R-09-31

Statistical analysis of results from the quantitative mapping of fracture minerals in Laxemar

Site descriptive modelling – complementary studies

Martin Löfgren, Niressa AB

Magnus Sidborn, Kemakta Konsult AB

December 2010

Svensk Kärnbränslehantering AB
Swedish Nuclear Fuel
and Waste Management Co

Box 250, SE-101 24 Stockholm
Phone +46 8 459 84 00

ISSN 1402-3091
SKB R-09-31

Statistical analysis of results from the quantitative mapping of fracture minerals in Laxemar

Site descriptive modelling – complementary studies

Martin Löfgren, Niressa AB

Magnus Sidborn, Kemakta Konsult AB

December 2010

Keywords: Fracture, Minerals, Quantitative mapping, Coating, Infill, Laxemar.

Abstract

Within the Laxemar site investigation campaign, quantitative mapping of different fracture minerals has been performed. This has been done by studying fracture surfaces of drill core sections from many different boreholes at the Laxemar site /Eklund and Mattsson 2008/. The drill core mapping was focused on the rock in the vicinity of flow anomalies detected by the Posiva Flow Log (PFL). The quantitative mapping was performed only on open fractures. The fracture minerals that were mapped are calcite, chlorite, clay minerals (as a group), hematite, and pyrite. In this present report, data from the quantitative mineral mapping campaign are refined, sorted into different data subsets, and analysed by parametric and non-parametric statistical methods.

The data subsets are associated with 17 different rock volumes, representing different elevations, rock domains, fracture domains, and groups of deformation zones. In total 1,852 fractures were mapped at the site, and the most frequent mineral was calcite. Its amount could be quantitatively estimated in 51% of the mapped fractures. Of the other minerals, chlorite was quantitatively estimated in 46%, pyrite in 19%, clay minerals in 16%, and hematite in 0.05% of the mapped fractures. For fractures where the averaged fracture mineral thickness, d_{mean} [mm], and visible coverage, C_{vis} [%], could be quantitatively estimated, the following arithmetic means were found: calcite = 0.25 mm and 22%, chlorite = 0.29 mm and 41%, pyrite =1.3 μm and 0.2%, and clay minerals = 0.15 mm and 35%. These quantities are based on visual inspection of fracture surfaces and do not include the contribution from non-consolidated fracture fillings.

It is shown that there is significant spatial variability of d_{mean} and C_{vis} within the examined rock volumes. Furthermore, the non-parametric analyses indicate that there are differences in d_{mean} and C_{vis} between the different rock volumes. Even so, the differences are generally shown to be small and if comparing the cumulative distribution functions for the data subsets of the 17 rock volumes, more similarities than dissimilarities are found. No general trends can be observed in data with respect to elevation and location of the rock volumes. These conclusions are made from the perspective of radionuclide retention and groundwater composition modelling. Such modelling is not so sensitive to local deviations in fracture mineral abundances, as flow path averaging is of major importance. In other scientific fields, these deviations may be attributed greater importance.

It is shown from parametric analyses that the normal distribution fairly well describes the logarithm of d_{mean} data. Concerning the visible coverage, $\log_{10}(C_{vis})$ data are fairly well described by truncated normal distributions. The distributions fitted to data from the entire site fairly well represent the individual rock volumes.

In fractures where the mineral amounts could be quantified, the following means and standard deviations for the normal distribution of $\log_{10}(d_{mean}$ [mm]) are suggested: calcite $\mu = -1.21$ and $\sigma = 0.76$, chlorite $\mu = -0.83$ and $\sigma = 0.48$, clay minerals $\mu = -1.12$ and $\sigma = 0.51$, pyrite $\mu = -4.43$ and $\sigma = 1.17$.

In fractures where the mineral visible coverage could be estimated, the following parameters for a truncated normal distribution of $\log_{10}(C_{vis})$ are suggested: calcite $\alpha = 0.96$ and $\beta = 0.65$, chlorite $\alpha = 1.43$ and $\beta = 0.45$, clay minerals $\alpha = 1.39$ and $\beta = 0.41$, pyrite $\alpha = -1.90$ and $\beta = 1.08$.

For hematite, the data are so scarce that no well founded conclusion can be drawn.

The potential correlation between the abundance of fracture minerals and the local transmissivity (which is related to the groundwater flow rate) has been evaluated, but no apparent correlation has been found. However, this evaluation is of preliminary character.

Contents

1 Introduction

1.1 Background

When setting up a safety assessment for a repository for spent nuclear fuel, two important scientific fields are hydrogeochemistry and radionuclide transport. The former describes the present and evolving groundwater chemistry of the natural and engineered barriers of the repository system, and the latter describes radionuclide migration from the engineered part of the repository to ground surface.

Groundwater flowing through the natural barrier will interact with the rock surrounding the flow paths by way of mineral dissolution, precipitation, and various reactions. This may alter the groundwater composition, which is primarily of concern for the function of the engineered barrier. In case radionuclides escape from the engineered barrier, they may be transported with flowing water towards the surface. These radionuclides will interact with the rock surrounding the flow paths, resulting in retardation.

The rock surrounding the flow paths is comprised of undisturbed rock matrix, altered rock matrix adjacent to fractures, fracture coatings, and fracture fillings. The mineralogy of the rock matrix has been carefully characterised and its mineral content is quantitatively described. However, until recently there has been a lack of data concerning quantities and coverages of fracture coatings, although they have previously been characterised qualitatively (e.g. /Drake and Tullborg 2009/).

In recent investigations at the Laxemar site, the occurrence of a number of fracture minerals associated with more than 1,800 fractures have been quantitatively mapped /Eklund and Mattsson 2008/. The drill core mapping was focused on the rock in the vicinity of flow anomalies detected by the Posiva Flow Low (PFL). The mapping has been performed on drill cores from several boreholes and from different depths as shown in Table 2-1. The boreholes concerned are shown in Figure 1-1. In these studies, fracture coatings have been mapped but not loose non-consolidated fracture fillings, as they to a large extent are flushed away in the drilling of the borehole. For further information of the mapping campaign see /Eklund and Mattson 2008/.

Before using the observed data in hydrogeochemical and radionuclide transport modelling, analysis and data reduction is required. This is attempted in this present report.

In the quantitative mineral mapping campaign sections of the boreholes KLX03, KLX10, KLX10C, KLX11F, KLX15A, KLX16A, KLX17A, KLX19A, and KLX26B were investigated. In the data delivery from Sicada forming the basis for this present work, data from KLX17A were excluded. Thus, this present work is based on data from boreholes KLX03, KLX10, KLX10C, KLX11F, KLX15A, KLX16A, KLX19A, and KLX26B.

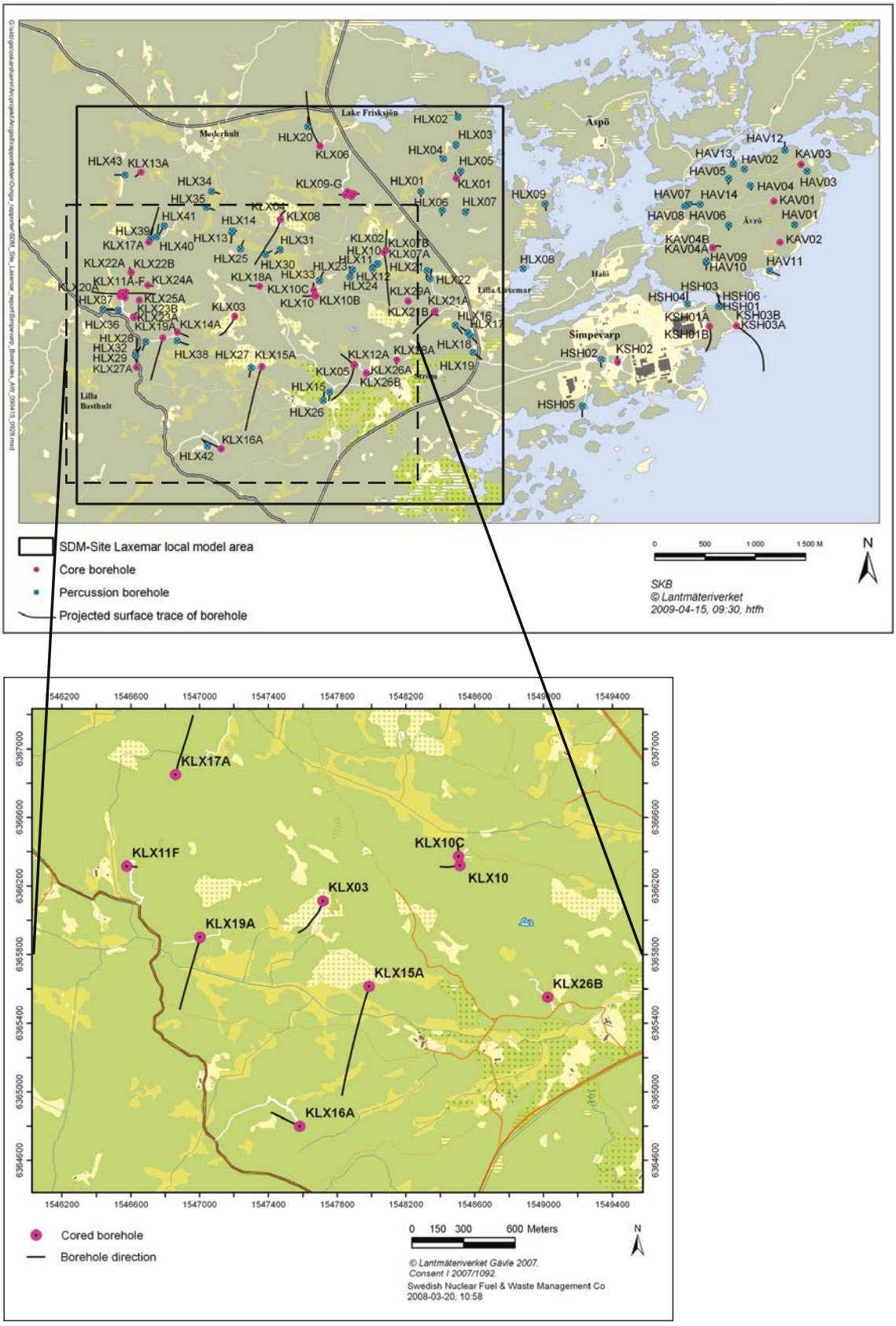

Figure 1-1. *Overview map of the site descriptive model domain (SDM-Site Laxemar) and location of the boreholes included in the quantitative mineral mapping campaign (inset map). The maps are adopted from /SKB 2009/ (top) and /Eklund and Mattsson 2008/ (inset).*

1.2 Scope and objectives

The objective of this report is to analyse the quantitative data reported within the Oskarshamn site investigation report /Eklund and Mattsson 2008/ and related files from the Sicada database. This will result in a set of distribution parameters recommended for subsequent modelling, for example in the SR-Site safety assessment. As part of performing data reduction, parametric and non-parametric statistical methods are used in the analysis with the aim to present mean values, histograms, and probability distributions of fracture mineral quantities and coverages. The quantity will be expressed as a thickness of each fracture mineral coating, as averaged over the entire fracture area. The coverage will be expressed as the fraction of the fracture surface that is covered by the particular fracture mineral.

The fracture minerals that were quantitatively mapped in the quantitative mineral mapping campaign are calcite, chlorite, clay minerals (as a group), hematite (may also include other iron oxides/hydroxides), and pyrite. It was also noted if the fracture mineral is pigmented (impregnated) by hematite. In addition, open fractures with fresh fracture surfaces of uncoated and unaltered rock matrix were mapped.

The results presented in this report concern the entire set of data obtained at the Laxemar site, but also a number of data subsets representing different rock volumes. This facilitates comparisons between different rock volumes that may be of use in subsequent analysis.

We acknowledge that conclusions are made from the perspective of radionuclide retention modelling. Such modelling is not so sensitive to minor deviations in fracture mineral abundances. If considering the data in the perspective of other scientific fields, what we judge as minor deviations in this report may be of considerable importance.

This report only aims at presenting analyses of the data obtained in the site investigation, and does not intend to interpret data in the light of, for example, geology, mineralogy, hydrogeochemistry, or radionuclide transport.

Parallel to performing the analyses in this report, efforts were made to identify which geological features mapped as fractures or crush zones that correspond to flow anomalies identified with the Posiva Flow Log method (e.g. /Teurneau et al. 2008/). It has not been within the scope for this report to include the results from these efforts.

1.3 Outline

This report consists of seven chapters. In Chapter 1, an introduction is given presenting the background, aim, and scope of this work. In Chapter 2, the methodology of this work is given. This includes both summarising the methodology of the data collection and presenting the methodology of the data refinement. Furthermore, the methods of non-parametric and parametric statistical analysis utilised are described. In Chapter 3, the averaged fracture mineral thickness, d_{mean}, is presented for a number of selected data subsets, representing the entire Laxemar site, different elevation ranges, rock domains, fracture domains, and groups of deformation zones. In Chapter 4, the visible coverage, C_{vis}, is presented for the same data subsets. In Chapter 5, distribution parameters are given as suggested for subsequent use in, for example, the SR-Site safety assessment. In Chapter 6 conclusions are given and Chapter 7 is the reference list.

Furthermore, for the different rock volumes and fracture minerals, figures showing histograms and fitted probability distributions are appended in Appendix A for d_{mean} and Appendix B for C_{vis}. Appendix C of this report has been structured to contain all sections requested by the data supplier in the instruction associated with the SR-Site Data report /SKB 2010/. This will simplify the integration of these data in the SR-Site safety assessment, if one chooses to do so.

2 Methodology

2.1 Methodology of data collection

The methodology of quantitative fracture mineral mapping is described in detail in the site investigation report /Eklund and Mattsson 2008/ and in the method description (MD 143.009). In this section, the methodology is summarised to facilitate a better understanding of the results presented in this present report.

2.1.1 Selection of drill core sections to map

The work done before the quantitative mineral mapping campaign, defining which drill core sections to map, is described in /Eklund and Mattsson 2008/. It was decided to focus the campaign upon open fractures (which apertures had previously been mapped to be > 0) that potentially constitute groundwater flow paths. Hydraulic data resulting from the Posiva flow log, a tool frequently used within the site investigations, were used. This tool is able to detect the locations where groundwater flows in or out of the borehole, through open fractures, with a resolution of 1 dm along the borehole. Such a detected in- or outflow is called a PFL-anomaly, where PFL is the abbreviation for Posiva flow log.

Prior to the quantitative mineral mapping campaign, there had been no coupling made between PFL-anomalies and discrete fractures detected in the drill core mapping. Therefore, it was decided to map all open fractures of a section of the drill core within a distance of one meter from a PFL-anomaly. Such a section is called a PFL-section.

At the time of the planning of the campaign, a great number of PFL-anomalies had been detected within the Laxemar site investigation area. In the initial planning, 400 anomalies out of these were chosen for mapping in the campaign, but due to time constraints, only 321 PFL-sections were finally mapped. The locations of these anomalies in terms of borehole name and elevation are given in Table 2-1. See Figure 1-1 for the location of the different boreholes.

Table 2-1. Number of mapped PFL-sections in different elevation (*E*) and transmissivity (*T*) ranges. Reproduced from Appendix 1 in /Eklund and Mattsson 2008/.

	$E > -100$ masl	$-100 \geq E \geq -300$ masl	$-300 > E \geq -600$ masl	$E < -600$ masl	$T < 10^{-8}$ m²/s	$10^{-8} \leq T \leq 10^{-6}$ m²/s	$T > 10^{-6}$ m²/s
KLX10	0	17	30	4	12	31	8
KLX10C	25	0	0	0	13	11	1
KLX15A	6	29	0	0	9	22	4
KLX26B	17	0	0	0	7	9	1
KLX17A	0	11	13	0	12	9	3
KLX03	0	0	10	18	8	18	2
KLX11F	23	0	0	0	4	17	2
KLX15A	0	14	11	2	13	14	0
KLX19A	0	12	27	3	21	19	2
KLX16A	12	34	3	0	12	32	5
Total	83	117	94	27	111	182	28

In addition to the selected PFL-sections, it was decided to map in total 74 m of drill core that is at least 5 m distant from any PFL-anomaly to facilitate comparisons between conducting and non-conducting rock volumes.

2.1.2 Methodology of fracture mineral mapping

Once the drill core sections included in the campaign had been selected, the previously performed drill core mapping was consulted and all discrete fractures previously mapped as open were revisited. In addition, crush zones were revisited. A crush zone is a section of the drill core with enhanced (open) fracture frequency, commonly with loose rock and fracture coating material of grain sizes ranging from clay to gravel. All other fractures or features were disregarded. The coverages and thickness of different fracture mineral layers were quantitatively mapped with respect to the following minerals:

- Calcite.
- Chlorite.
- Clay minerals (as a group).
- Hematite (may include other iron oxides/hydroxides).
- Pyrite.

It should be noted that chlorite found in fractures in Laxemar commonly consists of chlorite interlayered with the clay mineral corrensite (see e.g. /Drake and Tullborg 2009/). In addition, spot minerals were quantitatively mapped in the case of pyrite. Furthermore, a note was made in case:

- The fracture mineral is pigmented by hematite.
- Both the upper and lower fracture surface are fresh (no detectable fracture mineral and unaltered matrix rock).

Concerning the fracture mineral layers, the following parameters (in bold typeface) were estimated:

Mineral thickness: The mineral thickness is the integrated average of the thickness of a specific fracture mineral layer, where it covers the fracture surface, as estimated by the operator. This is done with a resolution of 0.1 mm. If the mineral layer is visible but significantly thinner than 0.1 mm, the mineral layer is noted for a qualitative purpose, but no quantitative thickness is assigned. Figure 2-1 and the discussion below aim at facilitating an understanding of how the mineral thickness is quantitatively estimated.

The rock sample in Figure 2-1 is covered by three fracture mineral layers. For the sake of simplicity, let us assume that the rock sample is a slab and not a cylinder, but keep in mind that the cylindrical shape of the drill core complicates the estimates made by the operator. Let us further assume that the layers do not vary along the z-axis in Figure 2-1. The mineral thickness is the average of the layer's thickness where it covers the underlying rock matrix. This means that the part of the fracture surface that is not covered by the specific layer should be disregarded. In Figure 2-1, fracture mineral layer A is represented by a triangle covering half the fracture surface, with the maximum thickness of 1 mm. In the mapping the correct estimate of the layer thickness should be 0.5 mm.

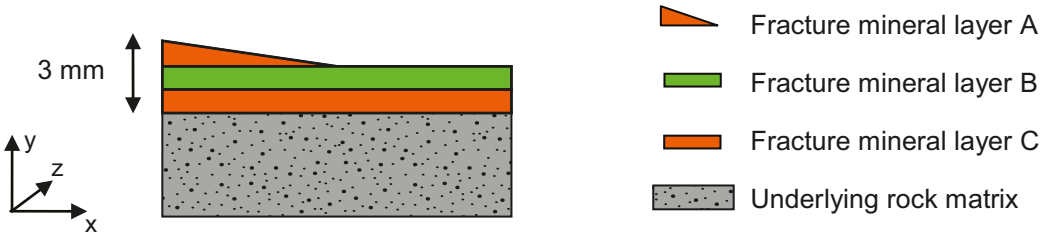

Figure 2-1. *Illustration of a rock sample covered by three layers of fracture minerals.*

Visible coverage of layer: The visible coverage of a specific layer is the fraction of the fracture surface that is covered by the layer, as estimated from visual inspection of the fracture surface from above. If inspecting the fracture surface in Figure 2-1 from above, mineral layer A would cover 50% of it, as would mineral layer B. Layer C would not be visible from above resulting in 0% visible coverage. In /Eklund and Mattsson 2008/ the visible coverage is also denoted as the surface coverage.

Total coverage: The total coverage is the actual fraction of the fracture surface that is covered by the mineral layer. In Figure 2-1, the total coverage would be 50% for mineral layer A, 100% for mineral layer B, and 100% for mineral layer C.

Some minerals commonly exist as spot minerals. In this campaign pyrite has been mapped as both spot mineral and layer mineral. Spot minerals are reported as *frequency* or number of crystals per cm^2, where the lower detection limit in the campaign is one crystal per ten cm^2. All mineral crystals on a fracture surface are assumed to be identical, with an average crystal size defined by the average squared base and an average thickness. The *length of the base* and the *thickness* are estimated with a resolution of 0.1 mm. The total as well as visible coverage of a spot mineral is the square of the length of the base times the frequency. It should be noted that only the uppermost crystal surface parallel to the fracture surface is included in the visible coverage, and not the surfaces of the sides of the pyrite grain.

For each of the upper and lower fracture surface of a fracture, up to four layers of fracture minerals are recorded, plus spot minerals if such exist. For crush zones, the same parameters are delivered as for discrete fractures, for three mineral layers and spot minerals. However, it is assumed that all fracture surfaces in a crush zone are identical. (It should be noted that the characteristics of the fracture surfaces in a crush zone can vary widely.) The delivered parameters are therefore estimated averages of the above parameters, based on the inspection of all fractures surfaces in the crush zone. In addition the number of fractures constituting the crush zone has been estimated.

In some fractures, the fracture minerals are pigmented (impregnated) with hematite. An investigation of such fracture minerals has indicated that their fraction of hematite is small, on the order of a couple of percents or less /Eklund and Mattsson 2008/. Furthermore, it has been concluded that by means of visual inspection only, the fraction of hematite cannot be determined. Therefore, the hematite associated with pigmented fracture minerals is not quantitatively mapped. It is only noted whether a fracture mineral is pigmented or not. This is done for calcite, chlorite, and clay minerals.

A special note is made concerning fractures where both the upper and lower fracture surfaces are fresh, as such fractures have recently become a focus of attention. In this campaign such fractures have been noted for a qualitative purpose, but only if previously assigned as open.

2.2 Methodology of data refinement

In the work presented in this report, data reported in the site investigation report /Eklund and Mattsson 2008/ and associated Sicada files have been refined and analysed. This is done by, as a first step, performing elementary arithmetic operations including the parameters underlined in Section 2.1. As a second step, the data are sorted into subsets associated with different rock volumes. These two steps are described in this section. In a third step, described in Sections 2.3 and 2.4, the data subsets are statistically analysed by non-parametric and parametric methods.

2.2.1 Defining output parameters

The parameters written in bold typeface in Section 2.1 are used to describe each layer, fracture, or crush zone. This present report aims at delivering output parameters representative for entire rock volumes. The data delivered as outputs in this report are:

- **Visible coverage C_{vis} (%):**
  The visible coverage for each fracture is calculated in two steps. Firstly, the visible coverages for the different mineral layers of the same mineral are summed. This includes layers on both the upper and lower fracture surfaces. Secondly, the sum is divided by two, in order to compensate for the fact that layers on both fractures surfaces are summed.
- **Average fracture mineral thickness d_{mean} (mm):**
  In the fracture mineral mapping, the output data concern different layers of fracture minerals in a fracture. From the product of the mineral thickness and total coverage for a specific layer, the *layer mean thickness* (mm) is obtained. If returning to the example of Figure 2-1, the layer mean thickness of mineral layer A is 0.25 mm, as its mineral thickness is 0.5 mm and only half the surface is covered. The layer mean thickness of mineral layer B and C is 1 mm.

  In some cases, different layers within a fracture (including both the upper and lower fracture surfaces) are of the same fracture mineral. If summarising the layer mean thicknesses of a specific fracture mineral in a fracture, the averaged fracture mineral thickness, d_{mean}, is obtained. If once more returning to the example of Figure 2-1; if mineral layers A and C are of the same fracture mineral and the upper fracture surface is uncoated by the mineral, d_{mean} is 1.25 mm.

  In case of spot minerals, the layer mean thickness is calculated by total coverage times the crystal thickness. For pyrite, which exists both as layer mineral and spot mineral, the averaged fracture mineral thickness is the sum of the layer mean thicknesses for both types of occurrences of the mineral.
- **Fraction of fractures where the averaged fracture mineral thickness could be quantitatively estimated f_{quant} (%):**
  In the fracture mineral mapping it has become apparent that not all of the investigated open fractures are coated by the fracture minerals studied. The fraction of fractures where the amount of a certain fracture mineral is sufficiently large to be quantitatively estimated is in this report called f_{quant}.
- **Fraction of fractures where the visible coverage could be quantitatively estimated f_{quant}^{c} (%):**
  The fraction of fractures where the visible coverage of a certain fracture mineral is sufficiently large to be quantitatively estimated is in this report called f_{quant}^{c}.
- **Fraction of fractures qualitatively populated by a certain mineral f_{qual} (%):**
  The parameter f_{qual} is similar to f_{quant}, except for the fact that f_{qual} also includes the fraction of fractures where a specific mineral is observed, but only in such small amounts that it cannot be quantitatively estimated. In other words, f_{qual} is the fraction of fractures where a specific mineral has been observed at any amounts.

2.2.2 Associating data subsets with different rock volumes

It is not known exactly how the information delivered by his report will be used, and what the demands are on coupling the results to different rock volumes. Therefore, it was decided to associate the data with a multitude of rock volumes. Different data subsets are assigned to different ranges of elevation, rock domains, fracture domains, and deformation zones as groups based on their orientation. Concerning elevation, six data subsets representing different elevation ranges are assigned as in the following:

- GS – 1,000: Ground surface to 1,000 mbsl (metres below sea level).
- GS – 100: Ground surface to 100 mbsl.
- 100 to 300 mbsl.
- 300 to 500 mbsl.
- 500 to 700 mbsl.
- 700 to 1,000 mbsl.

It should be noted that the first data subset, ground surface to 1,000 mbsl, includes the data set from the entire Laxemar site, as no drill core from below 1,000 mbsl was mapped. Concerning rock domains, the data subsets are based on the three rock domains defined in /SKB 2009, Section 5.4.4/ that are present in the target area.These are:

- RSMD01.
- RSMM01.
- RSMA01.

In addition, in /SKB 2009/ the rock domains RSMP01 and RSMP02 are defined, but in this campaign, no drill core from these rock domains is mapped.

Concerning fracture domains, the data subsets are based on five fracture domains defined in /SKB 2009, Section 5.6.1/:

- All FD: All fracture domains.
- FSM_EW007.
- FSM_NE005.
- FSM_W.
- FSM_C.
- FSM_S.

The first data subset includes all data in fracture domains, which excludes deformation zone data. In /SKB 2009/ the fracture domain FSM_N is also defined. However, no fracture from this domain has been mapped in this campaign. Concerning deformation zones, five data subsets are assigned according to /SKB 2009, Section 5.5.4/:

- All DZ: All deformation zones.
- NE-SW: Northeast-southwest striking, moderate to steeply dipping.
- N-S: North-south striking, moderate to steeply dipping.
- E-W/NW-SE: East-west and northwest-southeast striking moderate dip to the north.
- GDZ: Gently dipping.

The data set All DZ only includes data associated with deformation zones of a high confidence, and does not include data associated with possible deformation zones. In /SKB 2009, Section 5.5.4/, the additional group “East-west to northwest-southeast striking, steep to moderate dip to the south” is given. However, in this campaign no fracture was mapped that is associated to this group. In /SKB 2009, Section 8.4.1/ the zone klx19_dz5-8 is interpreted to be steep and mainly N-S oriented. In this work this zone is assigned as N-S.

As it turns out, and as described in Section 3.8, crush zones are fairly scarce within the investigated drill core sections. Only 21 crush zones were mapped. Furthermore, upon analysing the crush zones it is shown that their associated fracture minerals do not significantly differ in amount and coverage from those of discrete fractures. Therefore, it was decided to include only discrete open fractures in the assigned data subsets, and to use data from crush zones for a comparative purpose only.

2.2.3 Sorting of data into different subsets

In the Sicada files presenting the data from the quantitative mineral mapping campaign, all discrete fractures and crush zones are assigned a rock domain and fracture domain or deformation zone. As a result, sorting the data into different subsets representing the rock volumes presented no obstacle. A standard sorting routine was programmed in GNU Octave, automating the sorting process.

2.3 Non-parametric statistical analysis of data subsets

The data subsets were analysed by non-parametric statistical methods, as described below.

2.3.1 Kruskal-Wallis test

The first analysis made for the different data subsets is the Kruskal-Wallis test. This test aims to investigate whether different data sets are samples of the same population, which is the null hypothesis. In the test, two or more data sets are compared. This is done by sorting the data based on their values and assigning each data point a rank. For each data set, the ranks of its data points are summed. By comparing the sum of the ranks for the different data sets, the likeliness that they are samples of the same population can be evaluated. The test returns a confidence, or *p*-value. If the *p*-value is high, this indicates that the null hypothesis may be true, and that the data sets may be samples of the same population. If the *p*-value is small, this indicates that the null hypothesis should be rejected. For further explanation of the test, /NIST 2009/ is recommended.

2.3.2 Arithmetic mean and standard deviation of data subset

For each data subset, the arithmetic mean $\bar{X}$ and standard deviation *STD* are computed by standard methods. The arithmetic mean $\bar{X}$ of the data subset should not be mistaken for the mean value μ of the population which is sampled. Likewise, the standard deviation *STD* of the data subset should not be mistaken for the standard deviation σ of the sampled population.

2.3.3 Two-sided confidence limits for the mean

If sampling a number of data sets from the same population, it is unlikely that their arithmetic means $\bar{X}$ all coincide with the mean μ of the population. If one has access to a single data set, one may assign confidence limits around the arithmetic mean $\bar{X}$ of the sample. Within these limits, it is likely that the population mean μ is found. Confidence limits are expressed in terms of a confidence coefficient, and in this work the confidence coefficient used is 0.95. For further explanation of the confidence limits of the mean, /NIST 2009/ is recommended.

2.3.4 Histograms and cumulative distribution functions

In this work, data have been visualised by histograms and cumulative distribution functions. Histograms are useful when visualising how data of one data subset are distributed, and also when making comparisons with fitted probability distributions. In Figure 2-2 this is done for $\log_{10}(d_{mean})$ data for calcite. The comparison is made with the normal distribution.

When comparing different data sets, this is better visualised by the cumulative distribution function, CDF. In Figure 2-3, this is exemplified for $\log_{10}(d_{mean})$ for calcite data from different elevation ranges. The blue curve represents the same data as the histogram does in Figure 2-2.

One can extract much information from Figure 2-3, for example that the median of $\log_{10}(d_{mean})$ for the different data subsets (CDF = 0.5) is about –1.1.

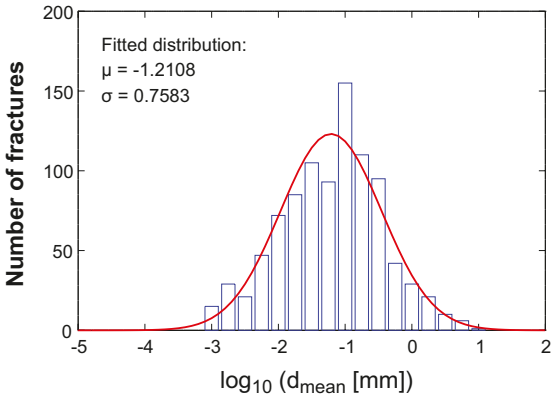

Figure 2-2. *Example of how data can be visualised by a histogram, facilitating visual comparisons with a fitted probability distribution.*

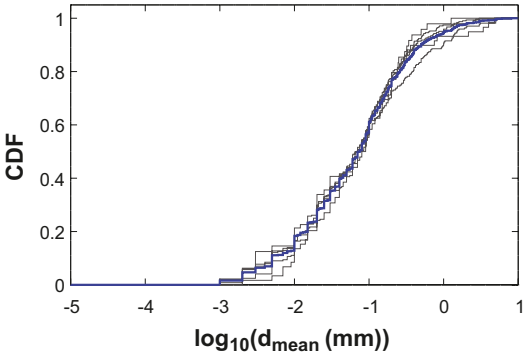

Figure 2-3. *Example of how several data subsets can be visualised by cumulative distribution functions.*

2.4 Parametric statistical analysis of data subsets

The distribution of a data set can be described by different probability distributions (also called probability density functions), such as the normal distribution, the chi square distribution, the beta distribution, etc. Due to bias issues discussed in Section 2.4.4, we have judged that there is no ground for making elaborate analyses with the aim at estimating possible skewness and kurtosis of the distribution. Based on the distributions of the sampled data, we have chosen to work with the normal distribution and truncated normal distribution in this report.

2.4.1 The normal distribution and truncated normal distribution

Equation 2-1 shows the equation for the normal distribution where φ is the probability that x will have a certain value, and x is the studied parameter that could be replaced with d_{mean}, C_{vis}, etc. One can also replace x with some expression including d_{mean} or C_{vis}, such as $\log_{10}(d_{mean})$. The parameters μ and σ are the mean and standard deviation of the distribution, respectively.

$$\varphi(x) = \frac{1}{\sigma\sqrt{2\pi}} \exp\left(-\frac{(x-\mu)^2}{2\sigma^2}\right) \qquad \text{Equation 2-1}$$

The logarithm of d_{mean} can in theory take any value while d_{mean} can only be ≥ 0. As the normal distribution permits both positive and negative values, it is strictly speaking not suitable for d_{mean}. For the visible coverage, the normal distribution is unsuitable for both $\log_{10}(C_{vis})$ and C_{vis}, as C_{vis} range from 0 to 100% and $\log_{10}(C_{vis})$ is ≤ 2. So solve this problem, the singly or doubly truncated normal distribution can be used /Cohen 1950, Barr and Sherrill 1999/. Equation 2-2 shows the singly truncated normal distribution that is used for $\log_{10}(C_{vis})$.

$$C_{vis} \le 100\% \;;\; \log_{10}(C_{vis}\,[\%]) \le 2: \quad \varphi\left(\log_{10}(C_{vis})\right) = \frac{\frac{1}{\beta\sqrt{2\pi}}\exp\left(-\frac{\left(\log_{10}(C_{vis})-\alpha\right)^2}{2\beta^2}\right)}{\int_{-\infty}^{2}\frac{1}{\beta\sqrt{2\pi}}\exp\left(-\frac{\left(\log_{10}(C_{vis})-\alpha\right)^2}{2\beta^2}\right)}$$

$$C_{vis} > 100\% \;;\; \log_{10}(C_{vis}\,[\%]) > 2: \quad \varphi\left(\log_{10}(C_{vis})\right) = 0 \qquad \text{Equation 2-2 a,b}$$

In the truncated normal distribution, we have chosen to denote the parameter corresponding to μ in the normal distribution by α. Furthermore, we have chosen to denote the parameter corresponding to σ in the normal distribution by β. This is done to minimise the risk that the parameter values for the truncated normal distribution are, by mistake, used for the normal distribution in subsequent modelling.

2.4.2 Shapiro-Wilk *W* test

The normality of a data set can be tested by the Shapiro-Wilk *W* test, also called the Shapiro-Wilk normality test. The theory behind the test can be read elsewhere, e.g. /Shapiro and Wilk 1965/, but it is based on linear regression of ordered observations. The test returns a *W*-value between zero and one. If one is returned, the data are normally distributed. The lower the *W*-value returned is, the less degree of normality the data set has. To exemplify, if taking the $\log_{10}(d_{mean})$ data for calcite of Figure 2-2, the *W*-value returned from the Shapiro-Wilk *W* test is 0.99. If instead using the d_{mean} data directly, as illustrated by the histogram in Figure 2-4, the *W*-value returned is 0.37. Clearly the d_{mean} values are not normally distributed.

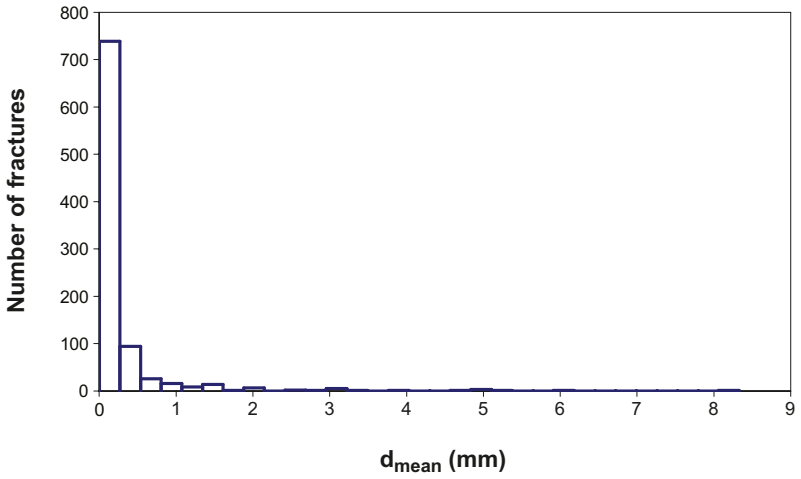

Figure 2-4. *Histogram of d_{mean} data for calcite (compare with Figure 2-2).*

If sampling a perfectly normally distributed population, the more data points one takes, the more likely it is that the data set agrees with the normal distribution. This would result in a returned W-value very close to one. In a development of the Shapiro-Wilk W test, the number of data points is taken into account, and a confidence (p-value) is given, which indicates whether or not the data set is a sample of a perfectly normally distributed population. The data set of Figure 2-2 contains hundreds of data points and still deviates from the normal distribution, for example at $\log_{10}(d_{mean}) \sim -1$. Even if one would sample more data points, it is unlikely that the situation would change. The p-value of the $\log_{10}(d_{mean})$ data displayed in Figure 2-2 is 0.0001, indicating that it is very unlikely that the data set is a sample of a perfectly normally distributed population.

It should be noted that a truncated distribution by definition deviates from normality. If the truncation is considerable, the Shapiro-Wilk W test is unsuitable. However, if the truncation is small, the errors introduced in the Shapiro-Wilk W test are small. Therefore, we have in some cases used the Shapiro-Wilk test to indicate which of d_{mean} or $\log_{10}(d_{mean})$ data to a larger degree are normally distributed, and whether C_{vis} or $\log_{10}(C_{vis})$ data to a larger degree are normally distributed.

2.4.3 Normal score plot

If a data set is fairly well normally distributed, one way of estimating the mean μ and standard deviation σ of the population is by the normal score plot (also called Q-Q plot). In a normal score plot, the data points are organised in ascending order depending on their value, and given a corresponding index. Based on the index and on the total number of data points in the data set, each data point is given a rank. Thereafter, each data point is assigned an x.y-coordinate. The y-coordinate is the actual value of the data point, for example $\log_{10}(d_{mean}) = -1.59$, while the x-coordinate depends on the rank. For further reading /Johnson 1994/ is recommended. In Figure 2-5, the normal score plot based on the same calcite $\log_{10}(d_{mean})$ data as displayed in Figure 2-2 are shown.

If the data would have been perfectly normally distributed, all the data points should have been in line with the linear fitting (red line). As this is not the case, this shows that there are some deviations from normality. For example, such a deviation can be seen at $\log_{10}(d_{mean}) \sim -1$ in both Figure 2-2 and Figure 2-5. As the r^2-value of the linear fitting is 0.99, one can say that the data are reasonably well normally distributed. From the slope and intercept of the linear fitting, the standard deviation σ and μ of the normal distribution can be obtained.

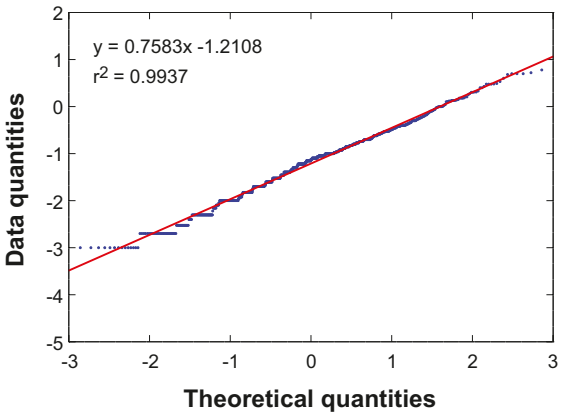

Figure 2-5. *Normal score plot of $\log_{10}(d_{mean})$ data for calcite.*

2.4.4 Underlying reasons to deviations from normality

As seen in Figure 2-5, the data in a normal score plot may deviate from the linear fitting. An obvious underlying reason is that the parameter studied is not normally distributed. This possible reason should be remembered throughout the reading of this report.

An additional reason may be that rounding issues in the estimations of the parameter give rise to bias. This is well illustrated by $\log_{10}(d_{mean})$ data for chlorite, a fracture mineral that often covers the entire fracture surface. Below, a few examples of common situations are given. In all examples, the total coverage of the chlorite mineral layer(s) is 100%. Firstly, consider a fracture where both fracture surfaces are covered by chlorite, and where the mineral thickness of both layers is rounded to 0.1 mm (which is the minimum quantitative layer thickness that can be assigned with this methodology). This gives rise to a $\log_{10}(d_{mean}[\text{mm}])$ value of –0.7. Secondly consider a fracture where only one fracture surface is totally covered by chlorite, and the other fracture surface is uncovered by chlorite (this is not uncommon). If rounding the mineral thickness to 0.1 mm, $\log_{10}(d_{mean})$ becomes –1. Thirdly, consider the same situation but where the mineral thickness is rounded to 0.2 mm, giving rise to a $\log_{10}(d_{mean})$ value of –0.7.

There are a few combinations of common total coverages and mineral thicknesses giving rise to favoured d_{mean} values. As there is an element of rounding involved in the estimations, this gives rise to bias. This bias is shown in both the corresponding histogram and normal score plot in Figure 2-6.

In the histogram, one can see that the two bins around –1 and –0.75 feature more data points that expected, compared to the best fit normal distribution (red curve). In the normal score plot one can see two plateaus at –1 and –0.7, which are highlighted by dashed arrows. These plateaus indicate that there are more data with the exact values –1 and –0.7 than expected.

Another example that illustrates bias is that of $\log_{10}(d_{mean})$ data for pyrite, a fracture mineral that is mapped as both spot mineral and layer mineral. Figure 2-7 shows the histogram and normal score plot for pyrite data from the entire site.

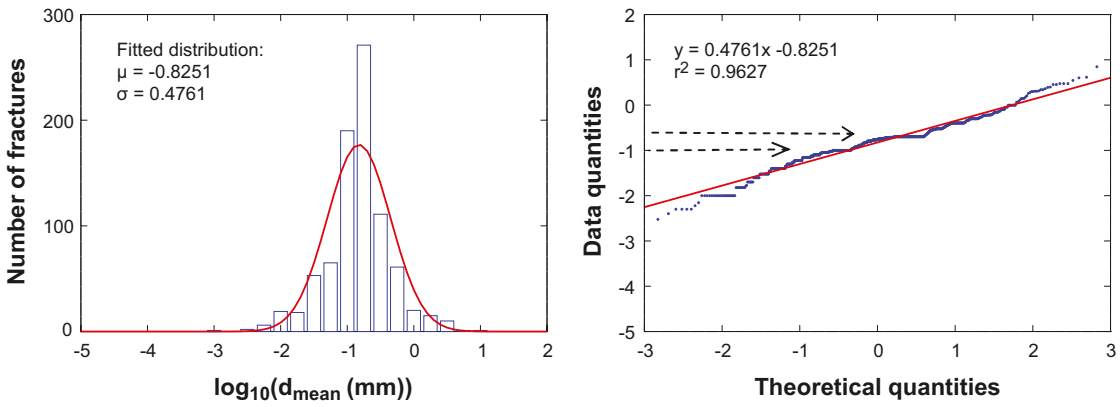

Figure 2-6. *Histogram and normal score plot of chlorite $\log_{10}(d_{mean})$ data.*

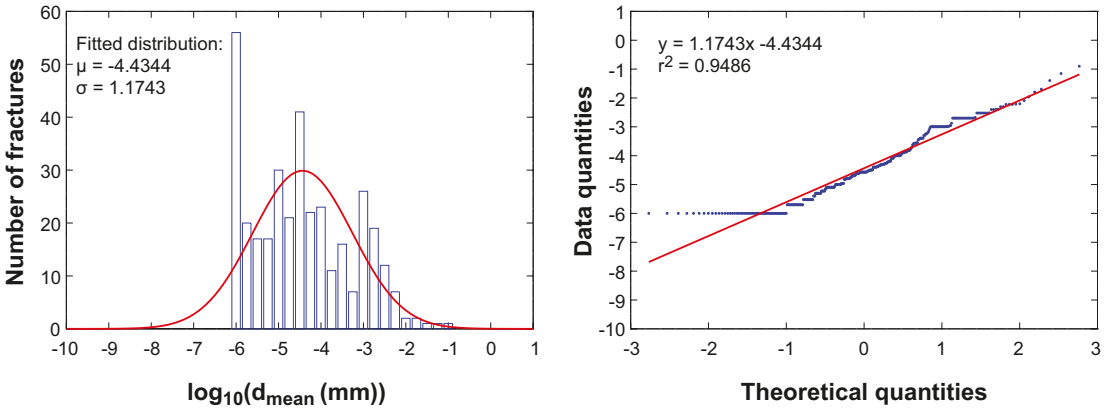

Figure 2-7. *Histogram and normal score plot of pyrite $\log_{10}(d_{mean})$ data.*

For pyrite as a layer mineral, it is common that there is a small speck of pyrite that is estimated to roundly cover 1% of the surface, with a 0.1 mm mineral thickness. This results in $\log_{10}(d_{mean}) = -3$. A few combinations of common total coverages and mineral thicknesses result in the plateaus at about –3 in the normal score plot in Figure 2-7. For pyrite as spot mineral, if one only finds one or two small pyrite cubes in a fracture, the frequency may be rounded to 1 crystal per 10 cm^2. Furthermore it is common that the length of the base and mineral thickness are rounded to 0.1 mm. This give rise to a $\log_{10}(d_{mean}) = -6$, which is seen as a distinct plateau in the normal score plot.

Due to the fact that rounding (and resolution) issues affect the shape of the histograms and normal score plots, it is judged that there is no ground for making elaborate analyses determining the potential skewness and kurtosis of the distributions.

2.4.5 Normal score plot for truncated normal distribution

In this work we have used the normal score plot to obtain the α and β parameters for the truncated normal distribution (see Equation 2-2). The α-value is obtained from the intercept of the linear fitting while the β value is obtained from the slope. In making the linear fit, we have censored all C_{vis} values $\geq 100\%$.

Figure 2-8 shows $\log_{10}(C_{vis})$ data for clay minerals from the entire site. The left image shows the histogram together with the truncated normal distribution. The right image shows the normal score plot.

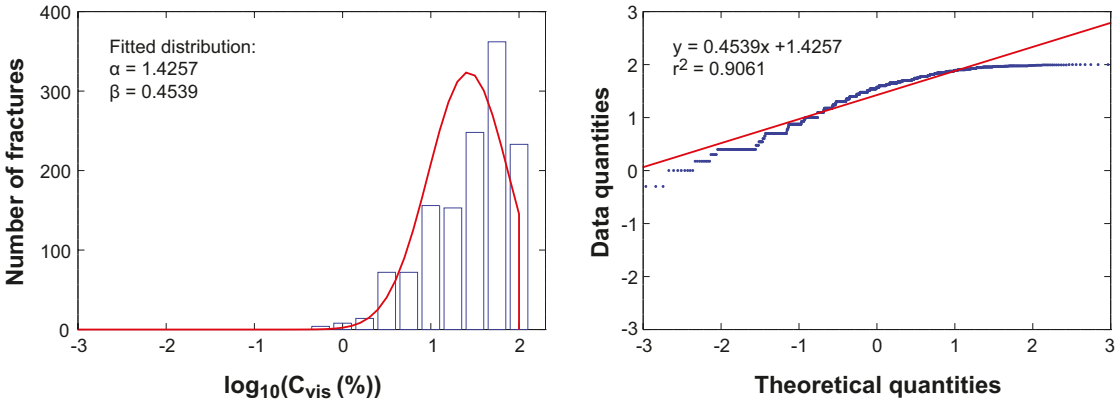

Figure 2-8. *Truncated distribution, histogram, and censored normal score plot for clay minerals $\log_{10}(C_{vis})$ data at the Laxemar site.*

3 Fracture mineral thickness, d_{mean}

The open fractures chosen for this campaign are predominantly located close to PFL anomalies. However, some fractures that are distant from any PFL anomaly are also included in the campaign, to facilitate comparisons between conducting and non-conducting rock volumes. As shown later in this chapter (Section 3.7), the location of the fracture with respect to PFL anomalies has little impact on the results. Neither does the occurrence of fracture minerals seem to be correlated with the measured transmissivities associated with the PFL anomalies. Therefore, the results presented for the different fracture minerals (Sections 3.1 to 3.6) are based upon all mapped open fractures.

In addition to open fractures, a few crush zones are mapped in this campaign. As seen in Section 2.1.2, the methodology of mapping crush zones differs from that of mapping discrete fractures. Even so, data from these crush zones are similar to data obtained from open fractures. It was decided to exclude these data from the general analysis in Sections 3.1 to 3.6 and instead include them in a separate study (see Section 3.8).

As described in Section 2.2.2, different data subsets of d_{mean} are assigned for different rock volumes. These rock volumes represent different ranges of elevation, rock domains, fracture domains, and deformation zones as groups based on orientation. In this chapter, these data subsets are analysed and results for d_{mean} are presented. For each fracture mineral, we will start with presenting the data subsets. Thereafter a non-parametric statistical analysis is presented. Finally a parametric statistical analysis is presented.

3.1 Calcite

3.1.1 The data subsets

In Table 3-1, information concerning calcite data subsets is summarised. For an introduction to the different rock volumes represented by the data subsets, Section 2.2.2 is recommended. In Table 3-1, firstly the total number of fractures mapped in the concerned rock volume is presented. Secondly, the number of data points in the subset is presented. This corresponds to the number of studied fractures in the rock volume holding a sufficient amount of calcite for quantitative mapping. Thirdly f_{quant} is presented, which is the fraction of all fractures holding quantitative amounts of calcite. Fourthly, f_{qual} is presented, which is the fraction of all fractures holding qualitative amounts of calcite.

Table 3-1. Amounts of data in different data subsets, calcite.

Calcite		Total number of fractures	Number of data points	f_{qual} (%)	f_{quant} (%)
Elevation (mbsl)	GS–1,000[1]	1,852	936	79	51
	GS–100	527	314	83	60
	100–300	502	244	83	49
	300–500	606	271	74	45
	500–700	134	59	73	44
	700–1,000	83	48	78	58
Rock domain	RSMA01	597	259	68	43
	RSMD01	1,067	564	84	53
	RSMM01	188	113	86	60
Fracture domain	All FD	797	405	82	51
	FSM_C	295	142	84	48
	FSM_EW007	146	68	77	47
	FSM_NE005	144	85	86	59
	FSM_S	115	56	76	49
	FSM_W	97	54	81	56
Deformation zone	All DZ	744	376	74	51
	GDZ	96	53	71	55
	E-W/NW-SE	57	41	82	72
	N-S	139	60	75	43
	NE-SW	452	222	73	49

[1]Data set represents the entire site.

The data are illustrated in Figure 3-1, showing the fractions of the fractures where calcite is found in quantitative amounts, qualitative amounts only, or not at all. With qualitative only, we mean the fractures holding so small fracture mineral amounts that although their occurrence can be qualitatively established, their amounts can not be quantitative estimated with the current methodology.

As can be seen from Table 3-1 and Figure 3-1, on average 51% of all fractures contain enough calcite to be quantitatively mapped, while 21% of all fractures contain no calcite at all. Furthermore, one can see that the occurrence of calcite in general is similar in the different rock volumes.

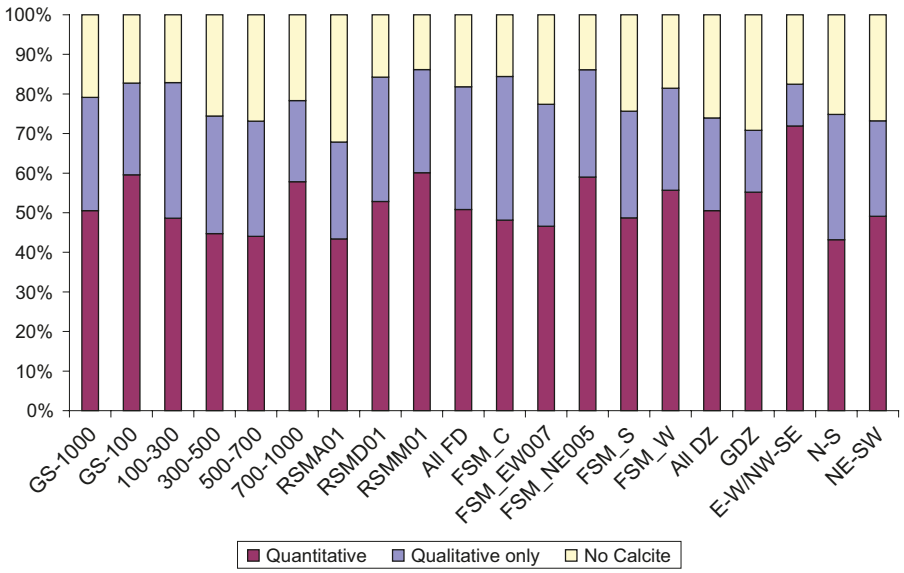

Figure 3-1. *Fractions of fractures populated or unpopulated by calcite.*

3.1.2 Non-parametric analysis

To determine whether or not the different calcite data subsets are samples of the same population, they were analysed by the Kruskal-Wallis test (see Section 2.3.1). There is no clear indication whether or not the data subsets are samples of the same population. For example, if comparing the five separate elevation data subsets for calcite, the *p*-value (confidence) returned from the Kruskal-Wallis test is 0.77. If comparing all separate data subsets, the *p*-value returned is 0.092. Simply put, this means that there is a 9% chance that the different data subsets are all samples of the same population. It should be noted that although the Kruskal-Wallis test gives information on whether the data subsets differ, it does not say whether the differences are large or small.

For all data subsets (including quantitative data only) the arithmetic mean $\bar{X}$ and the standard deviation *STD* of d_{mean} and $\log_{10}(d_{mean})$ were calculated. These data are shown in Table 3-2.

Table 3-2. Non-parametric data for calcite.

Calcite		Number of data points	$\bar{X}$ of d_{mean} [mm]	*STD of* d_{mean} *[mm]*	$\bar{X}$ of $\log_{10}(d_{mean}$ [mm])	*STD* of $\log_{10}(d_{mean}$ [mm])
Elevation (mbsl)	GS–1,000[1]	936	0.25	0.64	–1.21	0.76
	GS–100	314	0.19	0.54	–1.27	0.74
	100–300	244	0.20	0.42	–1.19	0.69
	300–500	271	0.35	0.83	–1.17	0.84
	500–700	59	0.35	0.93	–1.16	0.75
	700–1,000	48	0.15	0.21	–1.27	0.73
Rock domain	RSMA01	259	0.25	0.69	–1.28	0.83
	RSMD01	564	0.27	0.66	–1.15	0.72
	RSMM01	113	0.12	0.19	–1.38	0.71
Fracture domain	All FD	405	0.18	0.38	–1.27	0.75
	FSM_C	142	0.23	0.51	–1.24	0.80
	FSM_EW007	68	0.23	0.36	–1.24	0.92
	FSM_NE005	85	0.09	0.13	–1.43	0.63
	FSM_S	56	0.12	0.25	–1.30	0.61
	FSM_W	54	0.21	0.39	–1.11	0.68
Deformation zone	All DZ	376	0.30	0.82	–1.18	0.77
	GDZ	53	0.21	0.57	–1.23	0.71
	E-W/NW-SE	41	0.47	1.33	–1.10	0.87
	N-S	60	0.39	1.09	–1.28	0.81
	NE-SW	222	0.27	0.64	–1.16	0.76

[1]Data set represents the entire site.

The arithmetic mean of $\log_{10}(d_{mean})$ of each data subset is marked by a black ring in Figure 3-2 (left images). When sampling a number of data points from a population, the arithmetic mean $\bar{X}$ of the data subset may not coincide with the mean μ of the population. This gives rise to an uncertainty in how well the data subset's arithmetic mean represents the mean of the population. This uncertainty has been analysed resulting in a two-sided confidence limit for the mean (see Section 2.3.3) with the underlying assumption that the uncertainty is symmetrically distributed. For each data subset, the uncertainty range of μ is shown by the black line. In addition, in Figure 3-2 (left images), the standard deviation of $\log_{10}(d_{mean})$ for each data subset is illustrated by the green line. Here one standard deviation on each side of $\bar{X}$ is displayed. To avoid including too much information in Figure 3-2, we have refrained from including uncertainty ranges for how well the standard deviation *STD* of the sample represents the standard deviation σ of the population.

In Figure 3-2 a) and c), the combined data sets "All" for all elevations and all rock domains are identical. It is seen in Figure 3-2 (left images) that although there are differences in the arithmetic means $\bar{X}$ for the data subsets, the uncertainty ranges of the population means μ generally overlap (or almost overlap). In Figure 3-2 (right images) one can see that there are similarities in the cumulative distribution functions of the different data subsets. The results shown in Figure 3-1 and Figure 3-2 suggest that both the occurrence and amount of calcite are similar in different rock volumes at the Laxemar site.

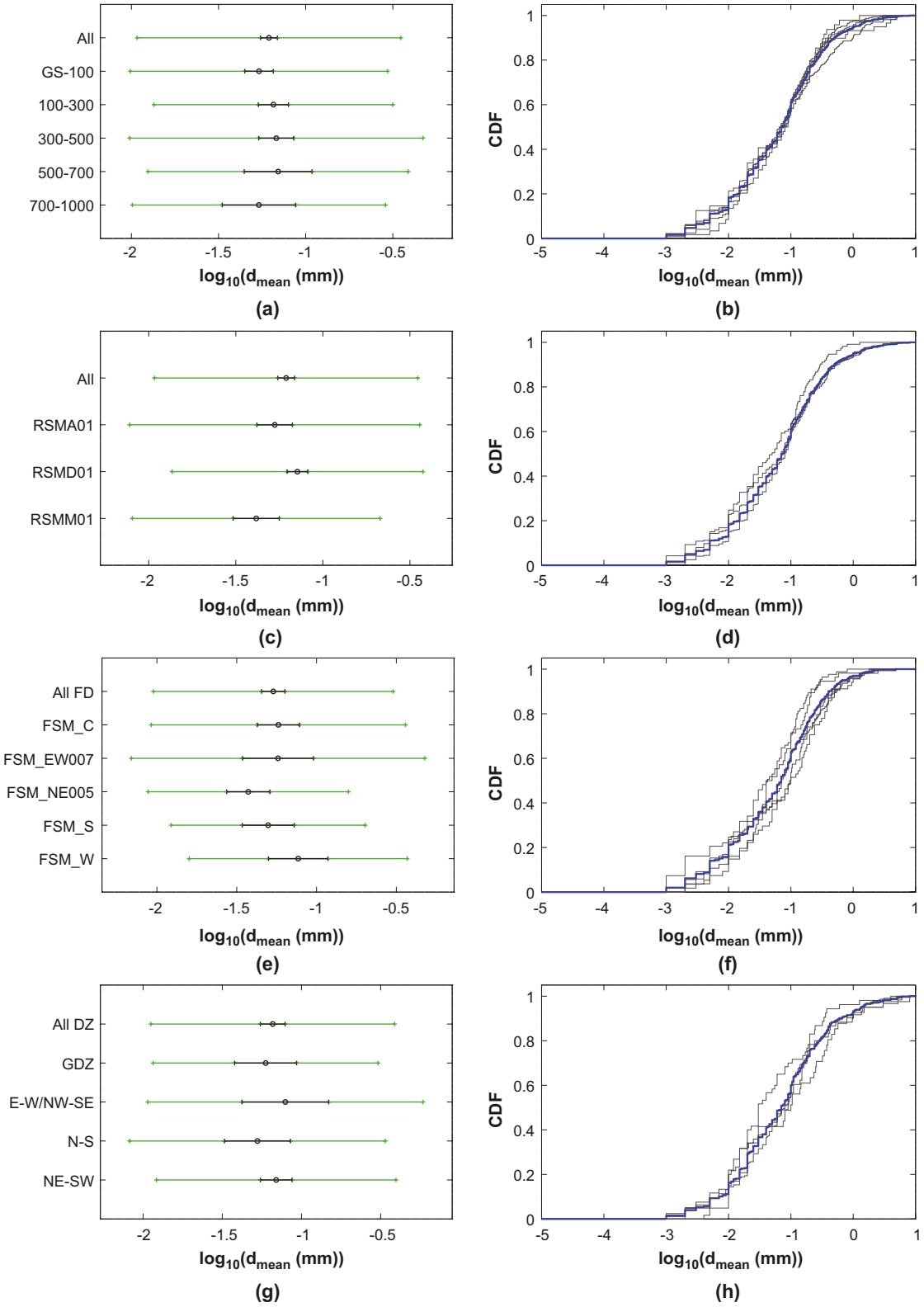

Figure 3-2. *Calcite: a, c, e, g) Arithmetic mean (black dot) and standard deviation (green range) of data subsets, and uncertainty range (black range) of population mean value. b, d, f, h) Cumulative distribution functions of the separate data subsets (black curves) and of the combined data set (blue curves).*

3.1.3 Parametric analysis

For the calcite data subsets from the entire site, it has been examined how well d_{mean} and $\log_{10}(d_{mean})$ data fit the normal distribution. This can be done by the Shapiro-Wilk W test for normality (see Section 2.4.2). In this test, the higher the W-value returned is, the higher degree of normality the data set has. If $W = 1$ is returned, this signify that the data are normally distributed. The Shapiro-Wilk W test can be performed for all data subsets but here, we only account for the tests on calcite data from the entire site. In this case, $W = 0.99$ is returned for $\log_{10}(d_{mean})$ data while $W = 0.37$ is returned for d_{mean} data. This clearly indicates a higher degree of normality for $\log_{10}(d_{mean})$ data. This is also supported in Figure 3-3, showing a histogram of $\log_{10}(d_{mean})$ for calcite data from the entire site. Furthermore, the best fit normal distribution (red curve in left figure) and the corresponding normal score plot (right figure) are shown. For an introduction to these concepts turn to Section 2.4.

It is seen in Figure 3-3 that the normal distribution reasonably well describes the $\log_{10}(d_{mean})$ data, with r^2=0.99 in the normal score plot. Similar figures are shown for all calcite data subsets in Appendix A.

With the Shapiro-Wilk W test one can also investigate whether or not the data set is a sample of a perfectly normally distributed population. However, for the data studied in this campaign, it is shown with great confidence that this is not the case. This can be exemplified with calcite data from the entire site, where the returned confidence is as low as $p = 0.0001$. This is not surprising, as one in Figure 3-3 clearly can see that the histogram deviates from the normal distribution, especially at $\log_{10}(d_{mean}) = -1$.

By making a normal score plot for each calcite data subset, taking μ from the intercept and σ from the slope, the data in Table 3-3 are obtained.

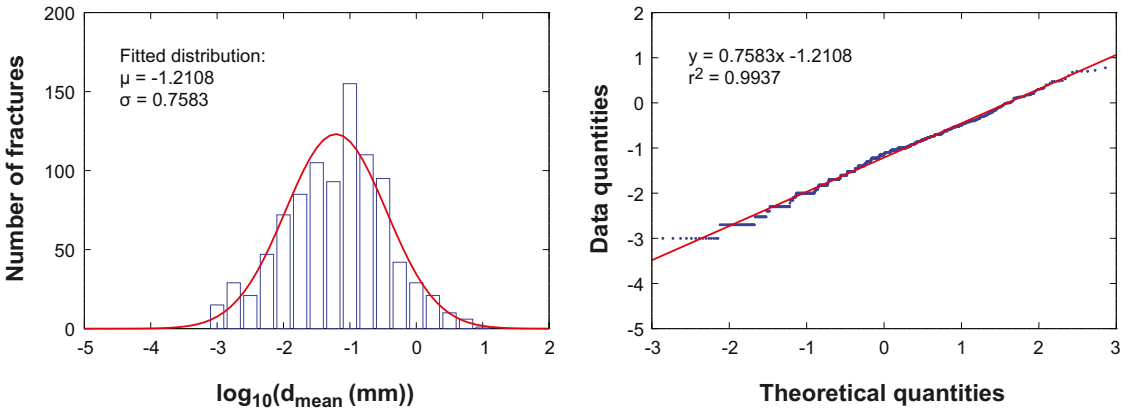

Figure 3-3. *Left: Histogram of $\log_{10}(d_{mean})$ data together with best fit normal distribution. Right: normal score plot of $\log_{10}(d_{mean})$ data. Data subset used: Calcite from the entire site.*

Table 3-3. Distribution parameters of populated fractures, calcite.

Calcite		Number of data points	$\log_{10}(d_{mean})$ μ	σ
Elevation (mbsl)	GS–1,000[1]	936	–1.21	0.76
	GS–100	314	–1.27	0.74
	100–300	244	–1.19	0.69
	300–500	271	–1.17	0.85
	500–700	59	–1.16	0.77
	700–1,000	48	–1.27	0.76
Rock domain	RSMA01	259	–1.28	0.84
	RSMD01	564	–1.15	0.73
	RSMM01	113	–1.38	0.73
Fracture domain	All FD	405	–1.27	0.75
	FSM_C	142	–1.24	0.81
	FSM_EW007	68	–1.24	0.93
	FSM_NE005	85	–1.43	0.65
	FSM_S	56	–1.30	0.64
	FSM_W	54	–1.11	0.72
Deformation zone	All DZ	376	–1.18	0.78
	GDZ	53	–1.23	0.74
	E-W/NW-SE	41	–1.10	0.92
	N-S	60	–1.28	0.82
	NE-SW	222	–1.16	0.77

[1]Data set represents the entire site.

Figure 3-4 illustrates the distributions of Table 3-3, where the distribution representing the entire site is shown by the red line.

Upon examination of Figure 3-4 one could suggest that the best fit distribution for data from the entire site well represents all the different rock volumes of the site.

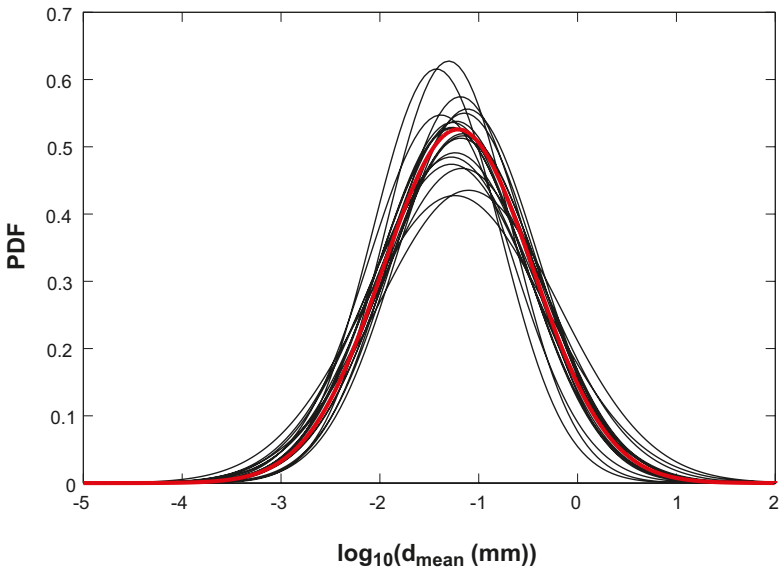

Figure 3-4. *Illustration of normal distributions of Table 3-3.*

3.2 Chlorite

In this section, equivalent tables and figures are presented for chlorite as for calcite in Section 3.1. In Section 3.1 information on how to interpret the tables, figures, and notations is found. An introduction to the rock volumes represented by the data subsets is found in Section 2.2.2.

3.2.1 The data subsets

In Table 3-4, information on the number of data points, f_{quant}, and f_{qual} is summarised for the different chlorite data subsets.

Table 3-4. Amounts of data in different data subsets, chlorite.

Chlorite		Total number of fractures	Number of data points	f_{qual} (%)	f_{quant} (%)
Elevation (mbsl)	GS–1,000[1]	1,852	844	72	46
	GS–100	527	260	73	49
	100–300	502	190	71	38
	300–500	606	295	77	49
	500–700	134	46	53	34
	700–1,000	83	53	69	64
Rock domain	RSMA01	597	242	73	41
	RSMD01	1,067	546	73	51
	RSMM01	188	56	61	30
Fracture domain	All FD	797	338	68	42
	FSM_C	295	128	67	43
	FSM_EW007	146	64	68	44
	FSM_NE005	144	31	62	22
	FSM_S	115	69	81	60
	FSM_W	97	46	68	47
Deformation zone	All DZ	744	340	73	46
	GDZ	96	50	58	52
	E-W/NW-SE	57	43	89	75
	N-S	139	80	81	58
	NE-SW	452	167	72	37

[1]Data set represents the entire site.

The data are illustrated in Figure 3-5, showing the fractions of the fractures where chlorite is found in quantitative amounts, qualitative amounts only, or not at all.

As can be seen from Table 3-4 and Figure 3-5, on average 46% of all fractures contain enough chlorite to be quantitatively mapped, while 28% of all fractures contain no chlorite at all. The bars for fracture domain FSM_NE005 and deformation zone group E-W/NW-SE deviates the most. Here, the deviation in f_{quant} as compared to that for the entire site is a factor of about two.

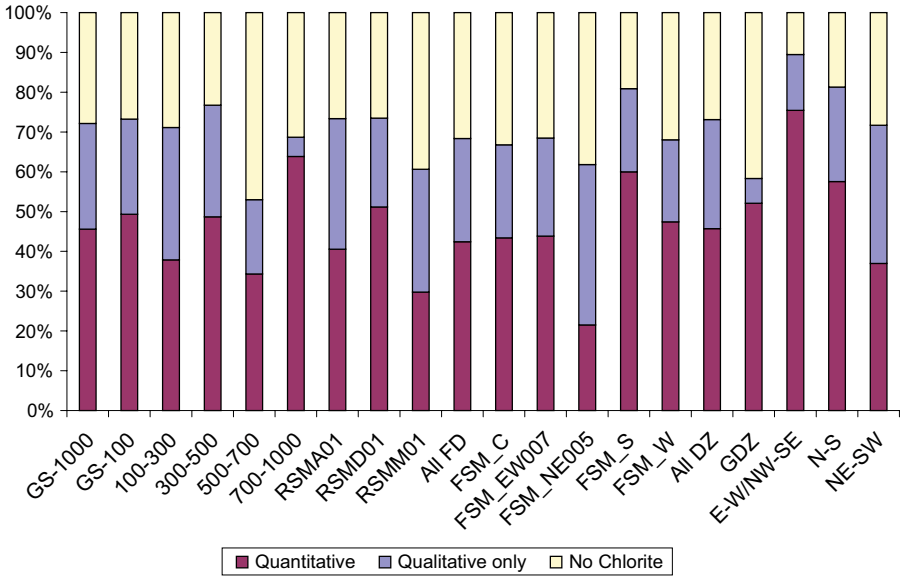

Figure 3-5. *Fractions of fractures populated or unpopulated by chlorite.*

3.2.2 Non-parametric analysis

As for calcite, an analysis was made by the Kruskal-Wallis test, clearly indicating that the different chlorite data subsets are not all samples of the exact same population. If comparing all separate data subsets, the *p*-value returned is 0.046.

For all data subsets (including quantitative data only) the arithmetic mean $\bar{X}$ and the standard deviation *STD* of d_{mean} and $\log_{10}(d_{mean})$ were calculated. These data are shown in Table 3-5**.**

Table 3-5. Non-parametric data for chlorite.

Chlorite		Number of data points	$\bar{X}$ of d_{mean} [mm]	*STD* of d_{mean} [mm]	$\bar{X}$ of $\log_{10}(d_{mean}$ [mm])	*STD* of $\log_{10}(d_{mean}$ [mm])
Elevation (mbsl)	GS–1,000[1]	844	0.29	0.59	–0.83	0.48
	GS–100	260	0.27	0.46	–0.88	0.53
	100–300	190	0.26	0.55	–0.78	0.38
	300–500	295	0.31	0.75	–0.83	0.49
	500–700	46	0.34	0.56	–0.76	0.49
	700–1,000	53	0.28	0.36	–0.80	0.49
Rock domain	RSMA01	242	0.26	0.46	–0.88	0.50
	RSMD01	546	0.31	0.67	–0.79	0.47
	RSMM01	56	0.19	0.16	–0.93	0.49
Fracture domain	All FD	338	0.24	0.38	–0.86	0.48
	FSM_C	128	0.27	0.37	–0.78	0.42
	FSM_EW007	64	0.31	0.59	–0.85	0.53
	FSM_NE005	31	0.16	0.12	–0.98	0.48
	FSM_S	69	0.23	0.31	–0.85	0.46
	FSM_W	46	0.15	0.14	–1.05	0.52
Deformation zone	All DZ	340	0.34	0.74	–0.79	0.50
	GDZ	50	0.30	0.37	–0.75	0.47
	E-W/NW-SE	43	0.37	0.69	–0.92	0.71
	N-S	80	0.50	1.25	–0.73	0.57
	NE-SW	167	0.26	0.43	–0.80	0.41

[1]Data set represents the entire site.

The arithmetic mean $\bar{X}$ of $\log_{10}(d_{mean})$ of each data subset is marked by a black ring in Figure 3-6 (left). The uncertainty range of μ is shown by the black line. In addition, in Figure 3-6 (left), the standard deviation of $\log_{10}(d_{mean})$ for each data subset is illustrated by the green line. Here one standard deviation on each side of $\bar{X}$ is displayed.

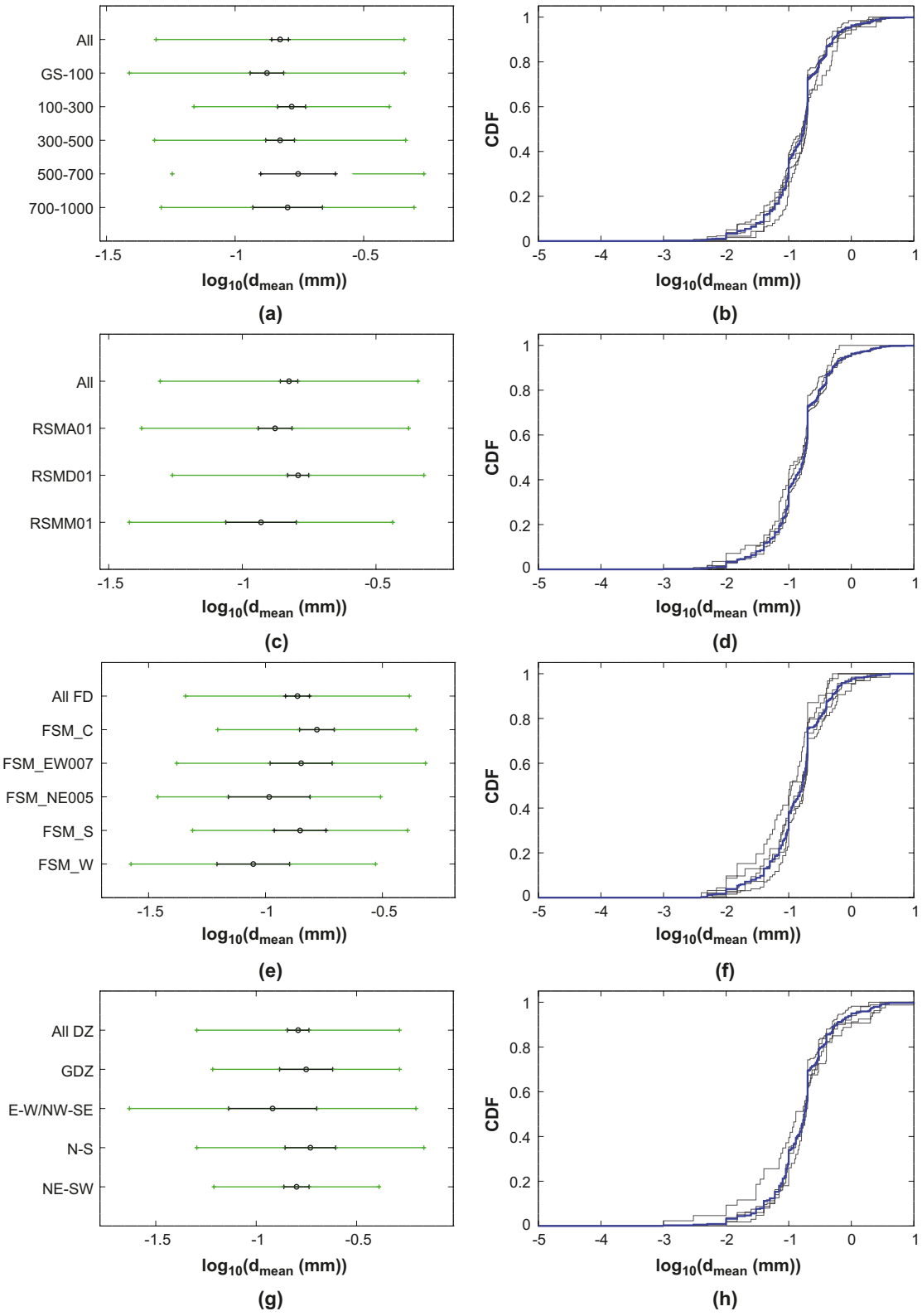

Figure 3-6. *Chlorite: a, c, e, g) Arithmetic mean (black dot) and standard deviation (green range) of data subsets, and uncertainty range (black range) of population mean value. b, d, f, h) Cumulative distribution functions of the separate data subsets (black curves) and of the combined data set (blue curves).*

It is seen in Figure 3-6 (left) that although there are differences in the arithmetic mean $\bar{x}$ for the data subsets, the uncertainty ranges of the population means μ generally overlap, or almost overlap. In Figure 3-6 (right images) one can see that there are similarities in the cumulative distribution functions of the different data subsets. The results shown in Figure 3-5 and Figure 3-6 suggest that both the occurrence and amount of chlorite are similar in different rock volumes at the Laxemar site.

3.2.3 Parametric analysis

As for calcite, the normality of the chlorite data subset from the entire site was investigated by means of the Shapiro-Wilk W test. It was shown that the normal distribution is much better fitted to $\log_{10}(d_{mean})$ data than to d_{mean} data. The W-value retuned for d_{mean} data is 0.35 and for $\log_{10}(d_{mean})$ data the returned W-value is 0.97. Figure 3-7 (left) shows a histogram of $\log_{10}(d_{mean})$ for chlorite data from the entire site, together with the normal distribution that is best fitted to the data. In the right image the associated normal score plot is shown.

It is seen in Figure 3-7 that the normal distribution fairly well describes the $\log_{10}(d_{mean})$ data, with $r^2 = 0.96$ in the normal score plot. The plateaus at $\log_{10}(d_{mean}) = -1$ and -0.7 (also seen in Figure 3-6) stems from a bias effect that is discussed in Section 2.4.4. Similar figures are shown for all chlorite data subsets in Appendix A.

By making a normal score plot for each chlorite data subset, taking μ from the intercept and σ from the slope, the data in Table 3-6 are obtained.

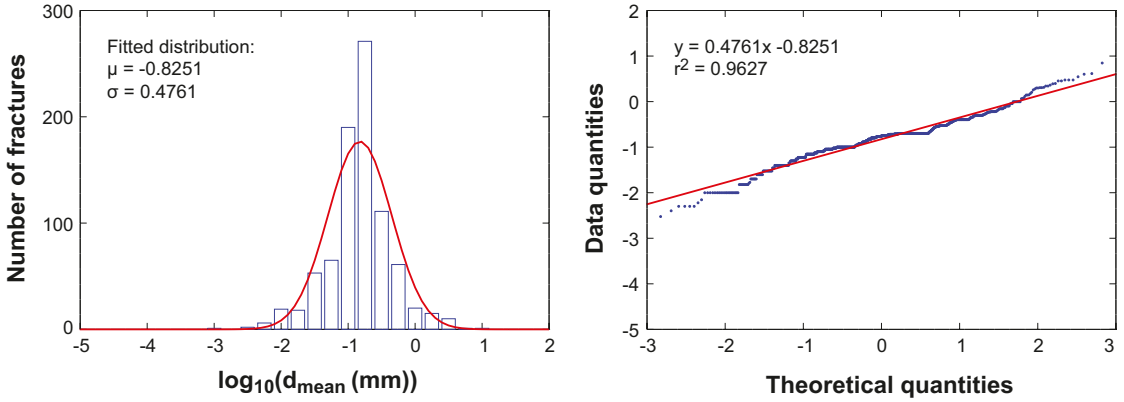

Figure 3-7. *Left: Histogram of $\log_{10}(d_{mean})$ data together with best fit normal distribution. Right: Normal score plot of $\log_{10}(d_{mean})$ data. Data subset used: Chlorite from the entire site.*

Table 3-6. Distribution parameters of populated fractures, chlorite.

Chlorite		Number of data points	$\log_{10}(d_{mean})$	
			μ	σ
Elevation (mbsl)	GS–1,000[1]	844	–0.83	0.48
	GS–100	260	–0.88	0.53
	100–300	190	–0.78	0.37
	300–500	295	–0.83	0.49
	500–700	46	–0.76	0.51
	700–1,000	53	–0.80	0.51
Rock domain	RSMA01	242	–0.88	0.49
	RSMD01	546	–0.79	0.47
	RSMM01	56	–0.93	0.50
Fracture domain	All FD	338	–0.86	0.48
	FSM_C	128	–0.78	0.43
	FSM_EW007	64	–0.85	0.55
	FSM_NE005	31	–0.98	0.48
	FSM_S	69	–0.85	0.47
	FSM_W	46	–1.05	0.54
Deformation zone	All DZ	340	–0.79	0.50
	GDZ	50	–0.75	0.48
	E-W/NW-SE	43	–0.92	0.74
	N-S	80	–0.73	0.58
	NE-SW	167	–0.80	0.41

[1]Data set represents the entire site.

Figure 3-8 illustrates the distributions of Table 3-6, where the distribution representing the entire site is shown by the red line.

Upon examination of Figure 3-8, one could suggest that the best fit distribution for data from the entire site well represents the different rock volumes of the site.

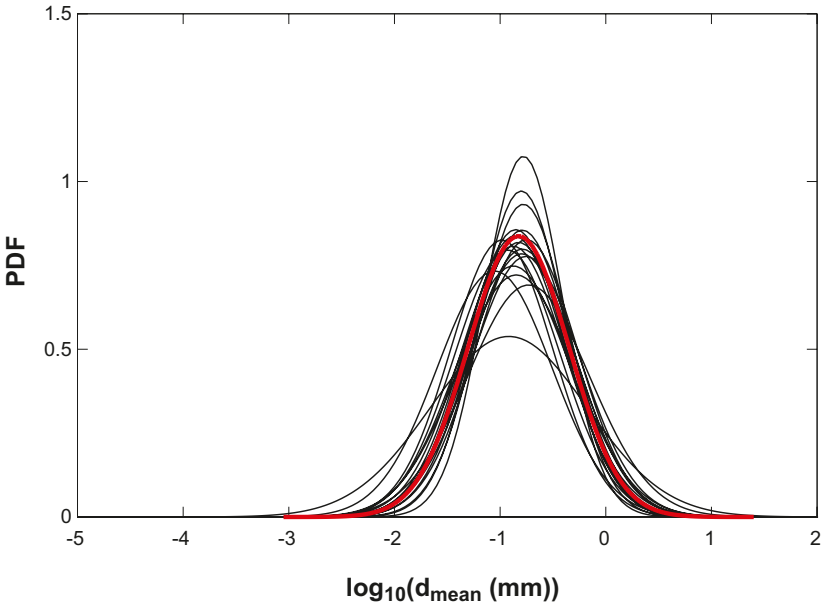

Figure 3-8. *Illustration of normal distributions of Table 3-6.*

3.3 Clay minerals, as a group

In this section results from what is mapped as “clay minerals as a group” are shown. In the following text we sometimes use the shorter notation “clay minerals”. In this section, equivalent tables and figures are presented for clay minerals, as for calcite in Section 3.1. In Section 3.1 information on how to interpret the tables, figures, and notations is found. An introduction to the rock volumes represented by the data subsets is found in Section 2.2.2.

3.3.1 The data subsets

In Table 3-7, information on the number of data points, f_{quant}, and f_{qual} is summarised for the different clay minerals data subsets.

Table 3-7. Amounts of data in different data subsets, clay minerals as a group.

Clay minerals, as a group		Total number of fractures	Number of data points	f_{qual} (%)	f_{quant} (%)
Elevation (mbsl)	GS–1,000[1]	1,852	301	34	16
	GS–100	527	78	29	15
	100–300	502	50	23	10
	300–500	606	105	41	17
	500–700	134	36	49	27
	700–1,000	83	32	57	39
Rock domain	RSMA01	597	97	44	16
	RSMD01	1,067	190	30	18
	RSMM01	188	14	26	7.4
Fracture domain	All FD	797	97	26	12
	FSM_C	295	37	24	13
	FSM_EW007	146	19	33	13
	FSM_NE005	144	10	30	6.9
	FSM_S	115	22	34	19
	FSM_W	97	9	10	9.3
Deformation zone	All DZ	744	142	40	19
	GDZ	96	39	71	41
	E-W/NW-SE	57	10	30	18
	N-S	139	21	31	15
	NE-SW	452	72	37	16

[1]Data set represents the entire site.

The data are illustrated in Figure 3-9, showing the fractions of the fractures where clay minerals are found in quantitative amounts, qualitative amounts only, or not at all.

As can be seen from Table 3-7 and Figure 3-9, on average 16% of all fractures contain enough clay minerals to be quantitatively mapped, while 66% of all fractures contain no clay mineral at all. The data indicate that the occurrence of clay minerals increases below repository depth. The occurrence is highest in gently dipping deformation zones and lowest in fracture domain FSM_NE005. Here, the deviation in f_{quant} as compared to that for the entire site is a factor of about two.

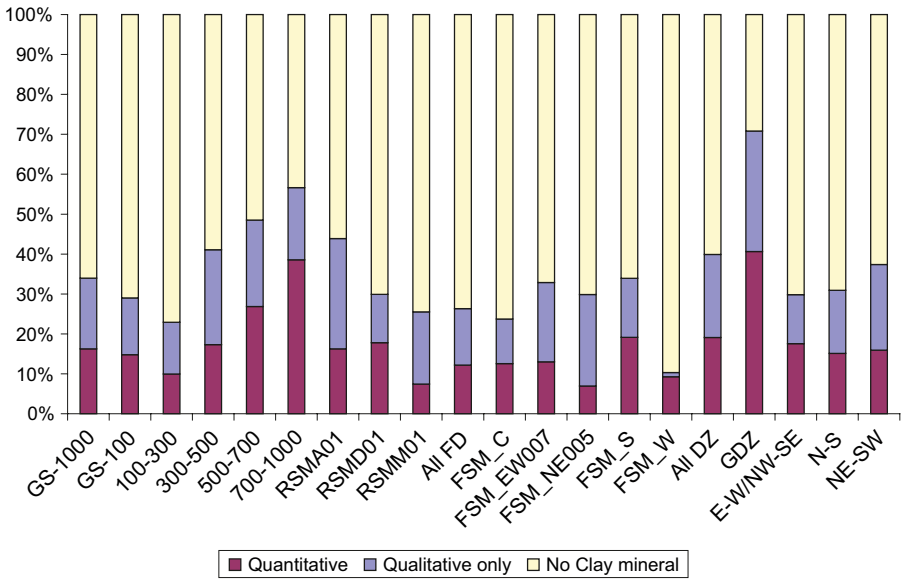

Figure 3-9. *Fractions of fractures populated or unpopulated by clay minerals, as a group.*

3.3.2 Non-parametric analysis

As for calcite, an analysis was made by the Kruskal-Wallis test, indicating that it is likely that the different data subsets are not all samples of the exact same population ($p = 0.22$ if comparing all separate data sets).

For all data subsets (including quantitative data only) the arithmetic mean $\bar{X}$ and the standard deviation *STD* of d_{mean} and $\log_{10}(d_{mean})$ were calculated. These data are shown in Table 3-8.

Table 3-8. Non-parametric data for clay minerals as a group.

Clay minerals, as a group		Number of data points	$\bar{X}$ of d_{mean} [mm]	*STD* of d_{mean} [mm]	$\bar{X}$ of $\log_{10}(d_{mean}$ [mm])	*STD* of $\log_{10}(d_{mean}$ [mm])
Elevation (mbsl)	GS–1,000[1]	301	0.15	0.24	–1.12	0.50
	GS–100	78	0.15	0.30	–1.20	0.52
	100–300	50	0.19	0.29	–1.04	0.54
	300–500	105	0.13	0.21	–1.14	0.48
	500–700	36	0.16	0.21	–1.05	0.49
	700–1,000	32	0.14	0.13	–1.04	0.49
Rock domain	RSMA01	97	0.11	0.15	–1.20	0.47
	RSMD01	190	0.17	0.28	–1.07	0.51
	RSMM01	14	0.13	0.13	–1.19	0.61
Fracture domain	All FD	97	0.15	0.22	–1.11	0.52
	FSM_C	37	0.17	0.27	–1.09	0.53
	FSM_EW007	19	0.12	0.093	–1.07	0.37
	FSM_NE005	10	0.11	0.12	–1.26	0.60
	FSM_S	22	0.16	0.19	–1.09	0.54
	FSM_W	9	0.22	0.34	–1.10	0.64
Deformation zone	All DZ	142	0.15	0.25	–1.16	0.53
	GDZ	39	0.17	0.21	–1.06	0.54
	E-W/NW-SE	10	0.05	0.05	–1.55	0.46
	N-S	21	0.14	0.28	–1.21	0.54
	NE-SW	72	0.15	0.27	–1.14	0.51

[1]Data set represents the entire site.

The arithmetic mean $\bar{X}$ of $\log_{10}(d_{mean})$ of each data subset is marked by a black ring in Figure 3-10 (left). The uncertainty range of μ is shown by the black line. In addition, the standard deviation of $\log_{10}(d_{mean})$ for each data subset is illustrated by the green line. Here one standard deviation on each side of $\bar{X}$ is displayed.

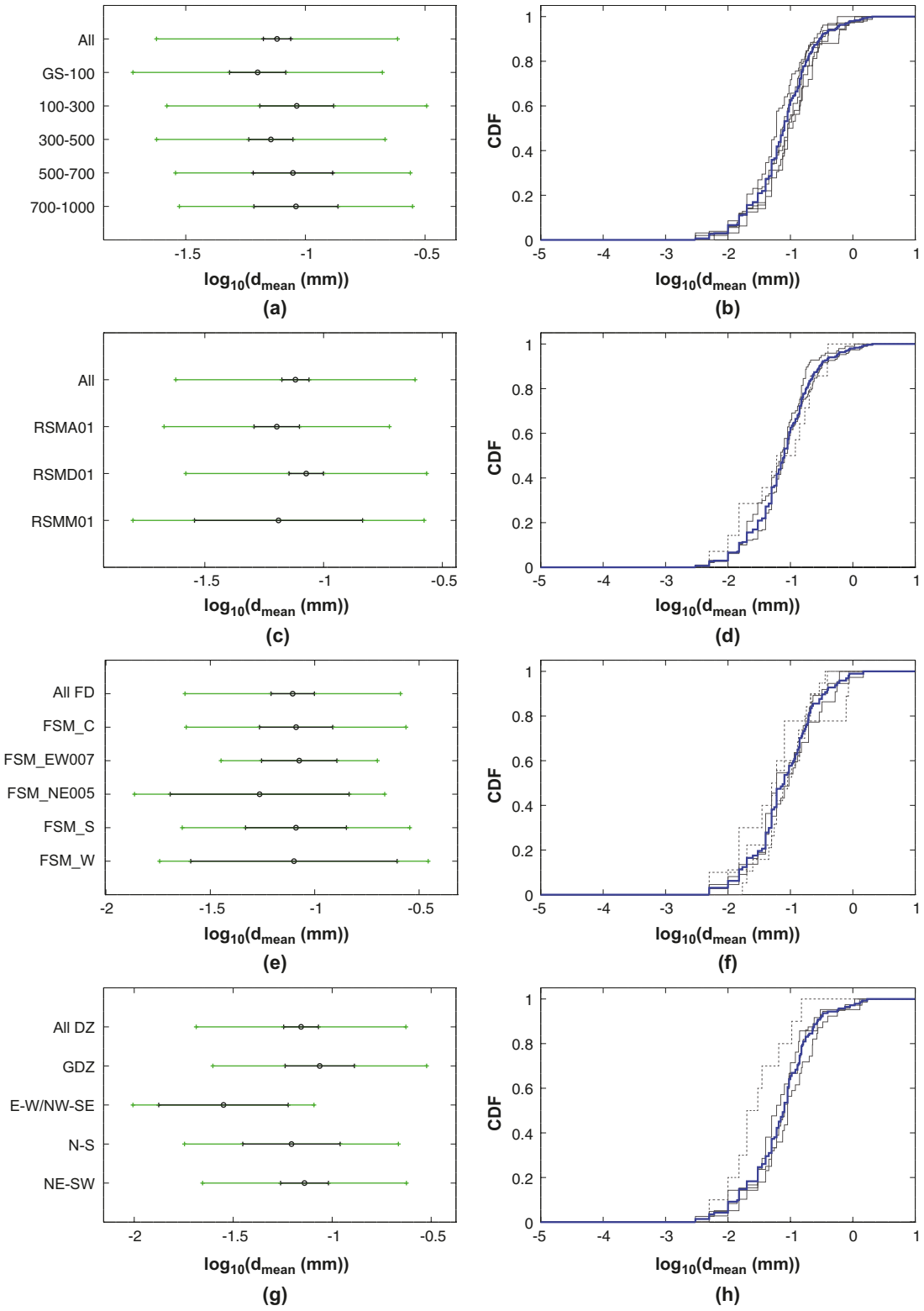

Figure 3-10. *Clay minerals: a, c, e, g) Arithmetic mean (black dot) and standard deviation (green range) of data subsets, and uncertainty range (black range) of population mean value. b, d, f, h) Cumulative distribution functions of the separate data subsets (black curves) and of the combined data set (blue curves). CDFs for data subsets with only up to 20 data points are dotted.*

As can be seen in Table 3-7, the data subsets for clay minerals do not include as many data points as for calcite and chlorite. Therefore, there is in many cases a larger uncertainty in μ. However, generally the uncertainty ranges overlap (note the different scales of the x-axes in the left hand figures). In Figure 3-10 (right) one can see that there are similarities in the cumulative distribution functions of the different data subsets. This is especially true for the data sets of more than 20 data points. CDFs representing data set with only up to 20 data points are shown by dotted lines. The results shown in Figure 3-9 and Figure 3-10 suggest that both the occurrence and amount of clay minerals are fairly similar in different rock volumes at the Laxemar site.

3.3.3 Parametric analysis

The normality of the clay minerals data set from the entire site was investigated by means of the Shapiro-Wilk W test. It was shown that the normal distribution is much better fitted to $\log_{10}(d_{mean})$ data than to d_{mean} data. The W-value retuned for d_{mean} data is 0.51 and for $\log_{10}(d_{mean})$ data the returned W-value is 0.99. Figure 3-11 (left) shows a histogram of $\log_{10}(d_{mean})$ for clay minerals data from the entire site, together with the normal distribution that is best fitted to the data (red curve in left figure). In the right image the associated normal score plot is shown.

It is seen in Figure 3-11 that the normal distribution well describes the $\log_{10}(d_{mean})$ data, with $r^2 = 0.99$ in the normal score plot. Similar figures are shown for all clay minerals data subsets in Appendix A.

By making a normal score plot for each clay minerals data subset, taking μ from the intercept and σ from the slope, the data in Table 3-9 are obtained.

Figure 3-12 illustrates the distributions of Table 3-9, where the distribution representing the entire site is shown by the red line. Distributions of data subsets with more than 20 data points are shown by the solid lines, while distributions of data subsets with up to 20 data points are shown by the shaded lines.

Upon examination of Figure 3-12, one can suggest that the best fit distribution for data from the entire site well represents the different rock volumes of the site.

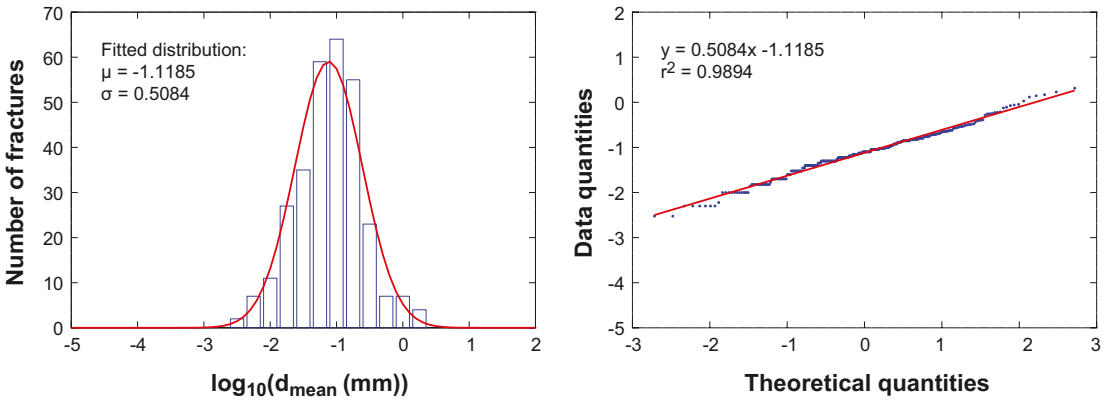

Figure 3-11. *Left: Histogram of $\log_{10}(d_{mean})$ data together with best fit normal distribution. Right: normal score plot of $\log_{10}(d_{mean})$ data. Data subset used: Clay minerals from the entire site.*

Table 3-9. Distribution parameters of populated fractures, clay minerals as a group.

Clay minerals, as a group		Number of data points	$\log_{10}(d_{mean})$	
			μ	σ
Elevation (mbsl)	GS–1,000[1]	301	–1.12	0.51
	GS–100	78	–1.20	0.54
	100–300	50	–1.04	0.57
	300–500	105	–1.14	0.49
	500–700	36	–1.05	0.52
	700–1,000	32	–1.04	0.51
Rock domain	RSMA01	97	–1.20	0.49
	RSMD01	190	–1.07	0.51
	RSMM01	14	–1.19	0.69
Fracture domain	All FD	97	–1.11	0.53
	FSM_C	37	–1.09	0.56
	FSM_EW007	19	–1.07	0.42
	FSM_NE005	10	–1.26	0.71
	FSM_S	22	–1.09	0.60
	FSM_W	9	–1.10	0.74
Deformation zone	All DZ	142	–1.16	0.54
	GDZ	39	–1.06	0.57
	E-W/NW-SE	10	–1.55	0.55
	N-S	21	–1.21	0.59
	NE-SW	72	–1.14	0.53

[1]Data set represents the entire site.

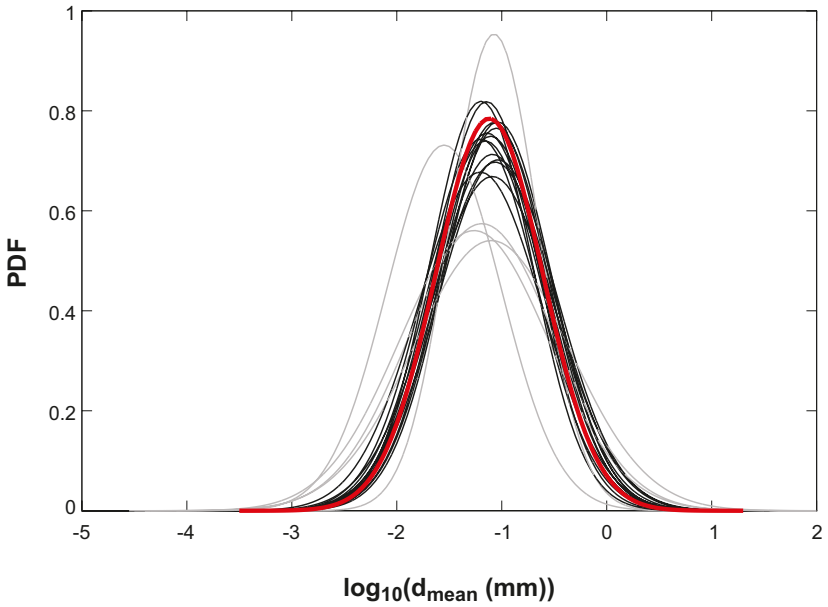

Figure 3-12. *Illustration of normal distributions of Table 3-9. Distributions of data subsets with only up to 20 data points are shaded.*

3.4 Hematite and hematite pigmented minerals

This section presents results for hematite and hematite pigmented minerals. Concerning hematite it was only found in two fractures in the campaign. Therefore, the analysis made is very limited. For hematite impregnated minerals, only qualitative results are presented. The reason for this is that there is little quantitative knowledge on the fraction of hematite that different hematite pigmented minerals hold, except for that the fraction is very small /Eklund and Mattsson 2008/.

In this section, some equivalent tables and figures are presented for hematite and hematite pigmented minerals as for calcite in Section 3.1. In Section 3.1 information on how to interpret the tables, figures, and notations is found. An introduction to the rock volumes represented by the data subsets is found in Section 2.2.2.

3.4.1 The data subsets and results

In Table 3-10, information on the number of data points, f_{quant}, and f_{qual} is summarised for the different hematite data subsets. In addition, the number of fractures containing any amount of hematite pigmented minerals is shown, together with f_{qual} for hematite pigmented minerals.

Table 3-10. Amounts of data in different data subsets, hematite and hematite pigmented minerals.

Hematite and hematite pigmented minerals		Total number of fractures	Hematite: Number of data points	Hematite: f_{qual} (%)	Hematite: f_{quant} (%)	Hem. pig.[2] Number of data points	Hem. pig.[2] f_{qual} (%)
Elevation (mbsl)	GS–1,000[1]	1,852	1	0.11	0.054	299	16
	GS–100	527	0	0	0	119	23
	100–300	502	0	0	0	51	10
	300–500	606	0	0.17	0	80	13
	500–700	134	1	0.75	0.75	28	21
	700–1,000	83	0	0	0	21	25
Rock domain	RSMA01	597	1	0.34	0.17	113	19
	RSMD01	1,067	0	0	0	152	14
	RSMM01	188	0	0	0	34	18
Fracture domain	All FD	797	0	0.13	0	92	12
	FSM_C	295	0	0	0	8	2.7
	FSM_EW007	146	0	0.68	0	20	14
	FSM_NE005	144	0	0	0	33	23
	FSM_S	115	0	0	0	28	24
	FSM_W	97	0	0	0	3	3.1
Deformation zone	All DZ	744	1	0.13	0.13	127	17
	GDZ	96	1	1.0	1.0	43	45
	E-W/NW-SE	57	0	0	0	19	33
	N-S	139	0	0	0	1	0.7
	NE-SW	452	0	0	0	64	14

[1]Data set represents the entire site.
[2]Hem. pig. = hematite pigmented minerals.

In Figure 3-13, the fractions of fractures containing hematite pigmented (impregnated) mineral are show. As seen, on average 16% of the fractures contain hematite pigmented mineral.

Only one of the two mapped occurrences of hematite had a layer mineral thickness, d_{mean} of 2.1 mm, large enough to be mapped quantitatively. This makes f_{quant} equal 0.05%.

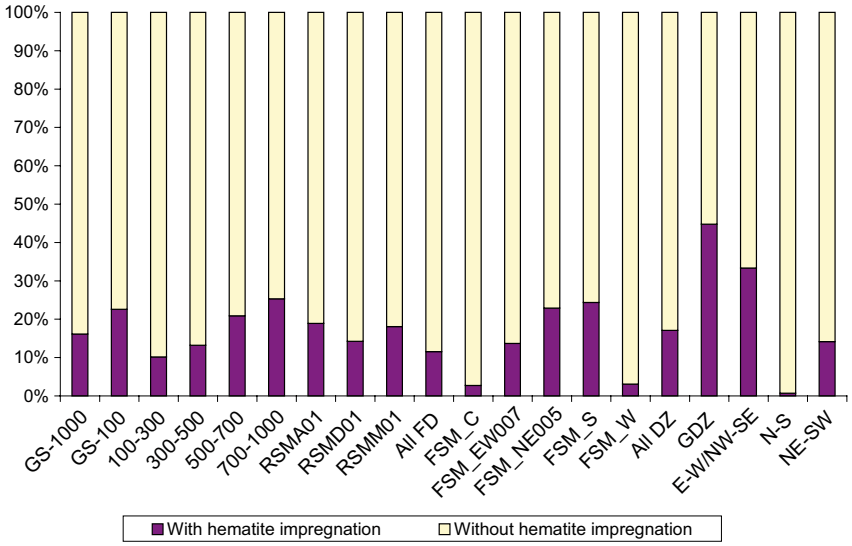

Figure 3-13. *Fractions of fractures populated or unpopulated by hematite pigmented mineral.*

3.5 Pyrite

In this section, equivalent tables and figures are presented for pyrite as for calcite in Section 3.1. In Section 3.1 information on how to interpret the tables, figures, and notations is found. An introduction to the rock volumes represented by the data subsets is found in Section 2.2.2.

3.5.1 The data subsets

In Table 3-11, information on the number of data points, f_{quant}, and f_{qual} is summarised for the different pyrite data subsets. As pyrite can also be mapped as minute spot minerals, where it was found it was in most cases mapped quantitatively, making f_{quant} and f_{qual} similar.

The data are illustrated in Figure 3-14, showing the fractions of the fractures where pyrite is found in quantitative amounts, qualitative amounts only, or not at all.

As can be seen from Table 3-11 and Figure 3-14, f_{quant} is on average 19%. Many of the deviating bars in Figure 3-14 represent rock volumes where only a few data points were obtained (e.g. GDZ with four data points).

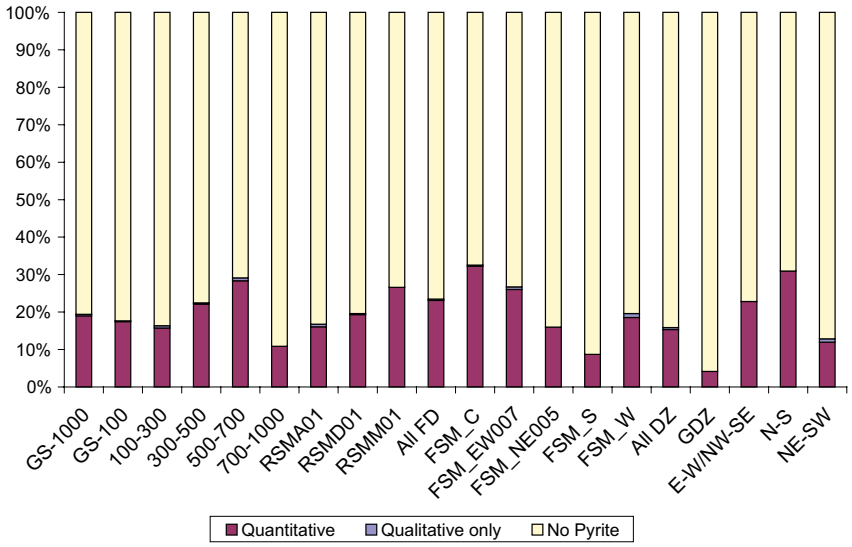

Figure 3-14. *Fractions of fractures populated or unpopulated by pyrite.*

Table 3-11. Amounts of data in different data subsets, pyrite.

Pyrite		Total number of fractures	Number of data points	f_{qual} (%)	f_{quant} (%)
Elevation (mbsl)	GS–1,000[1]	1,852	352	19	19
	GS–100	527	92	18	17
	100–300	502	79	16	16
	300–500	606	134	22	22
	500–700	134	38	29	28
	700–1,000	83	9	11	11
Rock domain	RSMA01	597	96	17	16
	RSMD01	1,067	206	20	19
	RSMM01	188	50	27	27
Fracture domain	All FD	797	184	23	23
	FSM_C	295	95	33	32
	FSM_EW007	146	38	27	26
	FSM_NE005	144	23	16	16
	FSM_S	115	10	8.7	8.7
	FSM_W	97	18	20	19
Deformation zone	All DZ	744	114	16	15
	GDZ	96	4	4.2	4.2
	E-W/NW-SE	57	13	23	23
	N-S	139	43	31	31
	NE-SW	452	54	13	12

[1]Data set represents the entire site.

3.5.2 Non-parametric analysis

An analysis was made by the Kruskal-Wallis test, indicating with great confidence that the different pyrite data subsets are not all samples of the exact same population. If comparing all separate data subsets, the *p*-value returned is 0.0022.

For all data subsets (including quantitative data only) the arithmetic mean $\bar{X}$ and the standard deviation *STD* of d_{mean} and $\log_{10}(d_{mean})$ were calculated. These data are shown in Table 3-12.

The arithmetic mean $\bar{X}$ of $\log_{10}(d_{mean})$ of each data subset is marked by a ring in Figure 3-15 (left). The uncertainty range of μ is shown by the black line. In addition, the standard deviation of $\log_{10}(d_{mean})$ for each data subsets is illustrated by the green line. Here one standard deviation on each side of $\bar{X}$ is displayed.

It is seen in Figure 3-15 (left) that although there are significant differences in the arithmetic mean $\bar{X}$ for the data subsets, the uncertainty ranges of the population means μ generally overlap. However, data indicates that there may be deviations between the rock volumes (on the order of a factor of few). In Figure 3-15 (right) one can see that there are similarities in the cumulative distribution functions of the different data subsets, but also some differences. The results shown in Figure 3-14 and Figure 3-15 suggest that the occurrence and amounts of pyrite are only fairly similar in the different rock volumes.

The larger ranges in the pyrite analyses as compared to the other minerals in the mapping campaign are partly due to the different methodolody used in the pyrite mapping (see Section 2.4.4).

Table 3-12. Non-parametric data for pyrite.

Pyrite		Number of data points	$\bar{X}$ of d_{mean} [mm]	*STD* of d_{mean} [mm]	$\bar{X}$ of $\log_{10}(d_{mean}$ [mm])	*STD* of $\log_{10}(d_{mean}$ [mm])
Elevation (mbsl)	GS–1,000[1]	352	$1.3 \cdot 10^{-3}$	$8.1 \cdot 10^{-3}$	–4.43	1.19
	GS–100	92	$6.1 \cdot 10^{-4}$	$2.1 \cdot 10^{-3}$	–4.43	1.08
	100–300	79	$6.3 \cdot 10^{-4}$	$1.4 \cdot 10^{-3}$	–4.34	1.10
	300–500	134	$9.6 \cdot 10^{-4}$	$4.0 \cdot 10^{-3}$	–4.54	1.26
	500–700	38	$3.9 \cdot 10^{-4}$	$7.9 \cdot 10^{-4}$	–4.55	1.18
	700–1,000	9	$2.2 \cdot 10^{-2}$	$4.5 \cdot 10^{-2}$	–3.24	1.47
Rock domain	RSMA01	96	$6.4 \cdot 10^{-4}$	$1.9 \cdot 10^{-3}$	–4.49	1.26
	RSMD01	206	$1.5 \cdot 10^{-3}$	$1.0 \cdot 10^{-2}$	–4.46	1.15
	RSMM01	50	$1.5 \cdot 10^{-3}$	$5.8 \cdot 10^{-3}$	–4.23	1.21
Fracture domain	All FD	184	$1.9 \cdot 10^{-3}$	$1.1 \cdot 10^{-2}$	–4.33	1.24
	FSM_C	95	$3.2 \cdot 10^{-3}$	$1.5 \cdot 10^{-2}$	–4.14	1.26
	FSM_EW007	38	$1.1 \cdot 10^{-3}$	$2.7 \cdot 10^{-3}$	–4.27	1.39
	FSM_NE005	23	$1.1 \cdot 10^{-4}$	$4.1 \cdot 10^{-4}$	–5.02	0.87
	FSM_S	10	$6.4 \cdot 10^{-4}$	$8.2 \cdot 10^{-4}$	–4.03	1.22
	FSM_W	18	$1.8 \cdot 10^{-4}$	$5.1 \cdot 10^{-4}$	–4.80	0.91
Deformation zone	All DZ	114	$6.2 \cdot 10^{-4}$	$2.1 \cdot 10^{-3}$	–4.48	1.09
	GDZ	4	$1.1 \cdot 10^{-4}$	$1.2 \cdot 10^{-4}$	–4.19	0.51
	E-W/NW-SE	13	$3.1 \cdot 10^{-4}$	$3.7 \cdot 10^{-4}$	–3.95	0.83
	N-S	43	$2.7 \cdot 10^{-4}$	$7.3 \cdot 10^{-4}$	–4.92	1.04
	NE-SW	54	$1.0 \cdot 10^{-3}$	$3.0 \cdot 10^{-3}$	–4.27	1.12

[1]Data set represents the entire site.

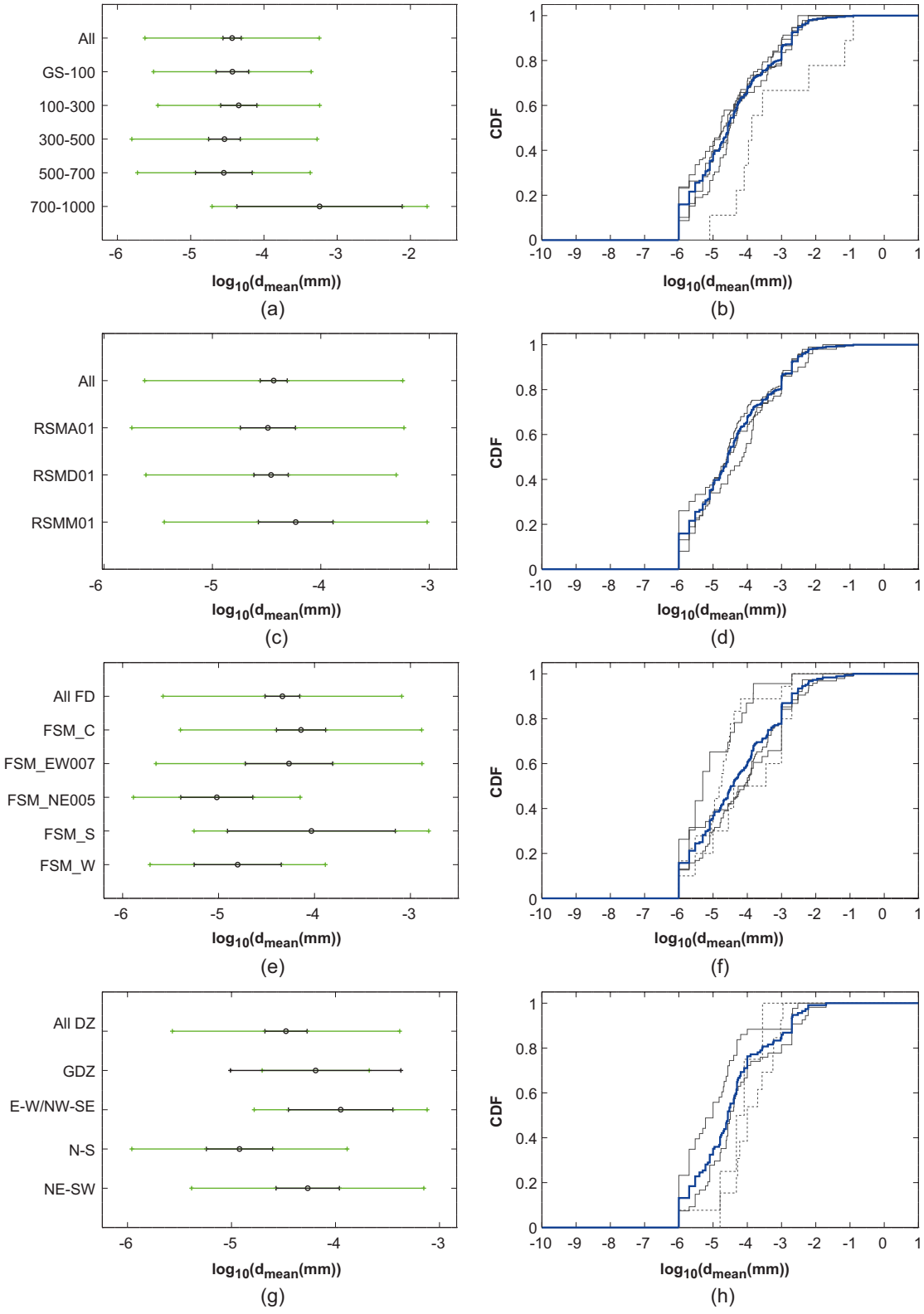

Figure 3-15. *Pyrite: a, c, e, g) Arithmetic mean (black dot) and standard deviation (green range) of data subsets, and uncertainty range (black range) of population mean value. b, d, f, h) Cumulative distribution functions of the separate data subsets (black curves) and of the combined data set (blue curves). CDFs for data subsets with only up to 20 data points are dotted.*

3.5.3 Parametric analysis

The normality of the pyrite data subset from the entire site was investigated by means of the Shapiro-Wilk W test. It was shown that the normal distribution is much better fitted to $\log_{10}(d_{mean})$ data than d_{mean} data. The W-value retuned for d_{mean} data is 0.13 and for $\log_{10}(d_{mean})$ data the returned W-value is 0.94.

Figure 3-16 (left) shows a histogram of $\log_{10}(d_{mean})$ for pyrite data from the entire site, together with the normal distribution that is best fitted to the data. In the right image the associated normal score plot is shown.

It is seen from Figure 3-16 that the normal distribution only fairly well describes the $\log_{10}(d_{mean})$ data, with r^2=0.95 in the normal score plot. Similar figures are shown for all pyrite data subsets in Appendix A. In this case resolution issues associated with the methodology clearly affect the appearance of the histogram and normal score plot, as discussed in Section 2.4.4.

By making a normal score plot for each pyrite data subset, taking μ from the intercept and σ from the slope, the data in Table 3-13 are obtained.

Figure 3-17 illustrates the distributions of Table 3-13, where the distribution representing the entire site is shown by the red line. Distributions of data subsets with more than 20 data points are shown by the solid lines, while distributions of data subsets with up to 20 data points are shown by the shaded lines.

Upon examination of Figure 3-17, one can suggest that the best fit distribution for data from the entire site fairly well represents the different rock volumes of the site. However, there is a notable difference in μ for fracture domain FSM_NE005 and deformation zone group N-S.

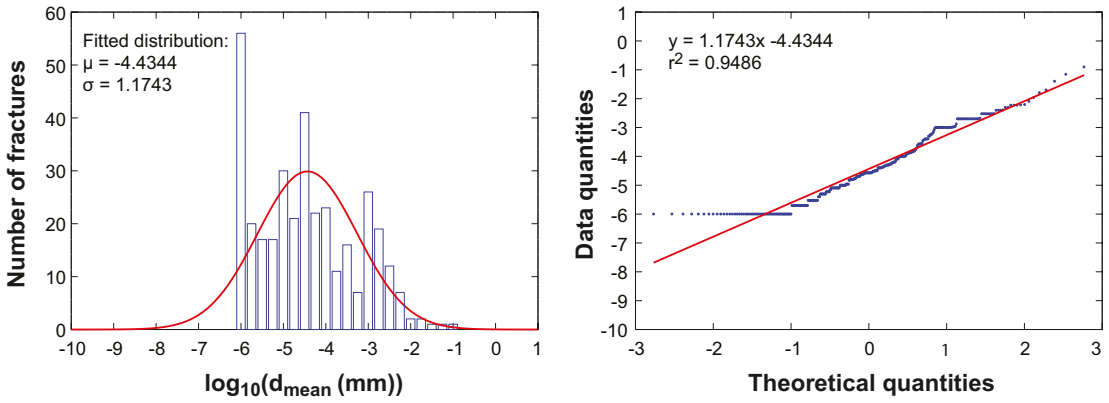

Figure 3-16. *Left: Histogram of $\log_{10}(d_{mean})$ data together with best fit normal distribution. Right: normal score plot of $\log_{10}(d_{mean})$ data. Data subset used: Pyrite from the entire site.*

Table 3-13. Distribution parameters of populated fractures, pyrite.

Pyrite		Number of data points	$\log_{10}(d_{mean})$	
			μ	σ
Elevation (mbsl)	GS–1,000[1]	352	–4.43	1.17
	GS–100	92	–4.43	1.10
	100–300	79	–4.34	1.12
	300–500	134	–4.54	1.25
	500–700	38	–4.55	1.22
	700–1,000	9	–3.24	1.70
Rock domain	RSMA01	96	–4.49	1.25
	RSMD01	206	–4.46	1.15
	RSMM01	50	–4.23	1.27
Fracture domain	All FD	184	–4.33	1.24
	FSM_C	95	–4.14	1.29
	FSM_EW007	38	–4.27	1.42
	FSM_NE005	23	–5.02	0.91
	FSM_S	10	–4.03	1.42
	FSM_W	18	–4.80	0.98
Deformation zone	All DZ	114	–4.48	1.10
	GDZ	4	–4.19	0.71
	E-W/NW-SE	13	–3.95	0.92
	N-S	43	–4.92	1.04
	NE-SW	54	–4.27	1.15

[1]Data set represents the entire site.

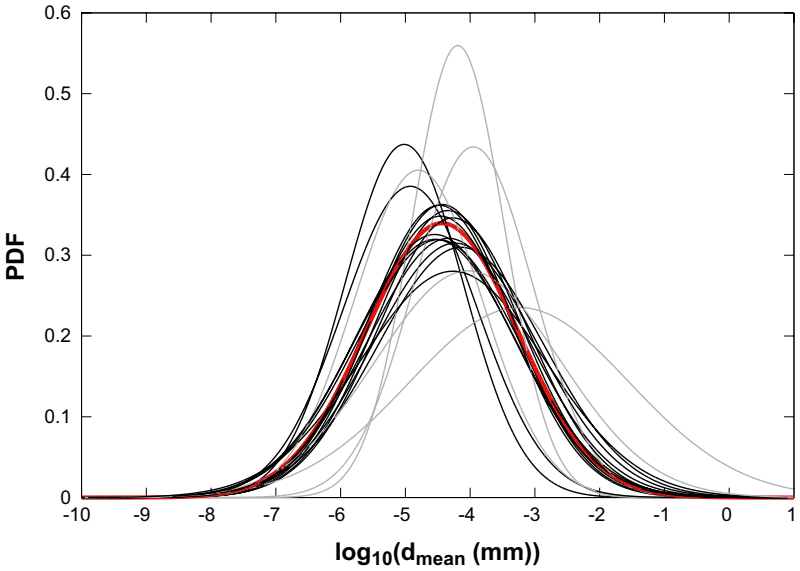

Figure 3-17. *Illustration of normal distributions of Table 3-13. Distributions of data subsets with only up to 20 data points are shaded.*

3.6 Fresh fracture surfaces

In the fracture mapping, some fracture surfaces were found to be fresh, meaning that no fracture mineral is detected by the visual mapping method used. It should be emphasised that small amounts of minerals undetectable without a microscope is likely to be present in these fractures. Table 3-14 shows the fraction of the fractures where both the upper and lower fracture surfaces are fresh. The data in Table 3-14 are illustrated in Figure 3-18.

As seen in Figure 3-18, only 4% of the investigated fractures display two fresh fracture surfaces. For the different rock volumes, this fraction varies between 1 and 8%.

Table 3-14. Amounts of data in different data subsets, fresh fracture surfaces.

Fresh fracture surfaces		Total number of fractures	Number of fresh fractures	Fraction (%)
Elevation (mbsl)	GS–1,000[1]	1,852	75	4.0
	GS–100	527	27	5.1
	100–300	502	22	4.4
	300–500	606	16	2.6
	500–700	134	8	6.0
	700–1,000	83	2	2.4
Rock domain	RSMA01	597	18	3.0
	RSMD01	1,067	43	4.0
	RSMM01	188	14	7.4
Fracture domain	All FD	797	46	5.8
	FSM_C	295	16	5.4
	FSM_EW007	146	5	3.4
	FSM_NE005	144	11	7.6
	FSM_S	115	7	6.1
	FSM_W	97	7	7.2
Deformation zone	All DZ	744	24	3.2
	GDZ	96	1	1.0
	E-W/NW-SE	57	2	3.5
	N-S	139	4	2.9
	NE-SW	452	17	3.8

[1]Data set represents the entire site.

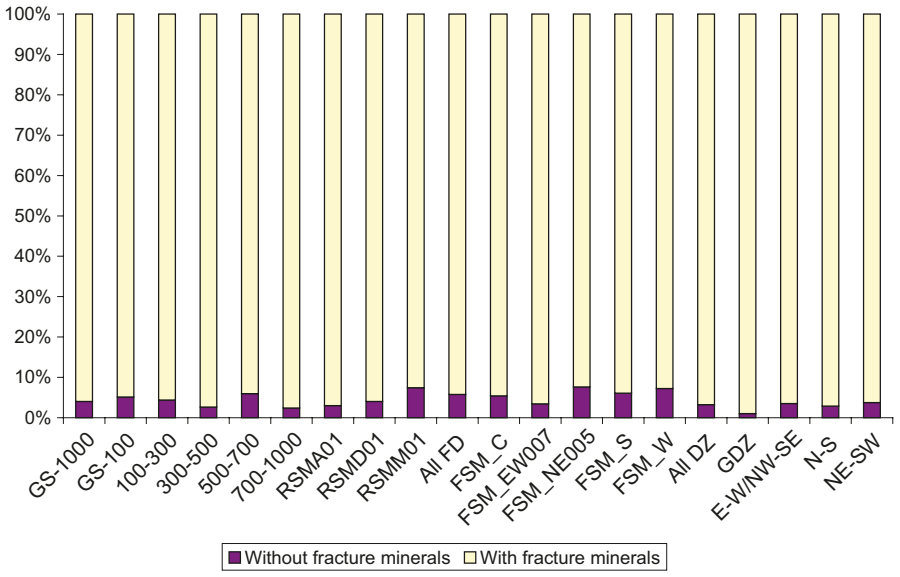

Figure 3-18. *Fractions of fractures with two fresh fracture surfaces for different data subsets.*

3.7 Influence of PFL anomaly

If the fracture minerals should have an impact on repository safety, they should be associated with flowing structures. Therefore, the great majority of fractures studied in this campaign are taken from within a meter of the nearest PFL-anomaly. In this section it is investigated if fracture mineral amounts are related to the transmissivity of the PFL-anomaly that the fracture is closest to. The transmissivity is correlated to the groundwater flow rate in the fracture (or fracture zone) at the imposed conditions of the measurements. As the hydraulic gradient is altered during the measurements, it is not certain that the fracture naturally conducts water. Even so, most transmissivities should in one way or another be related to the natural groundwater flow.

In order to do such a study it would be preferable if one had information on exactly which open fractures are conducting water in the PFL-logging. An effort has been initiated by SKB to couple PFL-anomalies with individual fractures, but no result from this effort has been a basis for this analysis. Instead, any open fracture within a distance of one decimetre from the location of a detected PFL-anomaly is coupled to the anomaly and its measured transmissivity. In case of two or more nearby PFL-anomalies, each fracture has been coupled to the nearest anomaly and its transmissivity.

The number of PFL-anomalies included in this comparative study is 297, and the number of fractures at distances up to 1 dm from such an anomaly is 422. Figure 3-19 to Figure 3-22 give plots of d_{mean} versus transmissivity for calcite, chlorite, clay minerals, and pyrite. Also the numbers of data points constituting the plots are shown.

As can be seen in Figure 3-19 to Figure 3-22, the fracture mineral thickness d_{mean} of the studied fracture minerals appears to be unrelated to the transmissivity. For hematite, the data are too scarce to make a comparison.

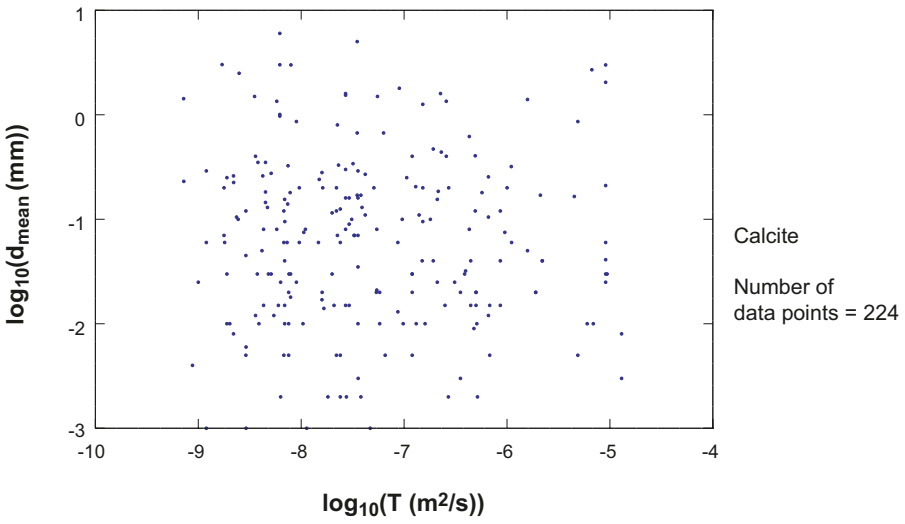

Figure 3-19. *Transmissivity vs. d_{mean} for calcite.*

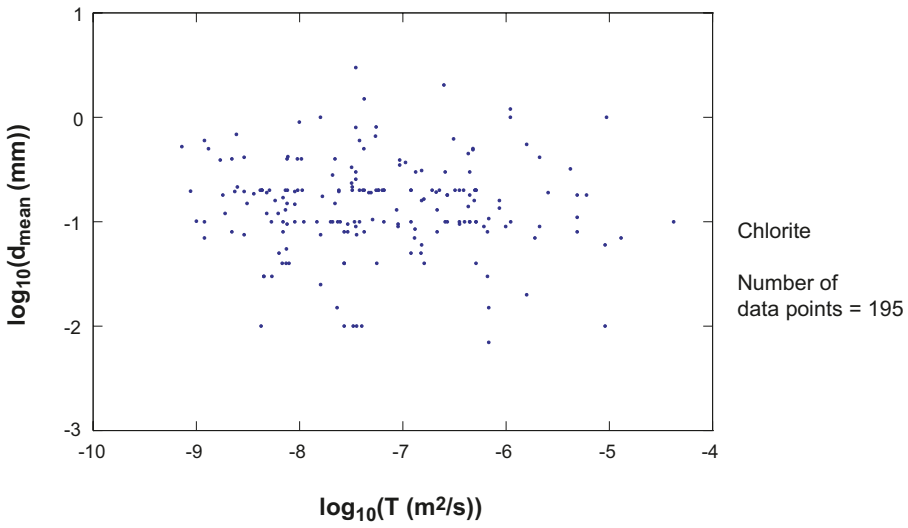

Figure 3-20. *Transmissivity vs. d_{mean} for chlorite.*

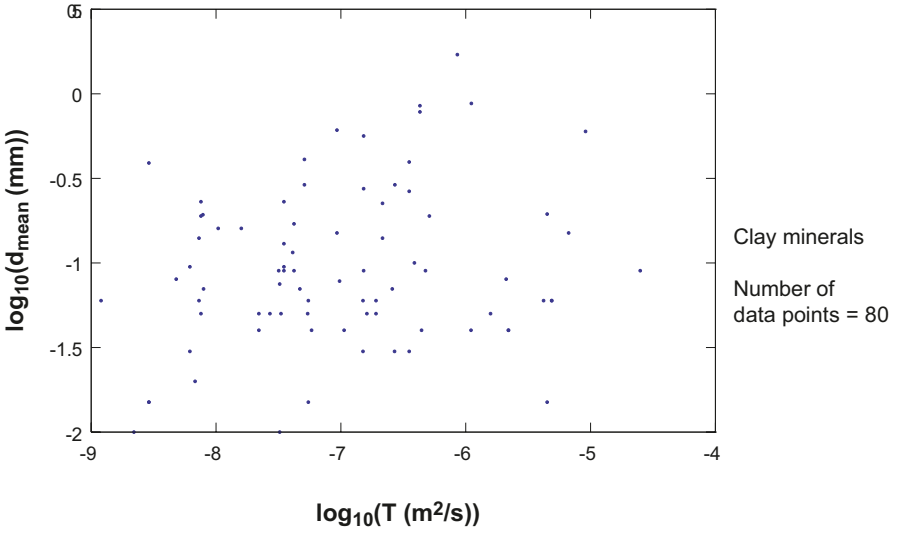

Figure 3-21. *Transmissivity vs. d_{mean} for clay minerals, as a group.*

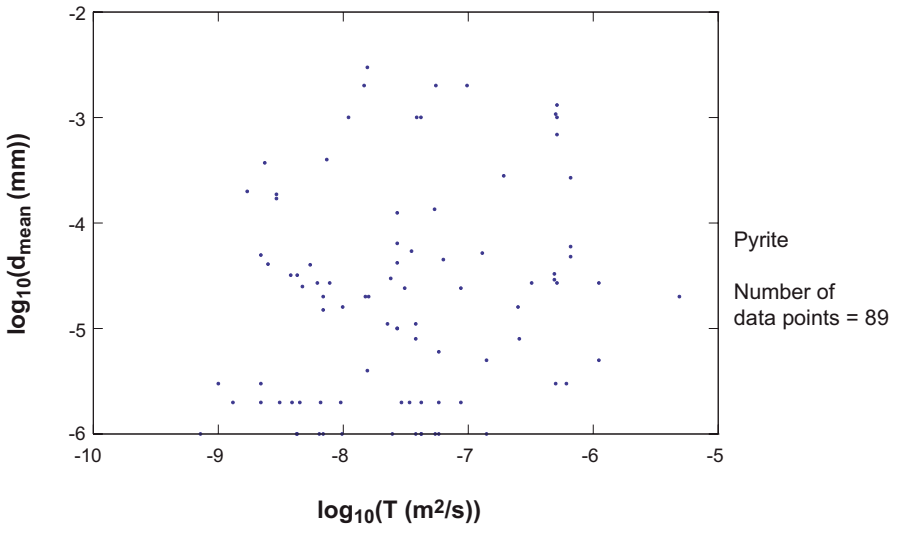

Figure 3-22. *Transmissivity vs. d_{mean} for pyrite.*

In the quantitative mineral mapping campaign a number of fractures (in total 93), which are located at least five metres distant from any detected PFL anomaly, were mapped. In Table 3-15, the number of data points, f_{qual}, f_{quant}, mean values, and standard deviations for the data subsets are shown.

Table 3-15. Data for fractures distant from any PFL-anomaly (in total 93 mapped fractures).

Mineral	Number of data points	f_{qual} (%)	f_{quant} (%)	d_{mean}		$\log_{10}(d_{mean})$	
				$\bar{X}$	STD	$\bar{X}$	STD
Calcite	41	71	44	0.19	0.28	–1.17	0.73
Chlorite	57	77	61	0.72	1.52	–0.57	0.58
Clay mineral	11	28	12	0.18	0.38	–1.30	0.73
Hematite	0	0	0	–	–	–	–
Pyrite	19	20	20	$4.1 \cdot 10^{-3}$	$9.6 \cdot 10^{-3}$	–4.00	1.57

For all fracture minerals, except for hematite, there are enough data for rough comparisons of d_{mean} data in Table 3-15 and data from fractures mainly associated with PFL-anomalies (cf. Table 3-2, Table 3-4, Table 3-8, and Table 3-12). If examining the mean values and standard deviations, there is no major difference. The comparisons do not contradict the earlier indications that the amount of fracture minerals is generally unrelated to the present groundwater flow in the fracture. For this reason, the decision taken early on to base the statistical analyses on data from all open fractures seems reasonable.

3.8 Influence of crush zone

Some drill core segments are so heavily fragmented that they cannot be pieced together into their original positions. Such segments are called crush zones and can be envisioned as gravel. Due to the difficulties in observing discrete fractures in crush zones, the methodology of mapping fracture minerals is somewhat different (see Section 2.1). Crush zones are scarce in the drill core mapped in this quantitative mineral mapping campaign, and only 21 crush zones have been studied (if excluding borehole KLX17A). In Table 3-16, the number of data points, f_{qual}, f_{quant}, mean values, and standard deviations for the crush zone data subsets are shown.

Table 3-16. Data for crush zones (in total 21 mapped crush zones).

Mineral	Number of data points	f_{qual} (%)	f_{quant} (%)	d_{mean}		$\log_{10}(d_{mean})$	
				$\bar{X}$	STD	$\bar{X}$	STD
Calcite	13	90	62	0.038	0.040	–1.67	0.56
Chlorite	15	95	71	0.49	1.53	–0.95	0.52
Clay mineral	16	86	76	0.22	0.49	–1.05	0.48
Hematite	0	0	0	–	–	–	–
Pyrite	1	4.8	4.8	$1.0 \cdot 10^{-6}$	–	–6.00	–

For calcite, chlorite and clay minerals there may be enough data for a rough comparison between crush zone data and discrete fracture data. If comparing the data in Table 3-16 with data in Table 3-2, Table 3-5, and Table 3-8 one can see no major differences. Due to the scarcity of crush zones and the differences in methodology when mapping crush zones and discrete fractures, it was decided not to include crush zone data in the general analyses in Sections 3.1 to 3.6.

4 Visible coverage C_{vis}

The visible coverage for the individual mineral layer is one of the parameters reported in the site investigation report /Eklund and Mattsson 2008/. In this section, the visible coverage is reported as averaged over both fracture surfaces of a fracture (see definition of C_{vis} in Section 2.2.1).

4.1 The data subsets

In Table 4-1 the number of data points in each data subset is given, together with f_{quant}^{c}. The latter is the fraction of the fractures covered by enough fracture minerals to be quantitatively estimated. An introduction to the rock volumes represented by the data subsets is found in Section 2.2.2.

Table 4-1. Number of data points in data subsets.

Rock volume		Calcite		Chlorite		Clay minerals		Hematite		Pyrite	
		No.	f_{quant}^{c} (%)	No.	f_{quant}^{c} (%)	No.	f_{quant}^{c} (%)	No.	f_{quant}^{c} (%)	No.	f_{quant}^{c} (%)
Elevation (mbsl)	GS–1,000[1]	1,459	79	1,322	71	626	34	2	0.11	355	19
	GS–100	434	82	384	73	151	29	0	0	92	17
	100–300	416	83	355	71	114	23	0	0	81	16
	300–500	450	74	457	75	249	41	1	0.17	135	22
	500–700	96	72	71	53	65	49	1	0.75	38	28
	700–1,000	63	76	55	66	47	57	0	0	9	11
Rock domain	RSMA01	402	67	435	73	262	44	2	0.34	99	17
	RSMD01	895	84	774	73	316	30	0	0	206	19
	RSMM01	162	86	113	60	48	26	0	0	50	27
Fracture domain	All FD	650	82	541	68	208	26	1	0.13	185	23
	FSM_C	248	84	196	66	70	24	0	0	95	32
	FSM_EW007	112	77	99	68	48	33	1	0.68	39	27
	FSM_NE005	124	86	89	62	43	30	0	0	23	16
	FSM_S	87	76	91	79	37	32	0	0	10	9.0
	FSM_W	79	81	66	68	10	10	0	0	18	19
Deformation zone	All DZ	546	73	538	72	296	40	1	0.13	116	16
	GDZ	65	68	54	56	68	71	1	1.0	4	4.0
	E-W/NW-SE	47	82	51	89	17	30	0	0	13	23
	N-S	104	75	112	81	43	31	0	0	43	31
	NE-SW	330	73	321	71	168	37	0	0	56	12

[1]Data set represents the entire site.

The fractions of fractures where quantitative visible coverages were obtained, f_{quant}^{c}, are displayed in Figure 4-1 for the different fracture minerals.

As can be seen, out of the fracture minerals investigated, the one that is most likely found at the site is calcite, followed by chlorite, clay minerals, pyrite, and hematite (that is practically not found at all). In some rock volumes it is more likely to find chlorite than calcite. In gently dipping deformation zones, the most common fracture mineral is clay minerals.

In the quantitative mineral mapping campaign, in the great majority of the cases when a fracture mineral was detected by inspecting the fracture surface from above, it was assigned a quantitative visible coverage. It appears that when very small specks of fracture minerals were found, the visible coverage of the layer was in many cases rounded up to 1% or down to non-existing. It should be noted that as the visible coverage of a fracture delivered from this report is averaged over both fracture surfaces, the minimum value possible is 0.5% (one surface with 0% coverage and the opposite surface with 1% coverage). The exception is for pyrite that exists as spot minerals, where the minimum value possible is 0.0005%[2].

[2] 0.0005% = 0.5 × 0.1 mm × 0.1 mm / 10 cm^2. See Section 2.1.2 for details.

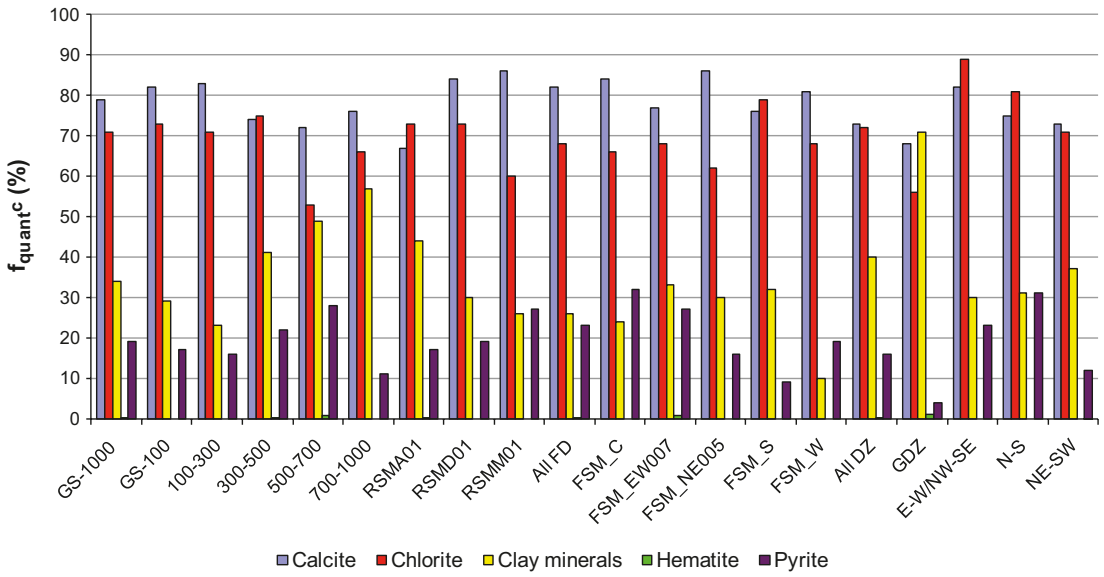

Figure 4-1. *f_{quant}^{c} of the different data subsets in Table 4-1.*

4.2 Calcite

4.2.1 Non-parametric analysis

For all data subsets (including quantitative data only) the arithmetic mean $\bar{X}$ and the standard deviation *STD* of C_{vis} and $\log_{10}(C_{vis})$ were calculated. These data are shown in Table 4-2.

Table 4-2. Non-parametric data for calcite.

Calcite		Number of data points	$\bar{X}$ of C_{vis} [%]	*STD* of C_{vis} [%]	$\bar{X}$ of $\log_{10}(C_{vis}$ [%])	*STD* of $\log_{10}(C_{vis}$ [%])
Elevation (mbsl)	GS–1,000[1]	1,459	22	24	0.96	0.67
	GS–100	434	23	24	1.01	0.65
	100–300	416	24	25	1.02	0.67
	300–500	450	21	25	0.91	0.70
	500–700	96	14	15	0.82	0.62
	700–1,000	63	16	22	0.79	0.66
Rock domain	RSMA01	402	17	21	0.85	0.66
	RSMD01	895	24	25	1.00	0.68
	RSMM01	162	22	22	1.01	0.62
Fracture domain	All FD	650	22	24	0.97	0.68
	FSM_C	248	22	25	0.91	0.71
	FSM_EW007	112	19	24	0.85	0.71
	FSM_NE005	124	21	21	1.02	0.60
	FSM_S	87	26	27	1.07	0.66
	FSM_W	79	27	24	1.14	0.61
Deformation zone	All DZ	546	21	23	0.95	0.67
	GDZ	65	16	19	0.85	0.61
	E-W/NW-SE	47	23	24	1.00	0.68
	N-S	104	18	23	0.83	0.70
	NE-SW	330	23	24	1.00	0.66

[1]Data set represents the entire site.

As seen in the table, C_{vis} of calcite is on average 22% in fractures where the mineral is found. For rock volumes where more than 100 data points were obtained, $\bar{X}$ of C_{vis} ranges from 18 to 24%.

By performing a Kruskal-Wallis test on the calcite C_{vis} data for the separate data subsets, it is strongly indicated that they are not all samples of the same population, with $p < 0.0001$.

Figure 4-2 shows the cumulative distribution functions of the data subsets. Combined data sets (All, All FD, and All DZ) are shown in blue lines while separate CDFs are shown in black lines.

As can be seen, the CDFs of the data subsets are similar. Based on Table 4-1**,** Table 4-2, and Figure 4-2 one can suggest that fracture surfaces in the different rock volumes at Laxemar are covered by similar fractions of calcite.

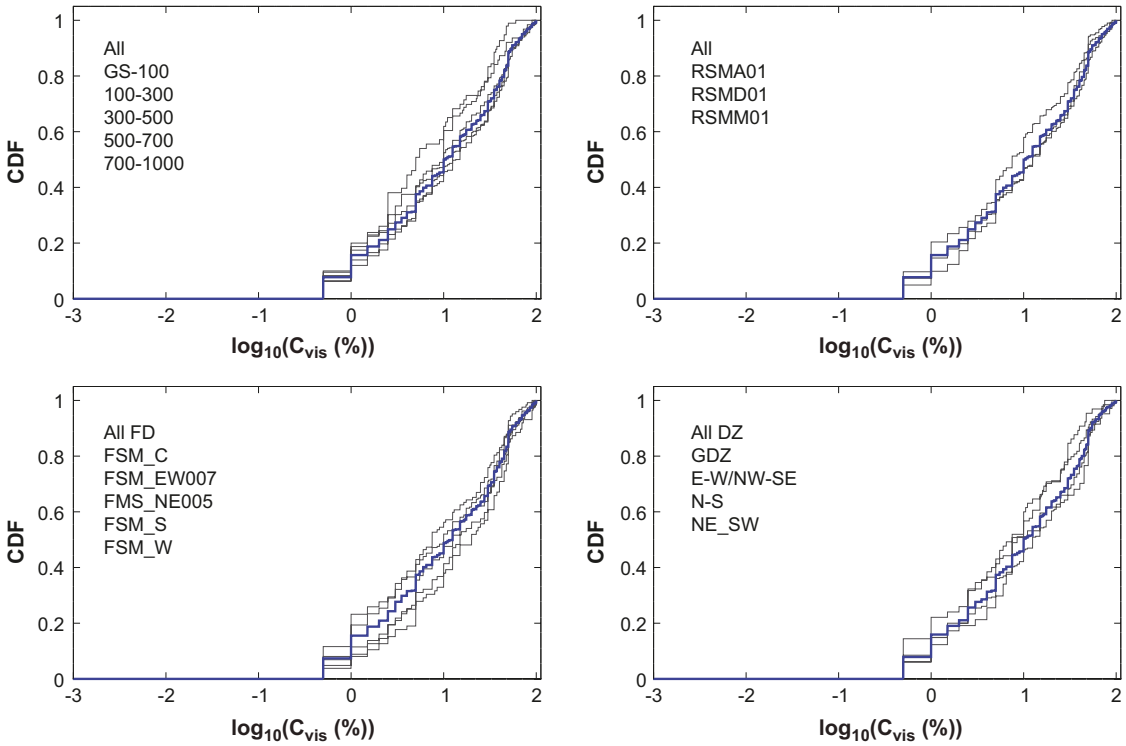

Figure 4-2. *Calcite: Cumulative distribution functions of the separate data subsets (black curves) and of the combined data sets (blue curves).*

4.2.2 Parametric analysis

As discussed in Section 2.4, the data are not expected to be normally distributed, as the visible coverage ranges from 0 to 100%. Instead the truncated normal distribution may be used. In case of using C_{vis} data, the distribution needs to be truncated at (below) 0% and at (above) 100%. In case of using $\log_{10}(C_{vis})$ data, the distribution needs to be truncated at 2 (100%). For calcite, the data are distributed in such a way that only few C_{vis} data are close to 100%. For example, only 1% of the data has a $C_{vis} > 95\%$. It is more common that the visible coverage for calcite is small, with 31% of the data having a $C_{vis} < 5\%$.

If performing the Shapiro-Wilk W test for $\log_{10}(C_{vis})$ data, the truncation at 2 will not affect the test too much. For calcite data from the entire site, the W-value returned is 0.94. For C_{vis} data it is advised against performing the Shapiro-Wilk W test, as the truncation in data at 0% would affect the test too much.

As the Shapiro-Wilk W test for $\log_{10}(C_{vis})$ data indicates fair normality, we have chosen to propagate the truncated normal distribution of $\log_{10}(C_{vis})$. Figure 4-3, shows the histogram of $\log_{10}(C_{vis})$ for calcite data from the entire site. Furthermore, the best fit truncated normal distribution (red curve in left figure) and the corresponding normal score plot (right figure) are shown. Similar figures are shown for all fracture mineral data subsets in Appendix B.

To compensate for the truncation in the normal score plot, the linear fit is only based on C_{vis} data $< 100\%$, while C_{vis} data $\geq 100\%$ are censored. As can be seen by the right hand figure, even if there is no theoretical truncation in the lower range, there is a practical truncation stemming from how the methodology was applied.

By making a linear fit in the normal score plot based only on data with $C_{vis} < 100\%$, the α and β parameters of Equation 2-2 (corresponding to μ and σ in a normal distribution) could be obtained from the intercept and slope. The data are shown in Table 4-3.

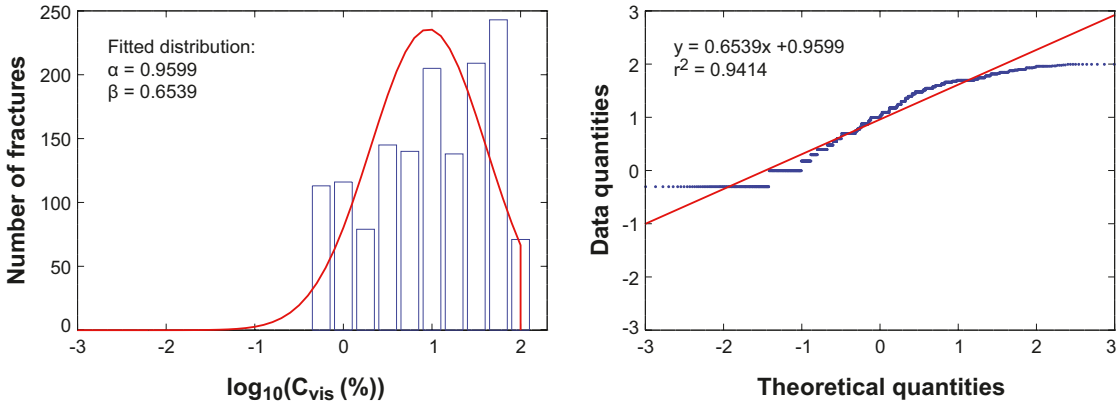

Figure 4-3. *Left: Histogram of $\log_{10}(C_{vis})$ data together with best fit truncated normal distribution. Right: Normal score plot of $\log_{10}(C_{vis})$ data. Data subset used: Calcite from the entire site.*

Table 4-3. Distribution parameters of populated fractures, calcite.

Calcite		Number of data points	$\log_{10}(C_{vis}[\%])$	
			α	β
Elevation (mbsl)	GS–1,000[1]	1,459	0.96	0.65
	GS–100	434	1.01	0.64
	100–300	416	1.02	0.65
	300–500	450	0.91	0.69
	500–700	96	0.82	0.63
	700–1,000	63	0.79	0.68
Rock domain	RSMA01	402	0.85	0.65
	RSMD01	895	1.00	0.66
	RSMM01	162	1.01	0.62
Fracture domain	All FD	650	0.97	0.66
	FSM_C	248	0.91	0.70
	FSM_EW007	112	0.85	0.72
	FSM_NE005	124	1.02	0.60
	FSM_S	87	1.07	0.67
	FSM_W	79	1.14	0.61
Deformation zone	All DZ	546	0.95	0.65
	GDZ	65	0.85	0.63
	E-W/NW-SE	47	1.00	0.69
	N-S	104	0.83	0.71
	NE-SW	330	1.00	0.65

[1]Data set represents the entire site.

Figure 4-4 illustrates the truncated distributions of Table 4-3, where the distribution representing the entire site is shown by the red line.

From Figure 4-4 one can see that the best fit distributions for data from the entire site and for the different data subsets very much resemble each other. It should be made clear that the choice of probability distribution is not obvious, and that other choices may be equally valid.

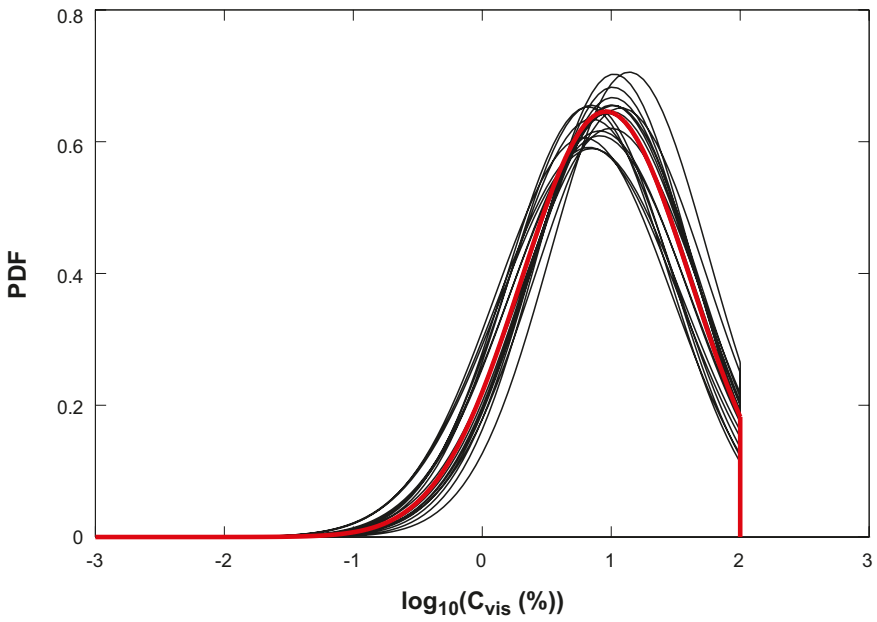

Figure 4-4. *Illustration of truncated normal distributions of Table 4-3.*

4.3 Chlorite

The analysis of C_{vis} for chlorite corresponds to that for calcite. In Section 4.2 more information on how the analysis is performed is given.

4.3.1 Non-parametric analysis

For all data subsets (including quantitative data only) the arithmetic mean $\bar{X}$ and the standard deviation *STD* of C_{vis} and $\log_{10}(C_{vis})$ were calculated. These data are shown in Table 4-4.

Table 4-4. Non-parametric data for chlorite.

Chlorite		Number of data points	$\bar{X}$ of C_{vis} [%]	*STD* of C_{vis} [%]	$\bar{X}$ of $\log_{10}(C_{vis}$ [%])	*STD* of $\log_{10}(C_{vis}$ [%])
Elevation (mbsl)	GS–1,000[1]	1,322	41	29	1.43	0.47
	GS–100	384	39	29	1.40	0.49
	100–300	355	44	29	1.49	0.42
	300–500	457	41	30	1.42	0.49
	500–700	71	34	26	1.33	0.50
	700–1,000	55	30	25	1.28	0.48
Rock domain	RSMA01	435	37	29	1.35	0.51
	RSMD01	774	43	29	1.48	0.44
	RSMM01	113	36	28	1.36	0.48
Fracture domain	All FD	541	40	29	1.42	0.48
	FSM_C	196	44	29	1.47	0.46
	FSM_EW007	99	30	25	1.27	0.50
	FSM_NE005	89	34	28	1.32	0.50
	FSM_S	91	49	30	1.57	0.39
	FSM_W	66	37	27	1.39	0.48
Deformation zone	All DZ	538	41	30	1.42	0.49
	GDZ	54	35	27	1.35	0.49
	E-W/NW-SE	51	38	32	1.31	0.61
	N-S	112	49	31	1.54	0.46
	NE-SW	321	39	29	1.41	0.48

[1]Data set represents the entire site.

As seen in the table, C_{vis} of chlorite is on average 41% in fractures where the mineral is found. For rock volumes where more than 100 data points were obtained, $\bar{X}$ of C_{vis} ranges from 36 to 49%.

By performing a Kruskal-Wallis test on the chlorite C_{vis} data for the separate data subsets, it is strongly indicated that they are not all samples of the same population, with $p < 0.0001$.

Figure 4-5 shows the cumulative distribution functions of the data subsets. Combined data sets (All, All FD, and All DZ) are shown in blue lines while separate CDFs are shown in black lines.

As can be seen, the CDFs of the data subsets are similar. Based on Table 4-1**,** Table 4-4, and Figure 4-5 one can suggest that the fracture surfaces of the different rock volumes in Laxemar are covered by similar fractions of chlorite.

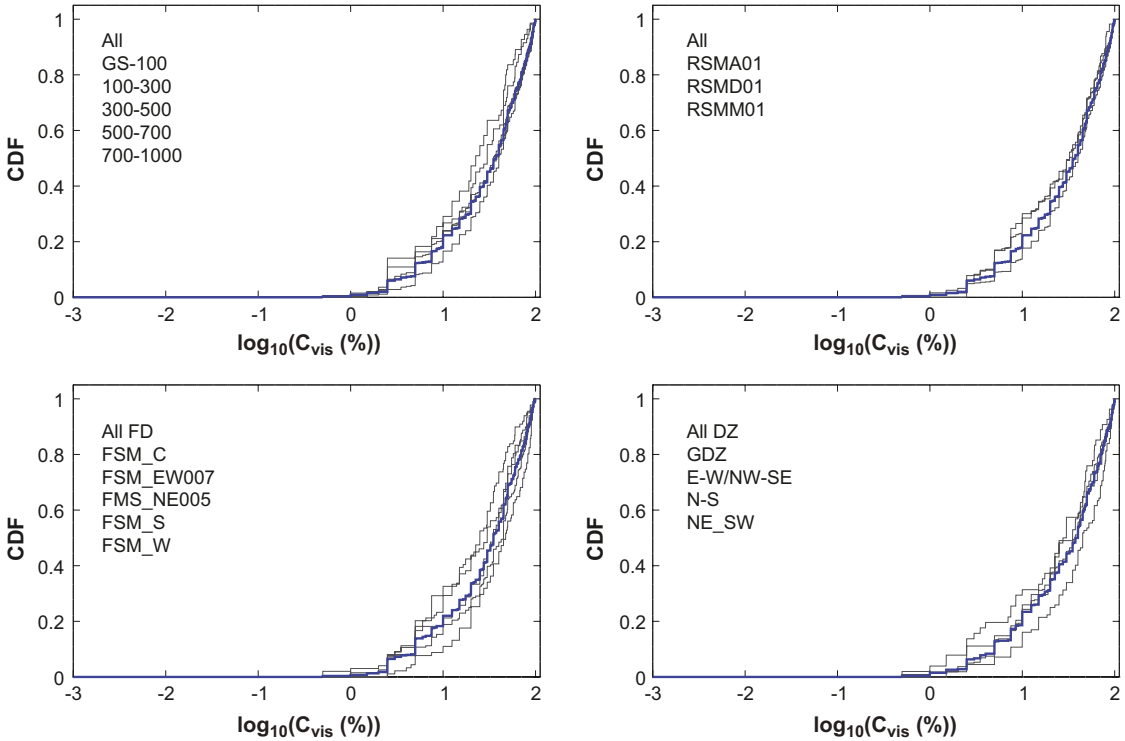

Figure 4-5. *Chlorite: Cumulative distribution functions of the separate data subsets (black curves) and of the combined data sets (blue curves).*

4.3.2 Parametric analysis

As for calcite, the truncation of C_{vis} data at 0% is more pronounced than at 100%. However, in this case there is also a significant truncation of data at 100%. Therefore, if intending to use the truncated normal distribution, the Shapiro-Wilk test may be a poor indication on whether to use C_{vis} or $\log_{10}(C_{vis})$ data. If still using the test the W-value returned for C_{vis} data is 0.93, while for $\log_{10}(C_{vis})$ data the W-value is 0.90. In the tests, data from the entire site were used. This gives no clear indication on whether to choose a singly truncated normal distribution for $\log_{10}(C_{vis})$ or a doubly truncated normal distribution for C_{vis}. As the $\log_{10}(C_{vis})$ representation was propagated for calcite, we chose to do the same for chlorite.

Figure 4-6 shows a histogram of $\log_{10}(C_{vis})$ for chlorite data from the entire site. Furthermore, the best fit truncated normal distribution (red curve in left figure) and the corresponding normal score plot (right figure) are shown.

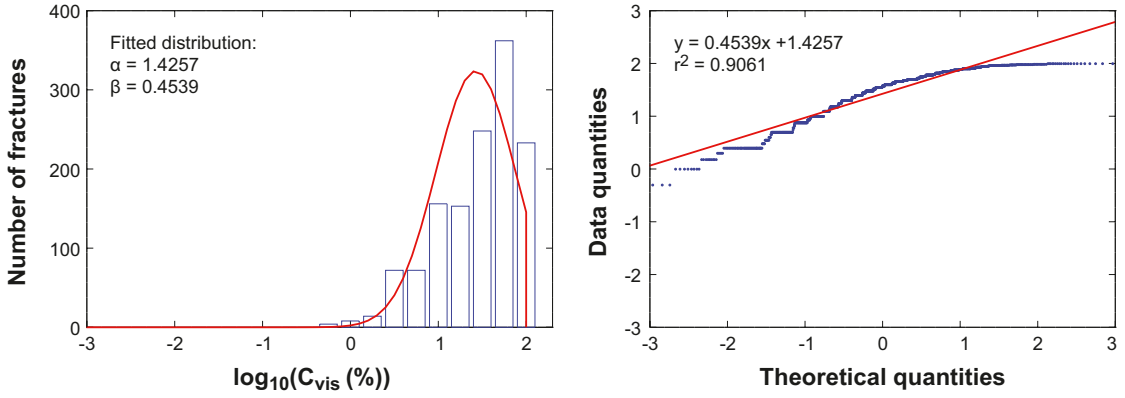

Figure 4-6. *Left: Histogram of $\log_{10}(C_{vis})$ data together with best fit truncated normal distribution. Right: Normal score plot of $\log_{10}(C_{vis})$ data. Data subset used: Chlorite from the entire site.*

By making a linear fit in the normal score plot based on all $C_{vis} < 100\%$, the α and β parameters of Equation 2-2 could be obtained from the intercept and slope. The data are shown in Table 4-5.

Table 4-5. Distribution parameters of populated fractures, chlorite.

Chlorite		Number of data points	$\log_{10}(C_{vis}[\%])$	
			α	β
Elevation (mbsl)	GS–1,000[1]	1,322	1.43	0.45
	GS–100	384	1.40	0.47
	100–300	355	1.49	0.40
	300–500	457	1.42	0.47
	500–700	71	1.33	0.50
	700–1,000	55	1.28	0.49
Rock domain	RSMA01	435	1.35	0.50
	RSMD01	774	1.48	0.42
	RSMM01	113	1.36	0.48
Fracture domain	All FD	541	1.42	0.46
	FSM_C	196	1.47	0.44
	FSM_EW007	99	1.27	0.50
	FSM_NE005	89	1.32	0.50
	FSM_S	91	1.57	0.38
	FSM_W	66	1.39	0.48
Deformation zone	All DZ	538	1.42	0.47
	GDZ	54	1.35	0.50
	E-W/NW-SE	51	1.31	0.62
	N-S	112	1.54	0.44
	NE-SW	321	1.41	0.46

[1]Data set represents the entire site.

Figure 4-7 illustrates the truncated distributions of Table 4-5, where the distribution representing the entire site is shown by the red line.

From Figure 4-7 one can see that the best fit distribution for data from the entire site well resembles the distributions for the different data subsets.

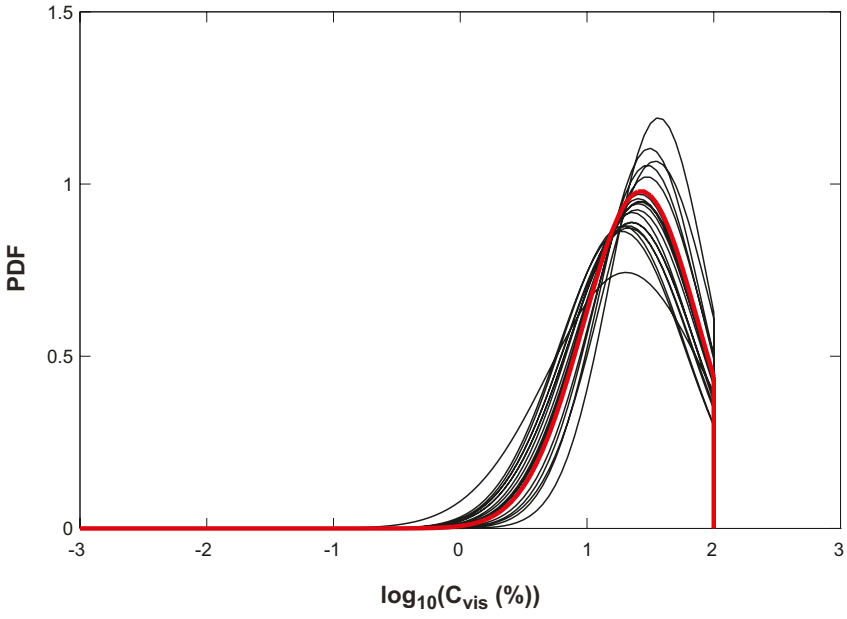

Figure 4-7. *Illustration of truncated normal distributions of Table 4-5.*

4.4 Clay minerals

The analysis of C_{vis} for clay minerals corresponds to that for calcite. In Section 4.2 more information on how the analysis is performed is given.

4.4.1 Non-parametric analysis

For all data subsets (including quantitative data only) the arithmetic mean $\bar{X}$ and the standard deviation *STD* of C_{vis} and $\log_{10}(C_{vis})$ were calculated. These data are shown in Table 4-6.

Table 4-6. Non-parametric data for clay minerals, as a group.

Clay minerals, as a group		Number of data points	$\bar{X}$ of C_{vis} [%]	*STD* of C_{vis} [%]	$\bar{X}$ of $\log_{10}(C_{vis}$ [%])	*STD* of $\log_{10}(C_{vis}$ [%])
Elevation (mbsl)	GS–1,000[1]	626	35	26	1.39	0.41
	GS–100	151	32	26	1.33	0.41
	100–300	114	35	25	1.39	0.43
	300–500	249	36	26	1.40	0.42
	500–700	65	35	24	1.41	0.39
	700–1,000	47	45	30	1.52	0.39
Rock domain	RSMA01	262	34	26	1.36	0.43
	RSMD01	316	38	26	1.44	0.39
	RSMM01	48	28	24	1.25	0.44
Fracture domain	All FD	208	33	25	1.36	0.43
	FSM_C	70	33	26	1.32	0.46
	FSM_EW007	48	37	26	1.43	0.40
	FSM_NE005	43	26	23	1.23	0.43
	FSM_S	37	38	25	1.46	0.36
	FSM_W	10	37	21	1.47	0.36
Deformation zone	All DZ	296	35	26	1.38	0.42
	GDZ	68	39	28	1.45	0.40
	E-W/NW-SE	17	17	14	1.07	0.39
	N-S	43	30	24	1.33	0.37
	NE-SW	168	36	26	1.39	0.43

[1]Data set represents the entire site.

As seen in the table, C_{vis} of clay minerals is on average 35% in fractures where the mineral is found. For rock volumes where more than 100 data points were obtained, $\bar{X}$ of C_{vis} ranges from 32 to 38%.

By performing a Kruskal-Wallis test on the clay minerals C_{vis} data for the separate data subsets, it is clearly indicated that they are not all samples of the same population, with $p = 0.0007$.

Figure 4-8 shows the cumulative distribution functions of the data subsets. Combined data sets (All, All FD, and All DZ) are shown in blue lines while separate CDFs are shown in black lines. CDFs representing data subsets of more than 20 data points are shown by solid lines while those representing fewer data are shown by dotted lines.

As can be seen, the CDFs of the data subsets are similar. Based on Table 4-1**,** Table 4-6, and Figure 4-8 one can suggest that the fracture surfaces in the different rock volumes in Laxemar are covered by fairly similar fractions of clay minerals. The somewhat deviating rock volumes are found below repository depth and in gently dipping deformation zones, where clay minerals are more abundant.

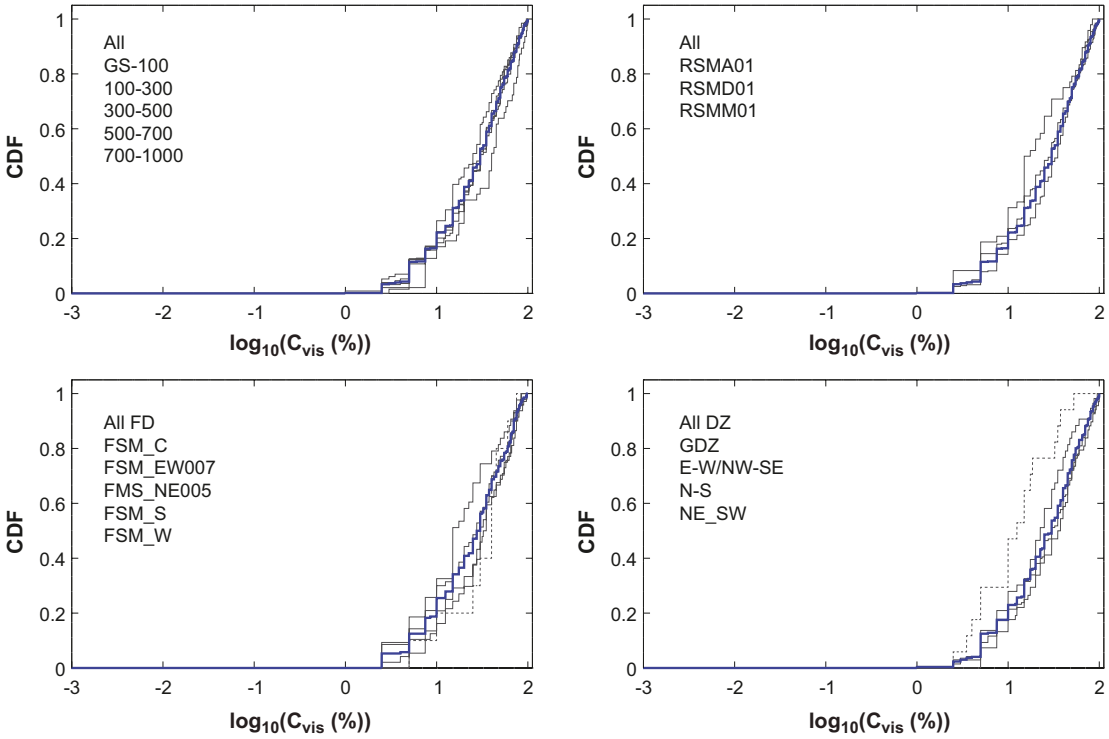

Figure 4-8. *Clay minerals: Cumulative distribution functions of the separate data subsets (black curves) and of the combined data sets (blue curves). CDFs for data subsets with up to 20 data points are dotted.*

4.4.2 Parametric analysis

The truncation situation for clay minerals is very much the same as for chlorite. If intending to use the truncated normal distribution, the Shapiro-Wilk test may be a poor indication on whether to use C_{vis} or $\log_{10}(C_{vis})$ data. If anyhow using the test, the W-value returned for C_{vis} is 0.92 while for $\log_{10}(C_{vis})$ the W-value returned is 0.94. In the tests, data from the entire site were used. This gives no indication on whether to choose a singly truncated normal distribution for $\log_{10}(C_{vis})$ or a doubly truncated normal distribution for C_{vis}. As the $\log_{10}(C_{vis})$ representation was propagated for calcite, we chose to do the same for clay minerals.

Figure 4-9 shows a histogram of $\log_{10}(C_{vis})$ for clay minerals data from the entire site. Furthermore, the best fit truncated normal distribution (red curve in left figure) and the corresponding normal score plot (right figure) are shown.

By making a linear fit in the normal score plot based on all $C_{vis} < 100\%$, the α and β parameters of Equation 2-2 could be obtained from the intercept and slope. The data are shown in Table 4-7.

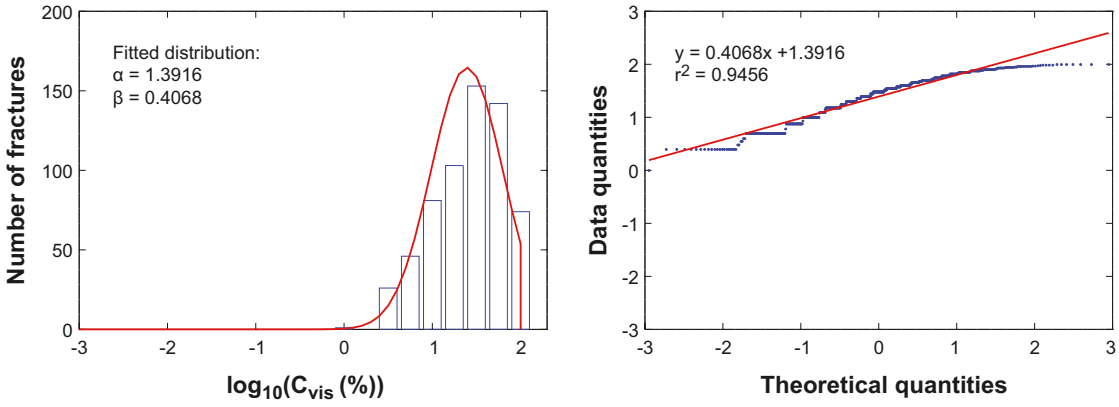

Figure 4-9. *Left: Histogram of $\log_{10}(C_{vis})$ data together with best fit truncated normal distribution. Right: Normal score plot of $\log_{10}(C_{vis})$ data. Data subset used: Clay minerals from the entire site.*

Table 4-7. Distribution parameters of populated fractures, clay minerals as a group.

Clay minerals, as a group		Number of data points	$\log_{10}(C_{vis}[\%])$	
			α	β
Elevation (mbsl)	GS–1,000[1]	626	1.39	0.41
	GS–100	151	1.33	0.42
	100–300	114	1.39	0.43
	300–500	249	1.40	0.41
	500–700	65	1.41	0.39
	700–1,000	47	1.52	0.40
Rock domain	RSMA01	262	1.36	0.42
	RSMD01	316	1.44	0.39
	RSMM01	48	1.25	0.46
Fracture domain	All FD	208	1.36	0.42
	FSM_C	70	1.32	0.47
	FSM_EW007	48	1.43	0.41
	FSM_NE005	43	1.23	0.46
	FSM_S	37	1.46	0.38
	FSM_W	10	1.47	0.40
Deformation zone	All DZ	296	1.38	0.41
	GDZ	68	1.45	0.41
	E-W/NW-SE	17	1.07	0.44
	N-S	43	1.33	0.39
	NE-SW	168	1.39	0.42

[1]Data set represents the entire site.

Figure 4-10 illustrates the truncated distributions of Table 4-7, where the distribution representing the entire site is shown by the red line. Distributions of data subsets with more than 20 data points are shown by the solid lines, while distributions of data subsets with up to 20 data points are shown in by the shaded lines.

From Figure 4-10 one can see that the best fit distribution for data from the entire site resembles all of the distributions for the different data subsets. The most deviating distribution is for E-W/NW-SE deformation zones, representing only 17 data points.

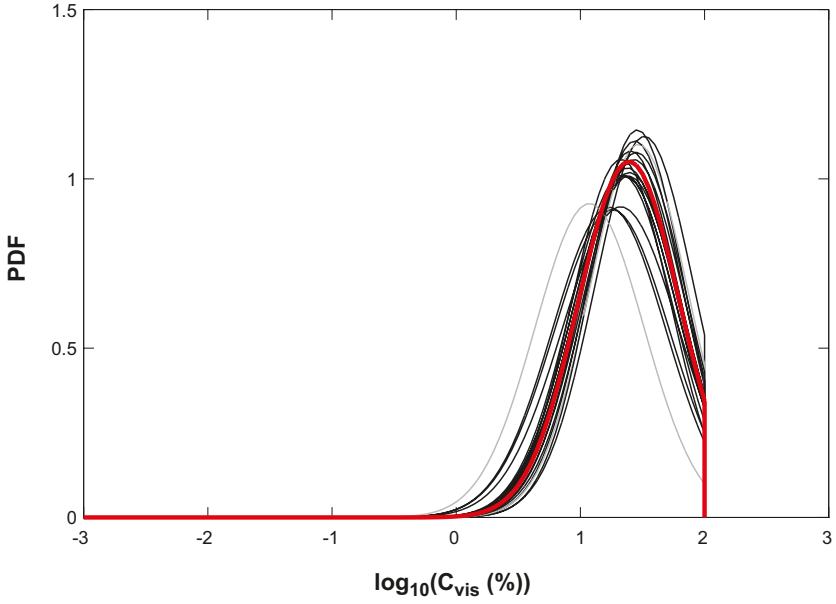

Figure 4-10. *Illustration of truncated normal distributions of Table 4-7. Distributions of data subsets with only up to 20 data points are shaded.*

4.5 Hematite

In the entire campaign hematite was found in two fractures, out of the 1,852 fractures mapped. This makes f_{quant}^{c} equal 0.1%. In these two fractures, C_{vis} of hematite was 25% and 55%. The arithmetic mean $\bar{X}$ of C_{vis} is thus 40%. No further analysis of hematite is performed.

4.6 Pyrite

The analysis of C_{vis} for pyrite corresponds to that for calcite. In Section 4.2 more information on how the analysis is performed is given.

4.6.1 Non-parametric analysis

For all data subsets (including quantitative data only) the arithmetic mean $\bar{X}$ and the standard deviation *STD* of C_{vis} and $\log_{10}(C_{vis})$ were calculated. These data are shown in Table 4-8.

Table 4-8. Non-parametric data for pyrite.

Pyrite		Number of data points	$\bar{X}$ of C_{vis} [%]	*STD* of C_{vis} [%]	$\bar{X}$ of $\log_{10}(C_{vis}$ [%])	*STD* of $\log_{10}(C_{vis}$ [%])
Elevation (mbsl)	GS–1,000[1]	355	0.23	0.71	–1.90	1.11
	GS–100	92	0.17	0.51	–1.92	1.01
	100–300	81	0.23	0.54	–1.81	1.08
	300–500	135	0.28	0.96	–1.97	1.20
	500–700	38	0.16	0.37	–1.97	1.12
	700–1,000	9	0.36	0.59	–1.28	1.01
Rock domain	RSMA01	99	0.22	0.53	–1.89	1.21
	RSMD01	206	0.18	0.44	–1.94	1.06
	RSMM01	50	0.44	1.50	–1.76	1.14
Fracture domain	All FD	185	0.27	0.89	–1.83	1.14
	FSM_C	95	0.35	1.14	–1.68	1.13
	FSM_EW007	39	0.34	0.71	–1.66	1.33
	FSM_NE005	23	0.05	0.21	–2.47	0.75
	FSM_S	10	0.17	0.23	–1.58	1.11
	FSM_W	18	0.060	0.16	–2.25	0.84
Deformation zone	All DZ	116	0.18	0.44	–1.92	1.03
	GDZ	4	0.018	0.020	–1.92	0.45
	E-W/NW-SE	13	0.10	0.14	–1.45	0.78
	N-S	43	0.14	0.36	–2.27	1.03
	NE-SW	56	0.24	0.54	–1.76	1.05

[1]Data set represents the entire site.

As seen in the table, C_{vis} of pyrite is on average only 0.13% in fractures where the mineral is found.

By performing a Kruskal-Wallis test on the pyrite C_{vis} data for the separate data subsets, it is indicated that they are not all samples of the same population, with $p = 0.020$.

Figure 4-11 shows the cumulative distribution functions of the data subsets. Combined data sets (All, All FD, and All DZ) are shown in blue lines while separate CDFs are shown in black lines. CDFs representing data subsets of more than 20 data points are shown by solid lines while those representing fewer data are shown by dotted lines.

The CDF of the data subsets that deviate the most is for fracture domain FSM_NE005, with 23 data points. Otherwise, the CDFs of the data subsets are fairly similar. Based on Table 4-1, Table 4-8, and Figure 4-11 one can suggest that the fracture surfaces of the different rock volumes in Laxemar are covered by fairly similar fractions of pyrite.

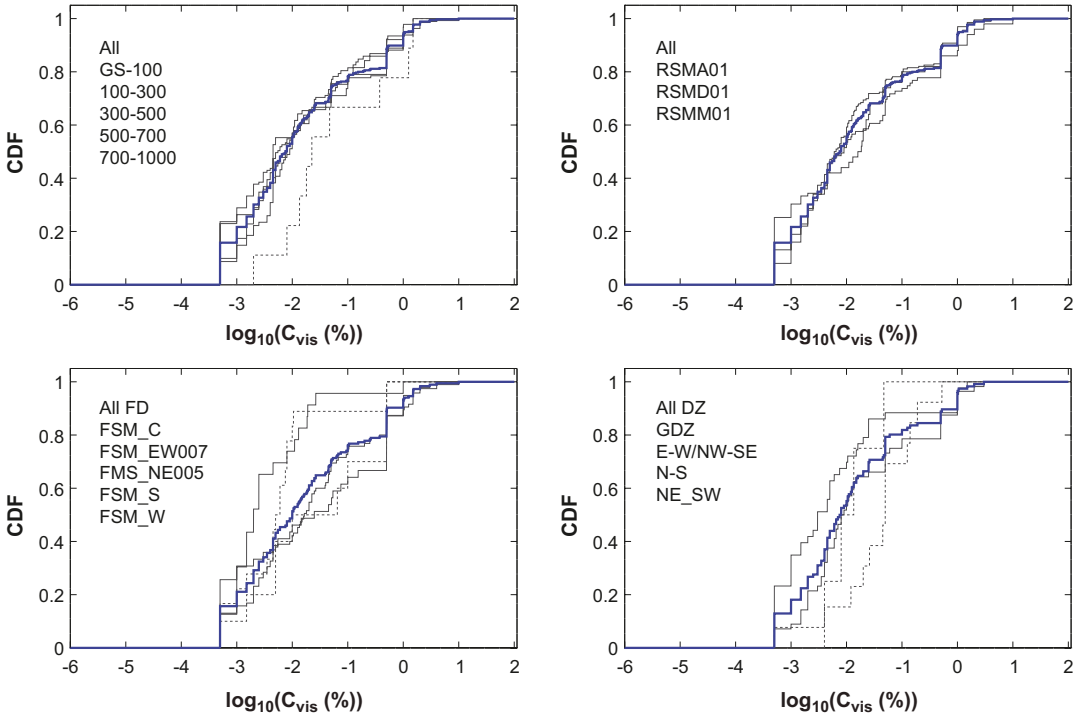

Figure 4-11. *Pyrite: Cumulative distribution functions of the separate data subsets (black curves) and of the combined data sets (blue curves). CDFs for data subsets with up to 20 data points are dotted.*

4.6.2 Parametric analysis

For pyrite, no C_{vis} is close to 100% and most C_{vis} data are below 1%. For pyrite, the Shapiro-Wilk test is a good test for normality for $\log_{10}(C_{vis})$ data. For C_{vis} data, however, the truncation issue at 0% affects the test too much. The returned W-value for $\log_{10}(C_{vis})$ data is 0.92, wherefore we have chosen to propagate this representation of the data.

Figure 4-12 shows a histogram of $\log_{10}(C_{vis})$ for pyrite data from the entire site. Furthermore, the best fit (truncated) normal distribution (red curve in left figure) and the corresponding normal score plot (right figure) are shown.

The resolution/rounding issue that applies for d_{mean} for pyrite (see Section 2.4.4) applies in a similar fashion for C_{vis}. Here, the minimum value of C_{vis} for layer minerals is 0.5% ($\log_{10}(C_{vis}) = -0.3$), a bar that is much overrepresented in Figure 4-12. The minimum value of $\log_{10}(C_{vis})$ for spot minerals is –3.3.

By making a linear fit in the normal score plot based on all $C_{vis} < 100\%$, which in this case is all data, the α and β parameters of Equation 2-2 could be obtained from the intercept and slope. The data are shown in Table 4-9.

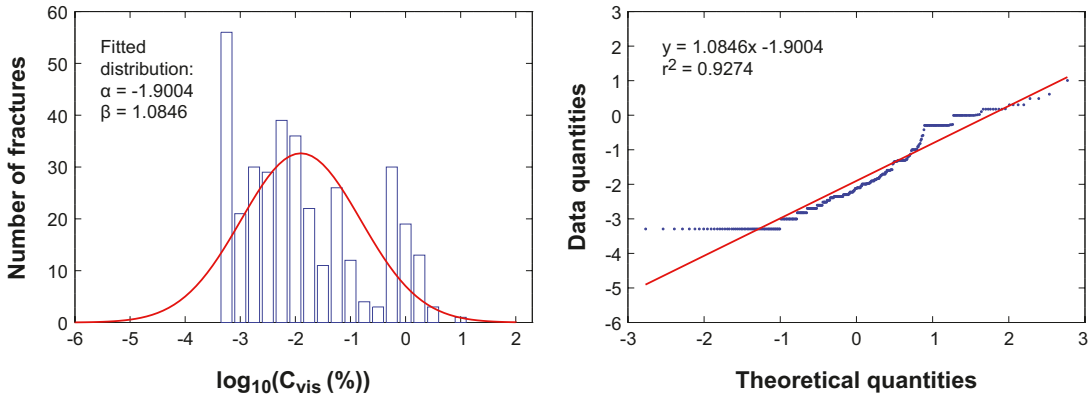

Figure 4-12. *Left: Histogram of $\log_{10}(C_{vis})$ data together with best fit truncated normal distribution. Right: Normal score plot of $\log_{10}(C_{vis})$ data. Data subset used: pyrite from the entire site.*

Table 4-9. Distribution parameters of populated fractures, pyrite.

Pyrite		Number of data points	$\log_{10}(C_{vis}[\%])$	
			α	β
Elevation (mbsl)	GS–1,000[1]	355	–1.90	1.08
	GS–100	92	–1.92	1.02
	100–300	81	–1.81	1.08
	300–500	135	–1.97	1.17
	500–700	38	–1.97	1.17
	700–1,000	9	–1.28	1.19
Rock domain	RSMA01	99	–1.89	1.20
	RSMD01	206	–1.94	1.03
	RSMM01	50	–1.76	1.18
Fracture domain	All FD	185	–1.83	1.13
	FSM_C	95	–1.68	1.15
	FSM_EW007	39	–1.66	1.36
	FSM_NE005	23	–2.47	0.76
	FSM_S	10	–1.58	1.30
	FSM_W	18	–2.25	0.87
Deformation zone	All DZ	116	–1.92	1.03
	GDZ	4	–1.92	0.62
	E-W/NW-SE	13	–1.45	0.87
	N-S	43	–2.27	1.02
	NE-SW	56	–1.76	1.07

[1]Data set represents the entire site.

Figure 4-13 illustrates the truncated distributions of Table 4-9, where the distribution representing the entire site is shown by the red line. Distributions of data subsets with more than 20 data points are shown by the solid lines, while distributions of data subsets with up to 20 data points are shown by the shaded lines.

From Figure 4-13 one can see that the best fit distribution for data from the entire site resembles nearly all the distributions for the different data subsets. The most deviating distribution is that representing fracture domain FSM_NE005.

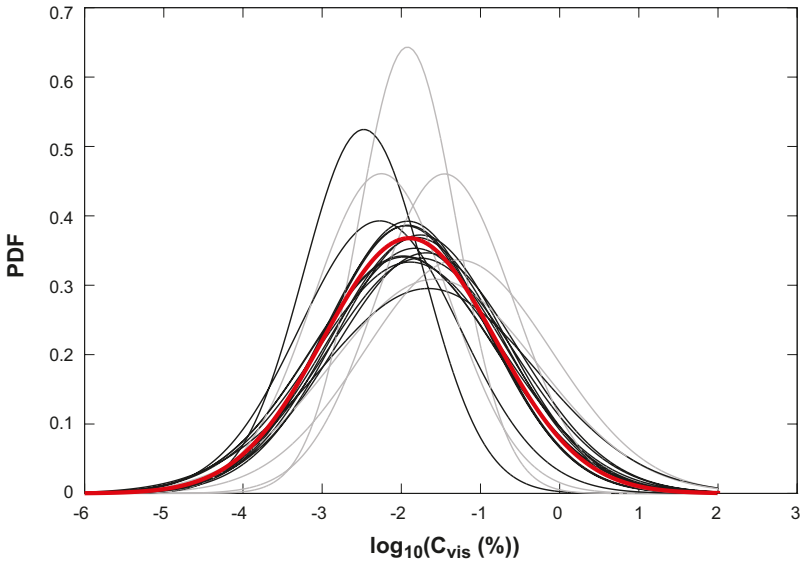

Figure 4-13. *Illustration of truncated normal distributions of Table 4-9. Distributions of data subsets with only up to 20 data points are shaded. Distributions for RFM044 and NNW are not shown.*

5 Distribution parameters suggested for use subsequent modelling

5.1 Tabulated distribution parameters

In Chapters 3 and 4 it has been shown that the different rock volumes of the Laxemar site generally hold fracture minerals of similar amounts and visible coverages. This is best seen from the cumulative distribution functions of $\log_{10}(d_{mean})$ and $\log_{10}(C_{vis})$ for the different data subsets. It is also shown that the normal distribution fairly well describes $\log_{10}(d_{mean})$ data while the truncated normal distribution fairly well describes $\log_{10}(C_{vis})$ data.

In this chapter we suggest a set of data for each fracture minerals in form of probability distribution function parameters for $\log_{10}(d_{mean})$ and $\log_{10}(C_{vis})$. The parameters of the distributions are given in Table 5-1 and Table 5-2. These data may be used as input in subsequent hydrogeochemical and radionuclide transport modelling. The background to the suggested data is summarised in Section 5.2.

Table 5-1. Normal distributions of $\log_{10}(d_{mean})$, suggested for use in SR-Site.

Fracture mineral	μ of $\log_{10}(d_{mean})$	σ of $\log_{10}(d_{mean})$	f_{quant} (%)
Calcite	–1.21	0.76	51
Chlorite	–0.83	0.48	46
Clay minerals, as a group	–1.12	0.51	16
Hematite	–	–	0.054
Pyrite	–4.43	1.17	19
Equation of PDF associated with the parameters	$\varphi(\log_{10}(d_{mean})) = \frac{1}{\sigma\sqrt{2\pi}}\exp\left(-\frac{(\log_{10}(d_{mean})-\mu)^2}{2\sigma^2}\right)$		

Table 5-2. Truncated normal distributions of $\log_{10}(C_{vis})$, suggested for use in SR-Site.

Fracture mineral	α of $\log_{10}(C_{vis})$	β of $\log_{10}(C_{vis})$	f_{quant}^c (%)
Calcite	0.96	0.65	79
Chlorite	1.43	0.45	71
Clay minerals, as a group	1.39	0.41	34
Hematite	–	–	0.11
Pyrite	–1.90	1.08	19
Equation of PDF associated with the parameters	For $C_{vis} \le 100\%$: $\varphi(\log_{10}(C_{vis})) = \frac{\frac{1}{\beta\sqrt{2\pi}}\exp\left(-\frac{(\log_{10}(C_{vis})-\alpha)^2}{2\beta^2}\right)}{\int_{-\infty}^{2}\frac{1}{\beta\sqrt{2\pi}}\exp\left(-\frac{(\log_{10}(C_{vis})-\alpha)^2}{2\beta^2}\right)}$ For $C_{vis} > 100\%$: $\varphi(\log_{10}(C_{vis})) = 0$		

5.2 Summarised background to suggested data

This section summarises the reasons for suggesting the probability distribution and distribution parameters in Table 5-1 and Table 5-2. In Chapters 3 and 4, the cumulative distribution functions and best fit probability distributions for the data subsets are given for the studied fracture minerals. In Figure 5-1 to Figure 5-8, all the CDFs for each mineral are shown, and also the CDF for the suggested best fit distribution of Table 5-1 or Table 5-2.

5.2.1 Calcite

In Figure 5-1 the CDFs for $\log_{10}(d_{mean})$ data for calcite are displayed. The CDF for data from the entire site is shown by a blue curve. The CDF for the best fit distribution for calcite, given in Table 5-1, is shown by the red curve.

The corresponding plot for the calcite $\log_{10}(C_{vis})$ is shown in Figure 5-2. The red curve shows the CDF of the best fit truncated normal distribution given in Table 5-2.

As can be seen in Figure 5-1 and Figure 5-2, the best fit distribution well describe the CDFs of the $\log_{10}(d_{mean})$ data subsets. For $\log_{10}(C_{vis})$ there is a deviation at the truncation, where the fitted distribution overestimates the fraction of fracture surfaces totally cover by calcite. Overall one could argue that the fit fairly well describe the CDFs. Based on the appearance of the figures, we suggest that the distributions for calcite in Table 5-1 and Table 5-2 reasonably well represent all rock volumes at the site. If a reduced data set is required as input data in subsequent modelling, these distributions may be used.

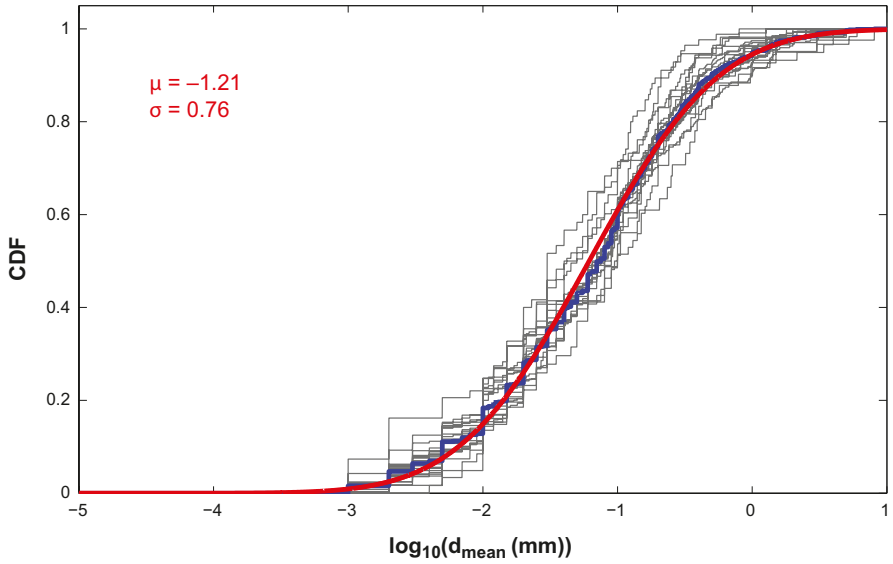

Figure 5-1. *Calcite – d_{mean}: Cumulative distribution functions of the separate data subsets (black curves) and of the data from the entire site (blue curve). The red curve represents the CDF of the best fitted normal distribution for data from the entire site.*

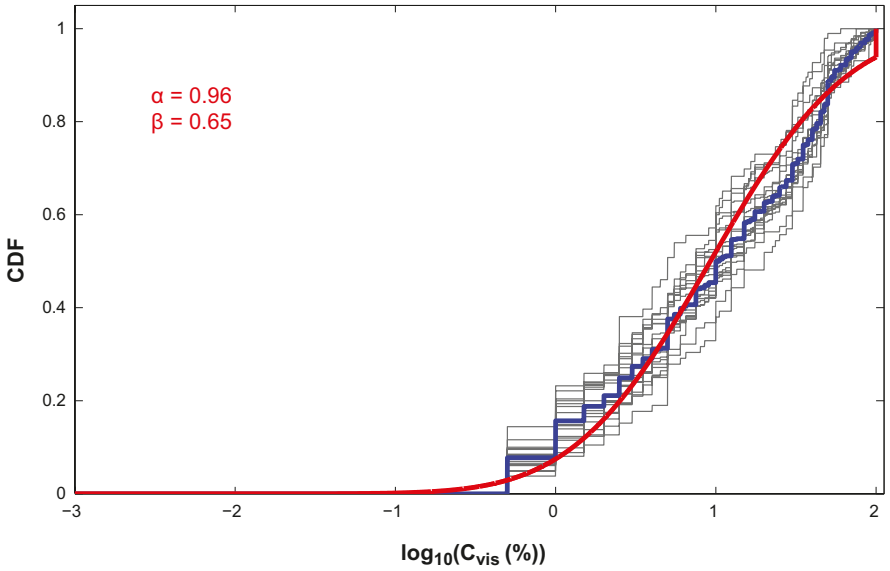

Figure 5-2. *Calcite – C_{vis}: Cumulative distribution functions of the separate data subsets (black curves) and of the data from the entire site (blue curve). The red curve represents the CDF of the best fitted truncated normal distribution for data from the entire site.*

5.2.2 Chlorite

The corresponding figures to Figure 5-1 and Figure 5-2 are displayed below for chlorite.

Based on the appearance of the figures, the same conclusions are drawn for chlorite as for calcite. We suggest that the distributions for chlorite in Table 5-1 and Table 5-2 reasonably well represent all rock volumes at the site.

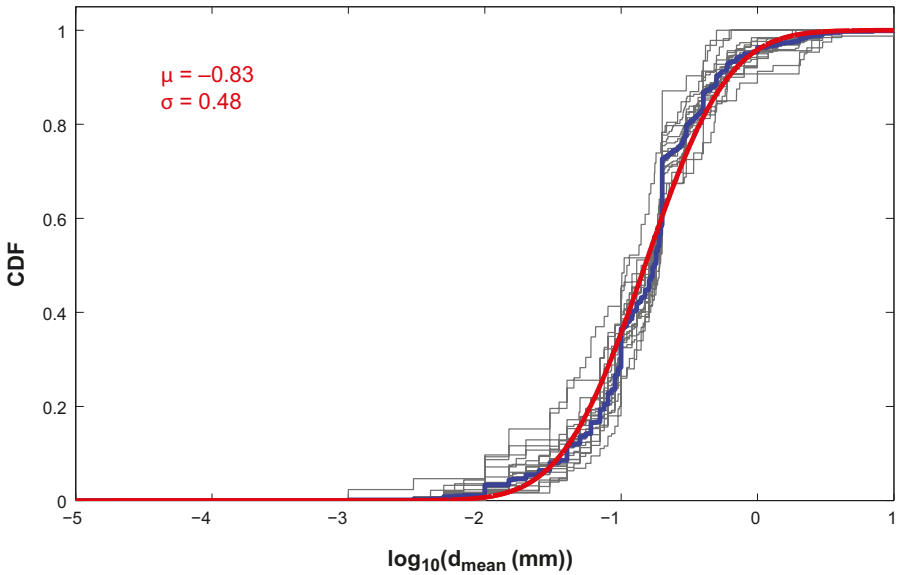

Figure 5-3. *Chlorite – d_{mean}: Cumulative distribution functions of the separate data subsets (black curves) and of the data from the entire site (blue curve). The red curve represents the CDF of the best fitted normal distribution for data from the entire site.*

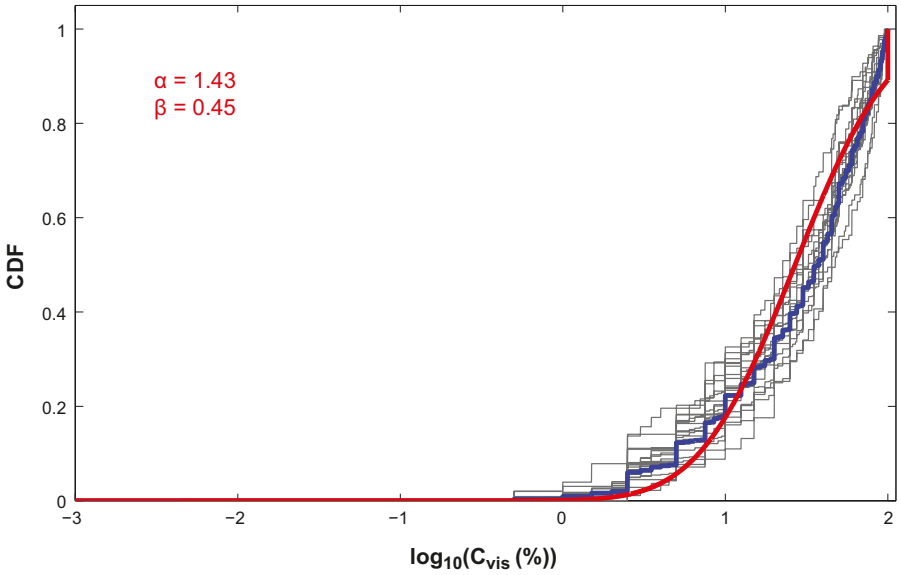

Figure 5-4. *Chlorite – C_{vis}: Cumulative distribution functions of the separate data subsets (black curves) and of the data from the entire site (blue curve). The red curve represents the CDF of the best fitted truncated normal distribution for data from the entire site.*

5.2.3 Clay minerals, as a group

The corresponding figures to Figure 5-1 and Figure 5-2 are displayed below for clay minerals, as a group. As in Chapter 3 and 4, CDFs representing data subsets of more than 20 data points are shown by solid lines. CDFs representing data subsets of up to 20 data points are shown by dotted lines.

Based on the appearance of the figures, the same conclusions are drawn for clay minerals as for calcite. We suggest that the distributions for clay minerals in Table 5-1 and Table 5-2 reasonably well represent all rock volumes at the site.

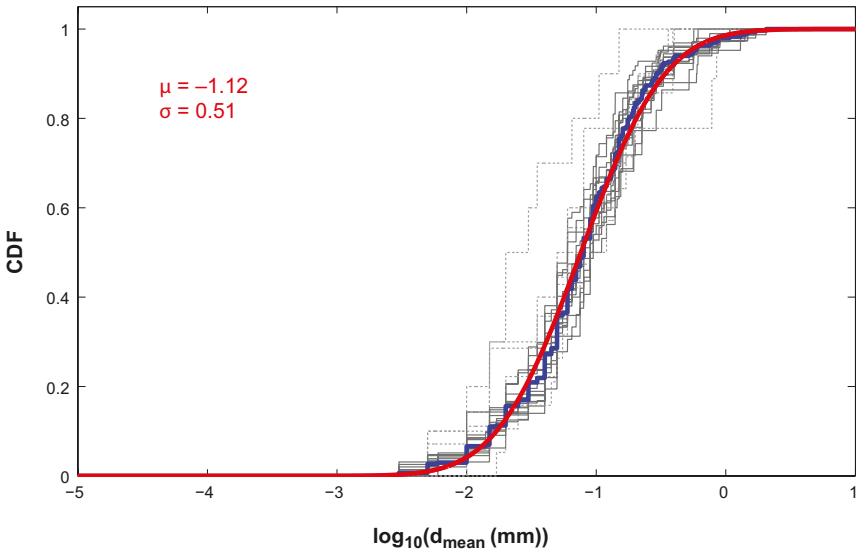

Figure 5-5. *Clay minerals – d_{mean}: Cumulative distribution functions of the separate data subsets (black curves) and of the data from the entire site (blue curve). CDFs for data subsets with up to 20 data points are dotted. The red curve represents the CDF of the best fitted normal distribution for data from the entire site.*

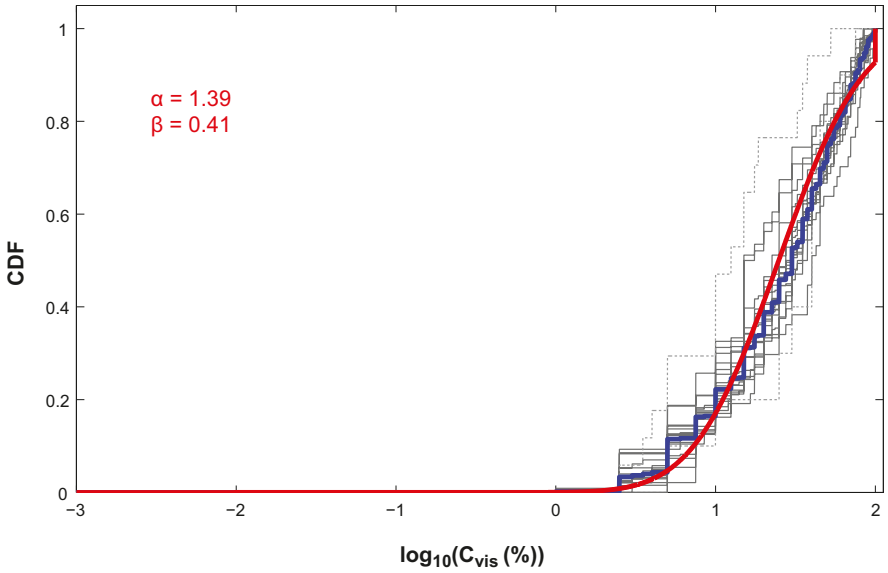

Figure 5-6. *Clay minerals – C_{vis}: Cumulative distribution functions of the separate data subsets (black curves) and of the data from the entire site (blue curve). CDFs for data subsets with up to 20 data points are dotted. The red curve represents the CDF of the best fitted truncated normal distribution for data from the entire site.*

5.2.4 Hematite

Only one quantitative d_{mean} data point was obtained for hematite. Two quantitative C_{vis} data points were obtained. Due to the lack of data, no CDFs are shown and no fitting of probabilistic distributions were made.

5.2.5 Pyrite

The corresponding figures to Figure 5-5 and Figure 5-6 are displayed below for pyrite.

As pyrite occurs as both spot mineral and layer mineral, the obtained CDFs range over more orders of magnitudes than those of the other studied minerals. Even so, based on the appearance of the figures, we suggest that the distributions for pyrite in Table 5-1 and Table 5-2 reasonably well represent all rock volumes at the site.

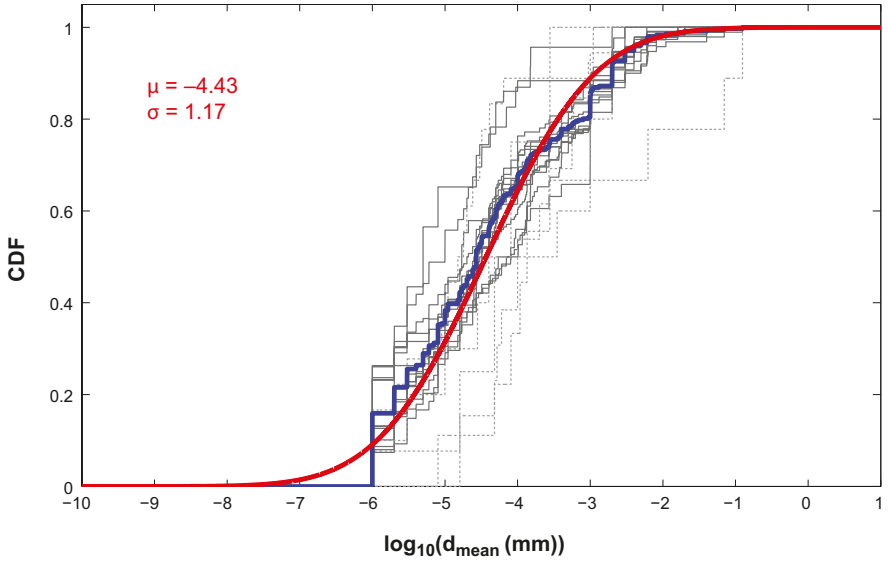

Figure 5-7. *Pyrite – d_{mean}: Cumulative distribution functions of the separate data subsets (black curves) and of the data from the entire site (blue curve). CDFs for data subsets with up to 20 data points are dotted. The red curve represents the CDF of the best fitted normal distribution for data from the entire site.*

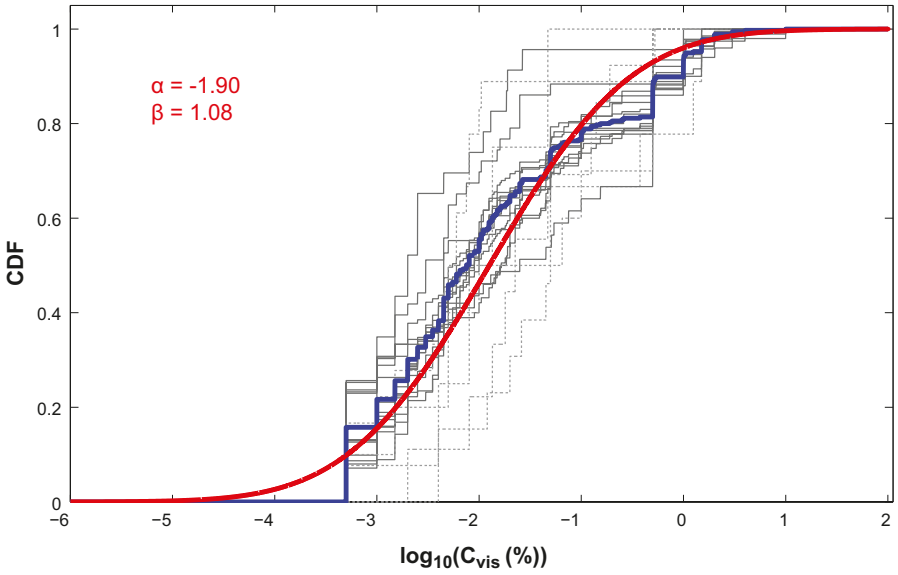

Figure 5-8. *Pyrite – C_{vis}: Cumulative distribution functions of the separate data subsets (black curves) and of the data from the entire site (blue curve). CDFs for data subsets with up to 20 data points are dotted. The red curve represents the CDF of the best fitted truncated normal distribution for data from the entire site.*

6 Conclusions

This document reports a statistical analysis of occurrences, amounts, and coverages of fracture minerals at the Laxemar site. In the quantitative mineral mapping campaign, over one thousand eight hundred open fractures have been quantitatively mapped. In total, hundreds of meters of drill core has been revisited. In more than half of the cases where a fracture mineral could be found, the averaged fracture mineral thickness d_{mean} could be estimated. In most cases where a fracture mineral could be observed as the outer layer on the fracture surface, the visible coverage C_{vis} could be estimated. As so many fractures were quantitatively mapped, and as so much data was delivered from the quantitative mineral mapping campaign, the statistical analysis made can in general be considered as reliable, and the results can be considered as representative for the site. The exception is for hematite, which was only found in two fractures. Except for the fact that hematite is scarce at the site, for this fracture mineral no other conclusion can be drawn.

A main conclusion from this work is that the occurrences, amounts, and coverages of the studied fracture minerals in general are similar for the different rock volumes at the site. One may have expected differences between, for example, fractures in deformation zones and fracture domains, but no such difference is easily detected. However, within the studied rock volumes there is a substantial spatial variability.

In the analysis, fractures were associated with closely located flow anomalies. For the studied fracture minerals, no relation between d_{mean} and the transmissivity of the flow anomalies could be seen. This indicates that there is no clear relation between the amounts of fracture minerals and the present groundwater flow situation in a fracture. This is not surprising, as many of the fractures and fracture minerals are considered to be old, even on a geologic time scale.

Both parametric and non-parametric methods have been used in the statistical analyses. From the parametric analyses, one can conclude that the normal distribution can be used to represent $\log_{10}(d_{mean})$ data, while the truncated normal distribution can be used to represent $\log_{10}(C_{vis})$ data. These distributions can be used as input to subsequent hydrogeochemical and radionuclide transport modelling. If the model can handle the parameterisation of the different rock volumes, the modeller can choose to import data for the individual volumes, given in Chapters 3 and 4. Such data may be based on few fractures and in such a case, the representativity and reliability can be questioned. If distribution parameters are required for the model, we suggest those given in Chapter 5, which can be used for the entire site. For calcite, chlorite, clay minerals, and pyrite, these distribution parameters are based upon many data points, making the results reliable.

All in all, both the quantitative mineral mapping campaign and the subsequent analysis of data can be considered as successful, delivering unprecedented data.

7 References

SKB's (Svensk Kärnbränslehantering AB) publications can be found at www.skb.se/publications.

Barr D R, Sherrill E T, 1999. Mean and variance of truncated normal distributions. The American Statistician, 53(4), pp 357–361.

Cohen A C, 1950. Estimating the mean and variance of normal populations from singly truncated and doubly truncated samples. The Annals of Mathematical Statistics, 21, pp 557–569.

Drake H, Tullborg E-L, 2009. Fracture mineralogy Laxemar. Site descriptive modelling**,** SDM-Site Laxemar. SKB R-08-99, Svensk Kärnbränslehantering AB.

Drake H, Sandström B, Tullborg E-L, 2006. Mineralogy and geochemistry of rocks and fracture fillings from Forsmark and Oskarshamn: compilation of data for SR-Can. SKB R-06-109, Svensk Kärnbränslehantering AB.

Eklund S, Mattsson K-J, 2008. Oskarshamn site investigation. Quantitative mapping of fracture minerals in Laxemar. SKB P-08-38, Svensk Kärnbränslehantering AB.

Johnson R A, 1994. Miller and Freund's probability & statistics for engineers. 5th ed. Englewood Cliffs, NJ: Prentice Hall.

NIST, 2009. NIST/SEMATECH e-Handbook of Statistical Methods. [Online]. Available at: http://www.itl.nist.gov/div898/handbook/. National Institute of Standards and Technology. [03 June 2009].

Shapiro S S, Wilk M B, 1965. An analysis of variance test for normality (complete samples). Biometrika, 52, pp 591–611.

SKB, 2009. Site description of Laxemar at completion of the site investigation phase. SDM-Site Laxemar. SKB TR-09-01, Svensk Kärnbränslehantering AB.

SKB, 2010. Data report for the safety assessment SR-Site. SKB TR-10-52, Svensk Kärnbränslehantering AB.

Teurneau B, Forsmark T, Forssman I, Rhén I, 2008. Oskarshamn site investigation. Correlation of Posiva Flow Log anomalies to core mapped features in KLX05, KLX06, KLX07A-B and KLX08. SKB P-07-212, Svensk Kärnbränslehantering AB.

Fracture mineral thickness, d_{mean}, in Laxemar

A1 All fractures in Laxemar (1,852 fractures)

A1.1 Calcite (All)

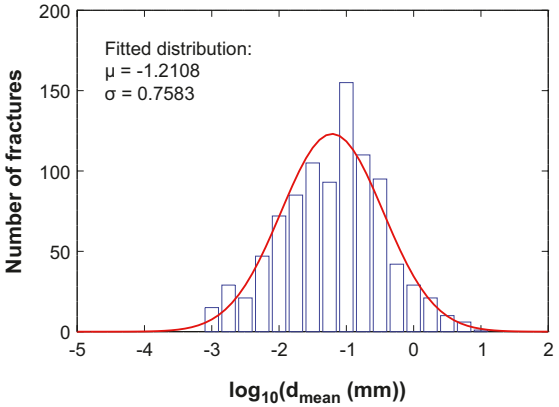

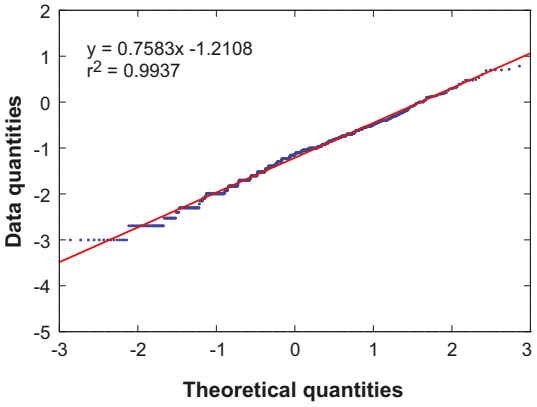

A1.2 Chlorite (All)

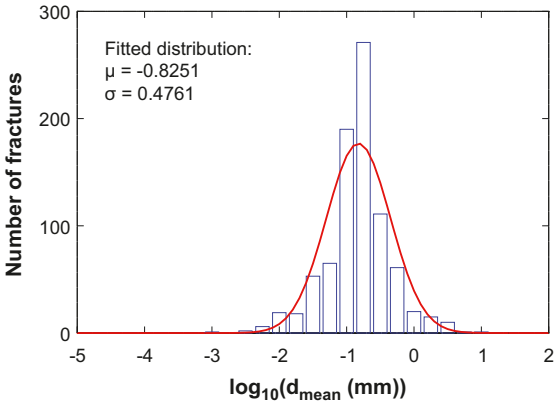

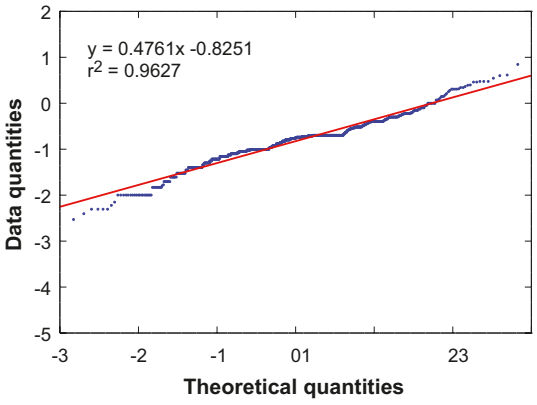

A1.3 Clay minerals (All)

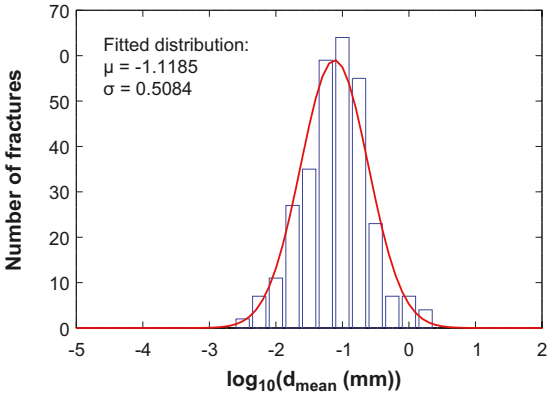

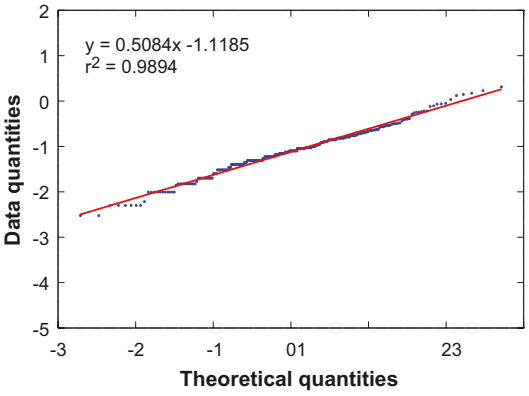

A1.4 Hematite (All)

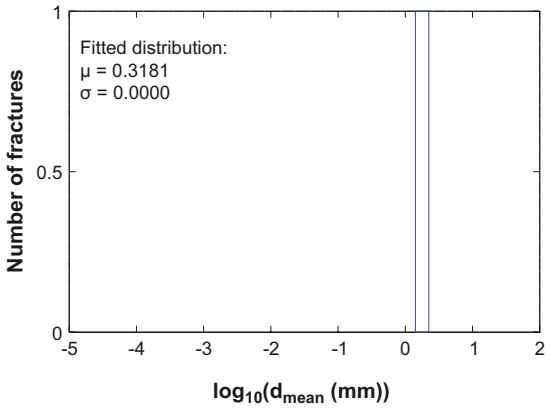

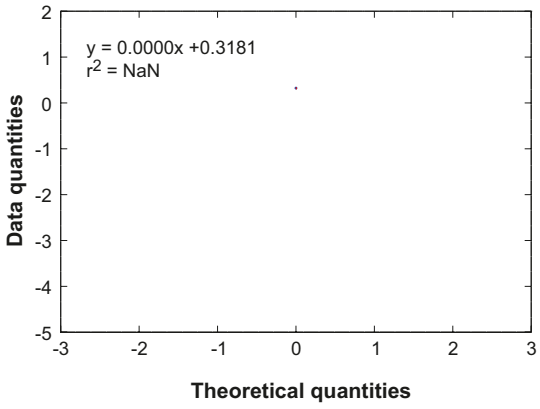

A1.5 Pyrite (All)

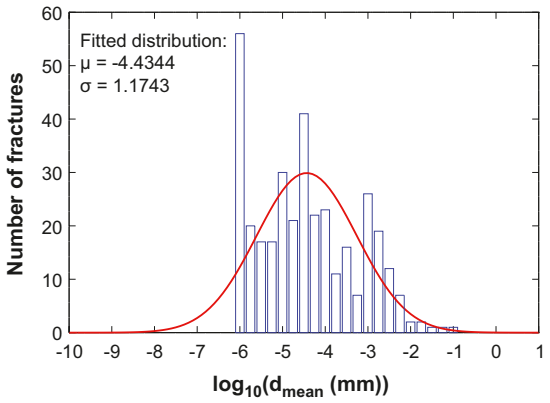

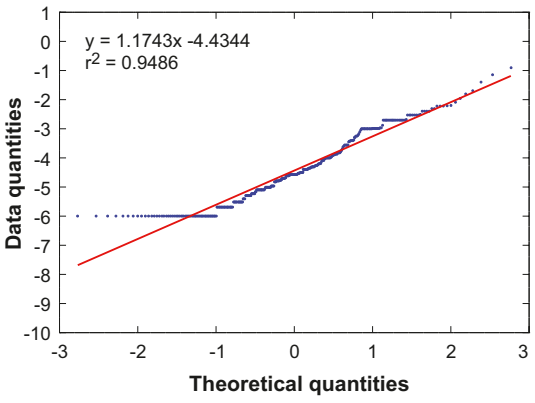

A2 Different elevations

A2.1 0–100 m (527 fractures)

Calcite (0–100 m)

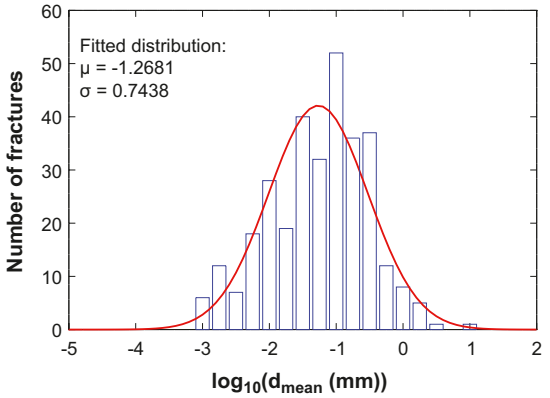

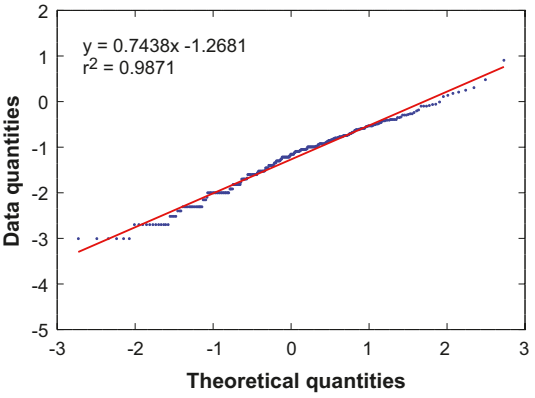

Chlorite (0–100 m)

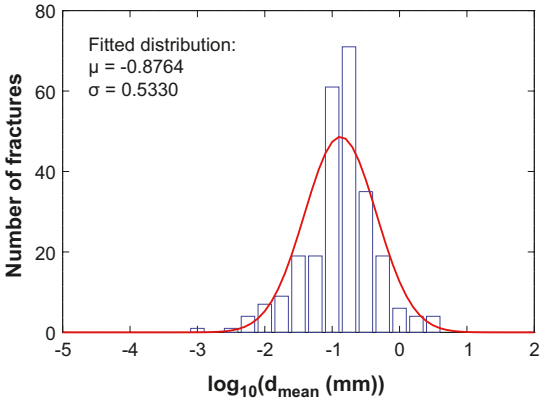

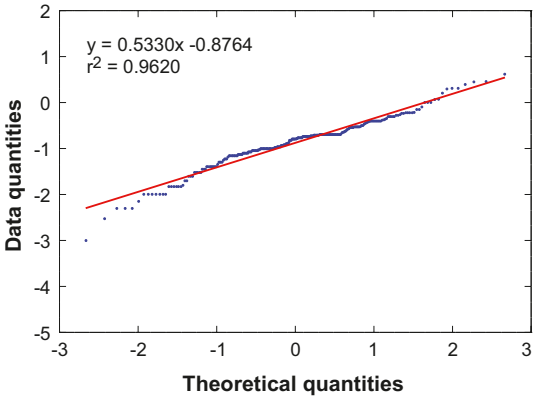

Clay minerals (0–100 m)

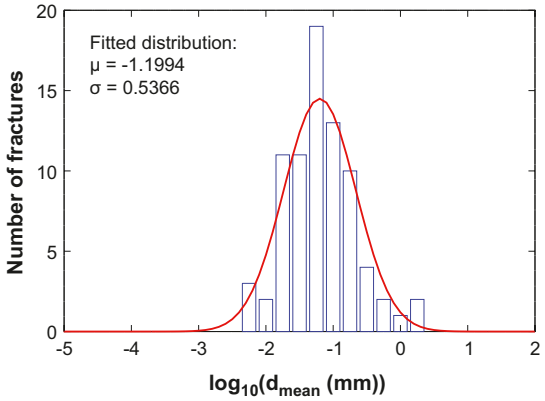

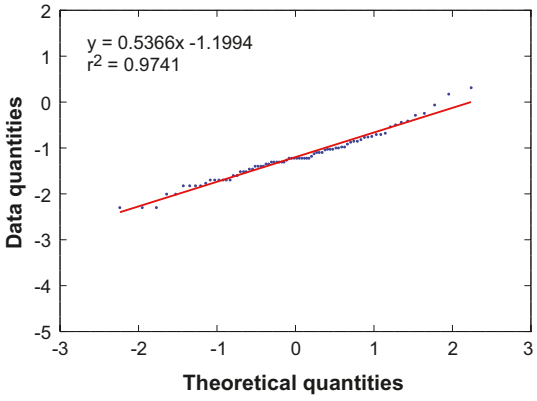

Hematite (0–100 m)

N/A

Pyrite (0–100 m)

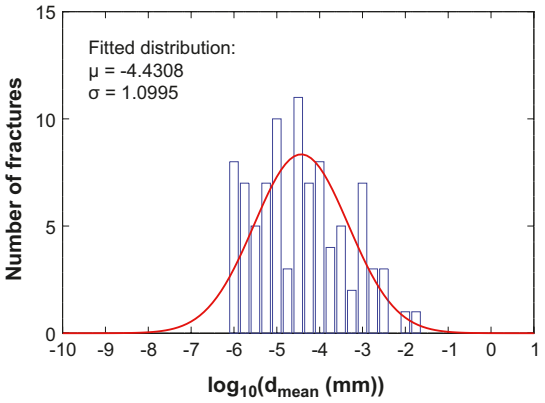

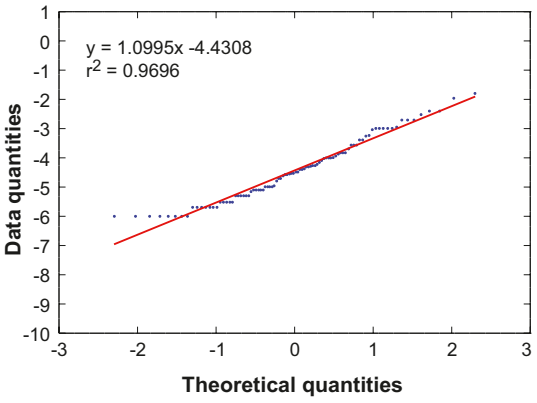

A2.2 100–300 m (502 fractures)

Calcite (100–300 m)

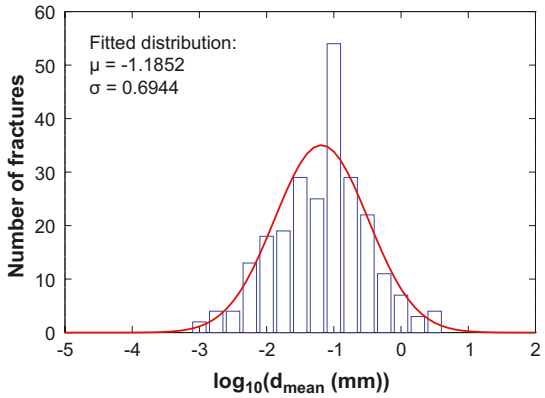

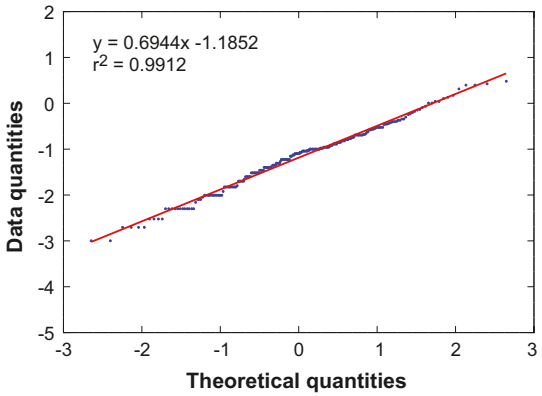

Chlorite (100–300 m)

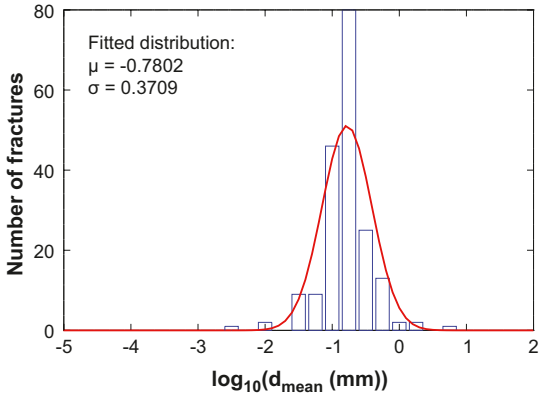

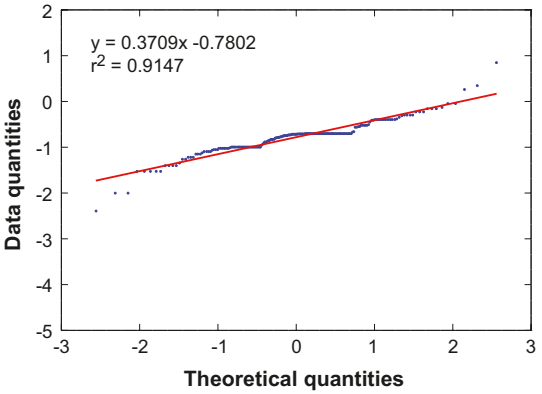

Clay minerals (100–300 m)

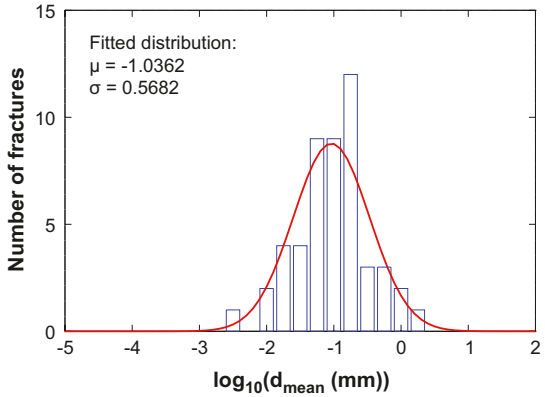

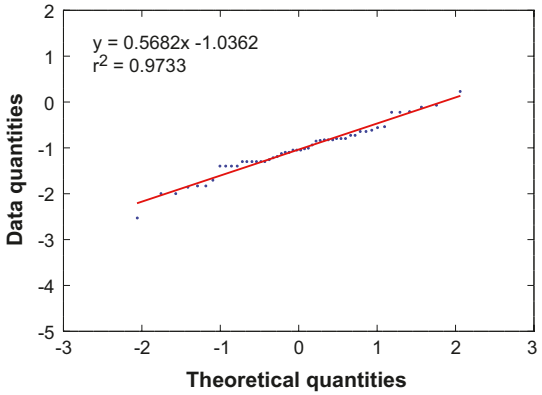

Hematite (100–300 m)

N/A

Pyrite (100–300 m)

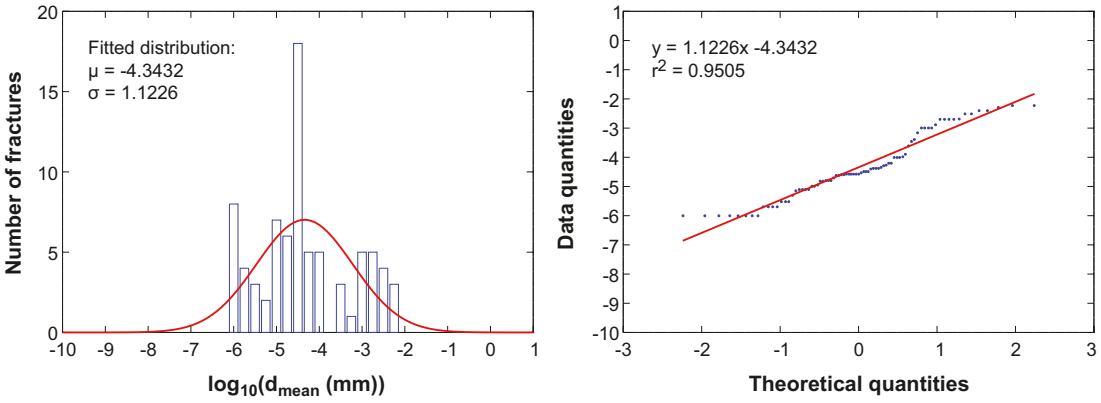

A2.3 300–500 m (606 fractures)

Calcite (300–500 m)

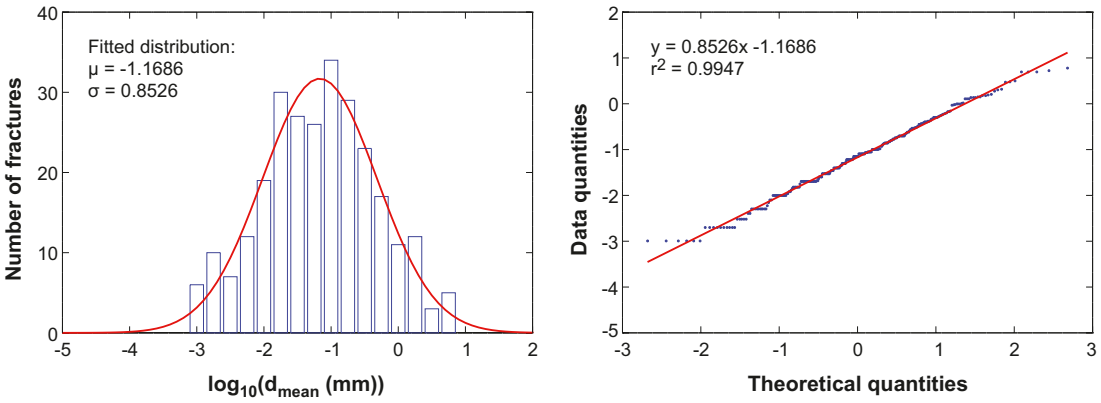

Chlorite (300–500 m)

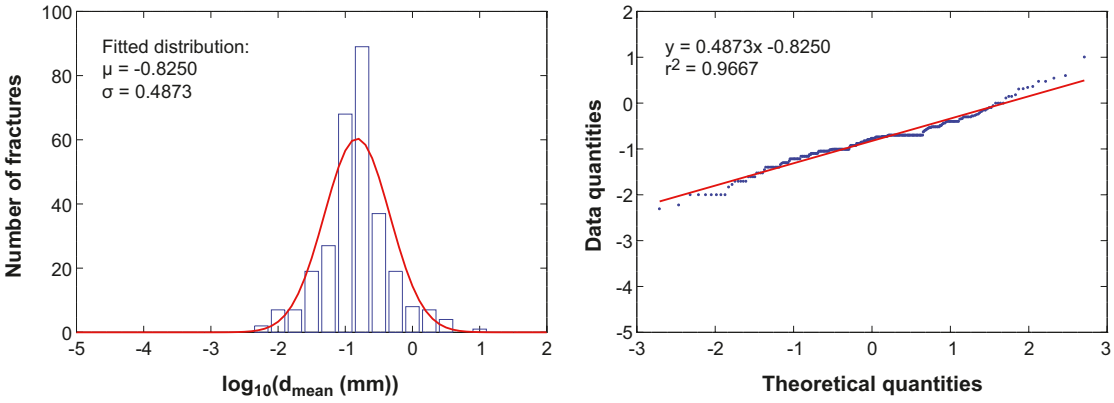

Clay minerals (300–500 m)

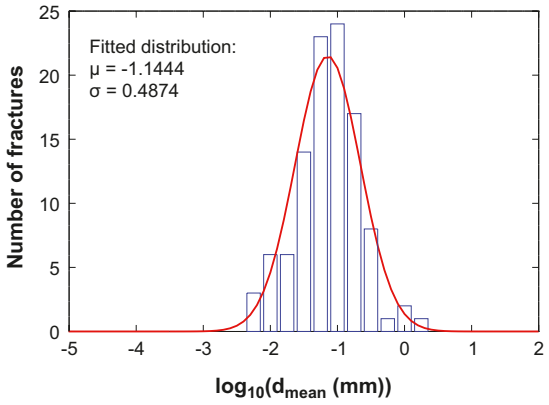

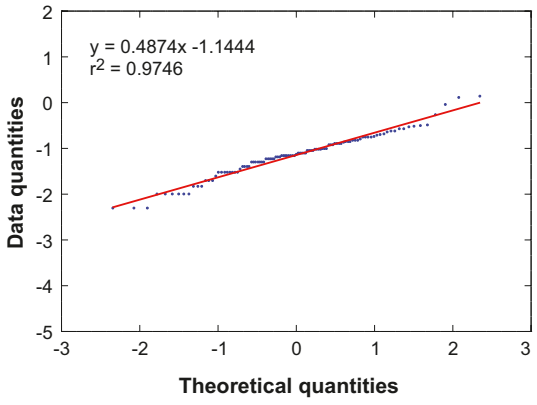

Hematite (300–500 m)

N/A

Pyrite (300–500 m)

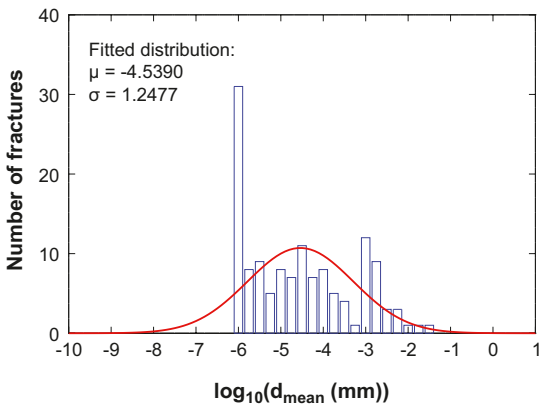

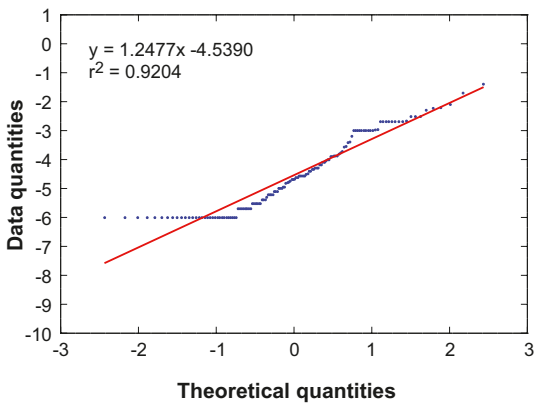

A2.4 500–700 m (134 fractures)

Calcite (500–700 m)

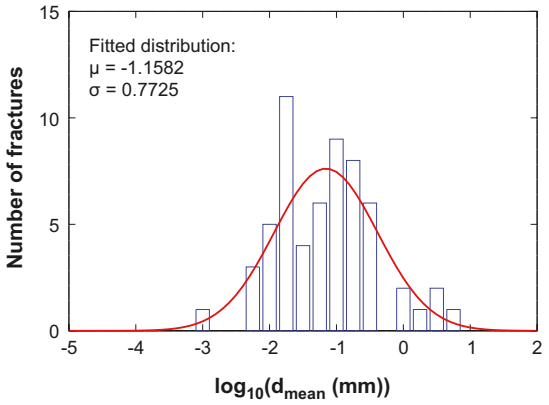

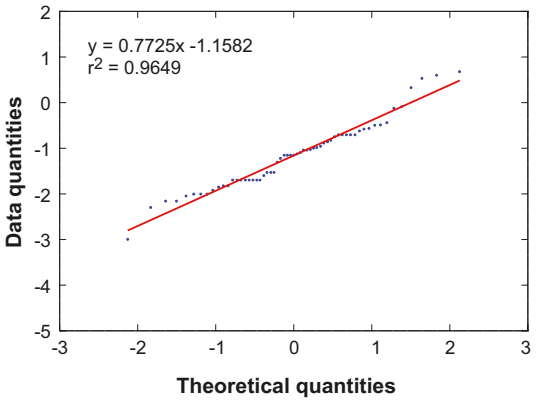

Chlorite (500–700 m)

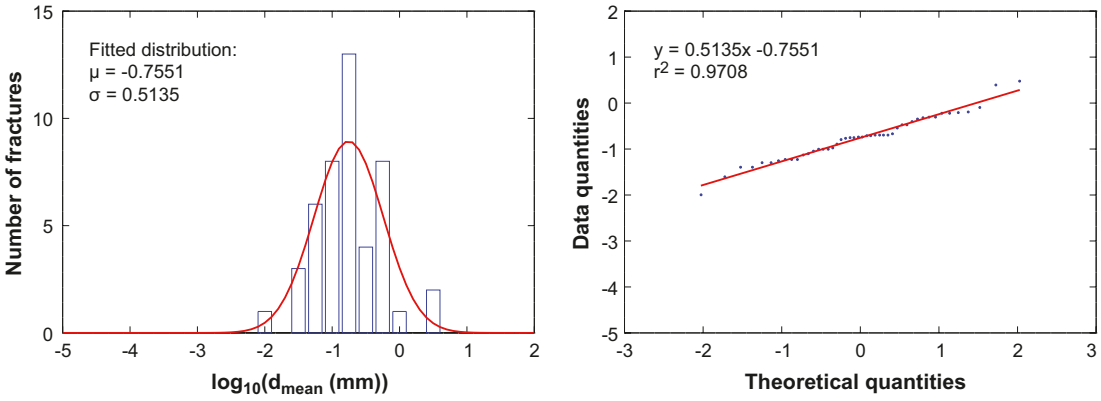

Clay minerals (500–700 m)

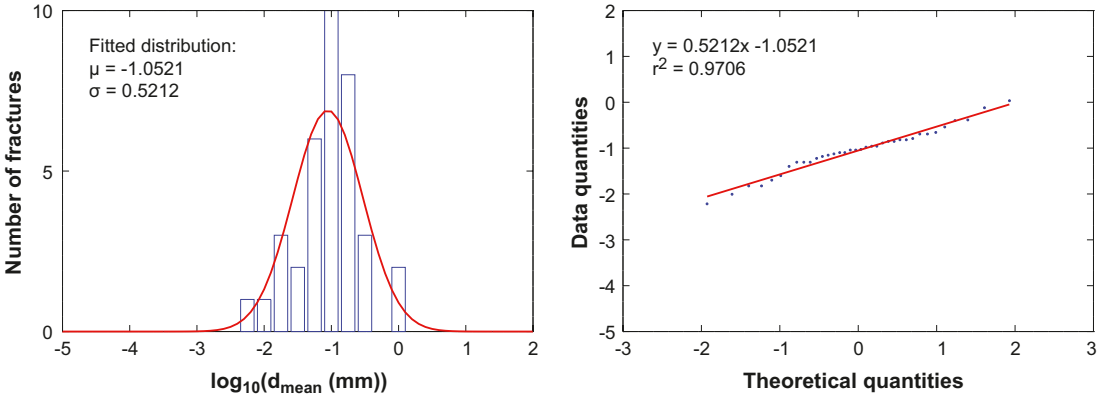

Hematite (500–700 m)

N/A

Pyrite (500–700 m)

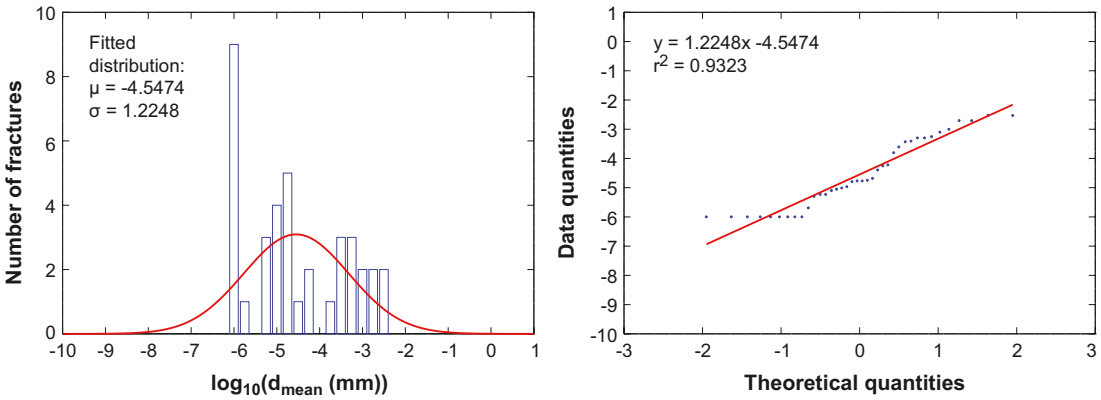

A2.5 700–1,000 m (83 fractures)

Calcite (700–1,000 m)

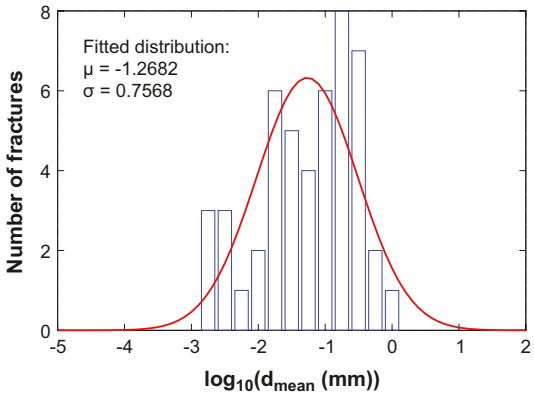

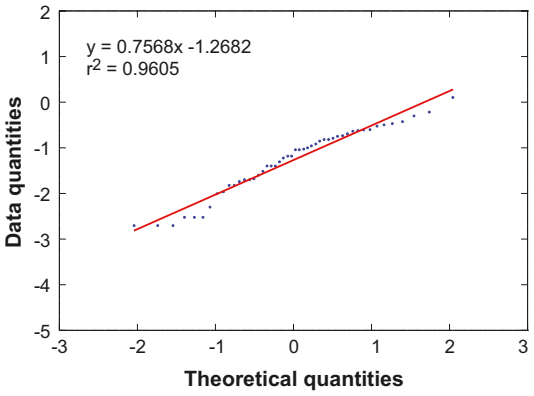

Chlorite (700–1,000 m)

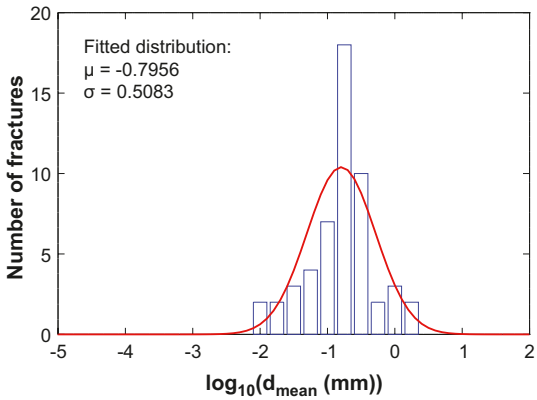

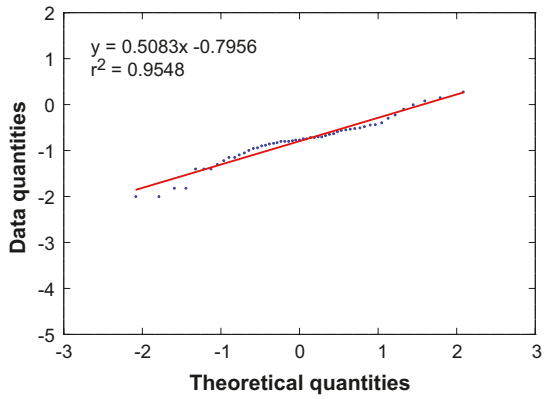

Clay minerals (700–1,000 m)

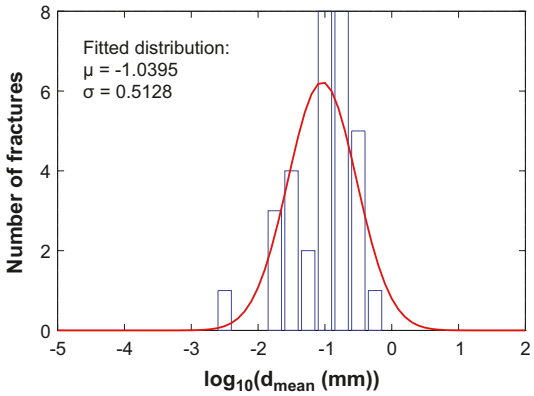

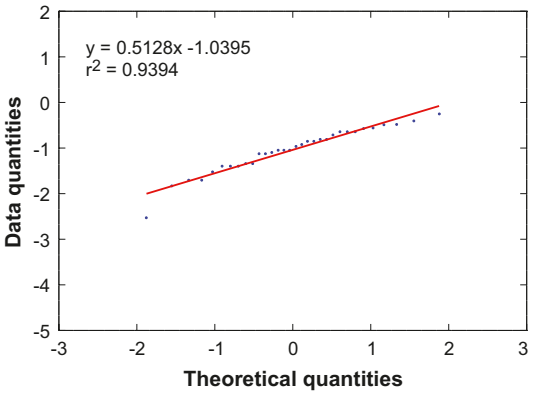

Hematite (700–1,000 m)

N/A

Pyrite (700–1,000 m)

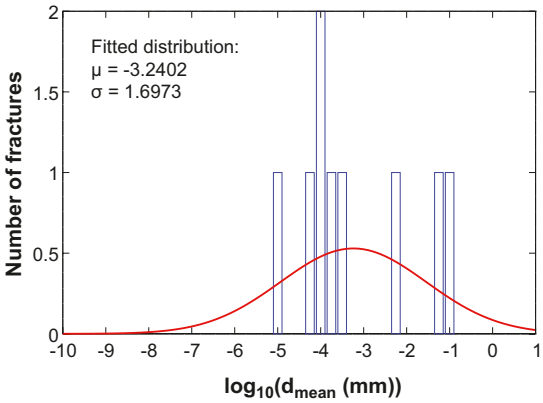

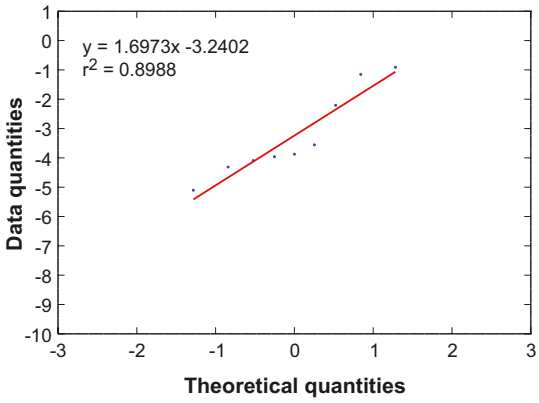

A3 Rock domains

A3.1 RSMA01 (597 fractures)

Calcite (RSMA01)

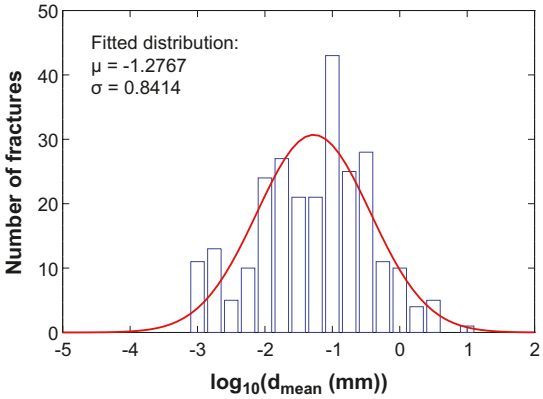

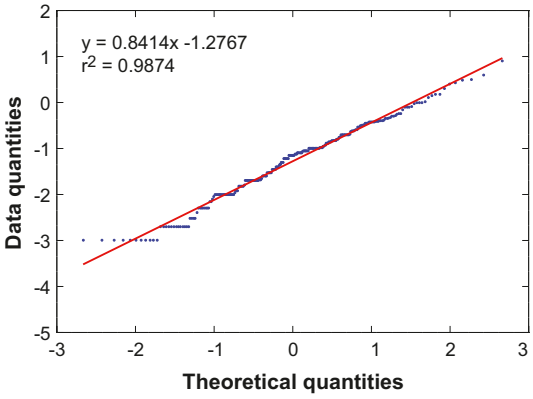

Chlorite (RSMA01)

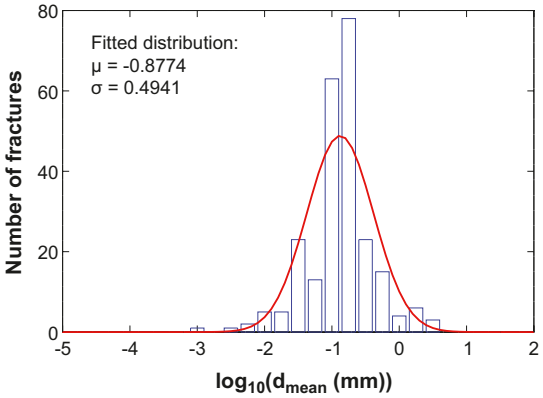

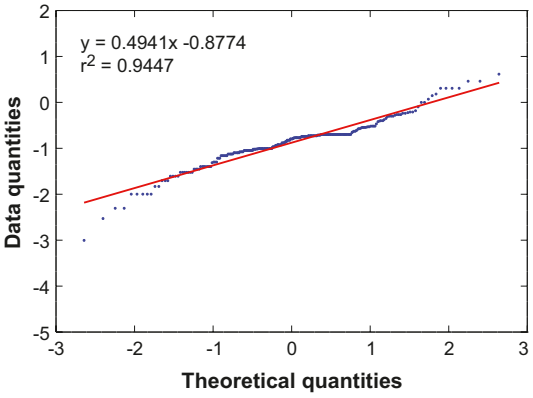

Clay minerals (RSMA01)

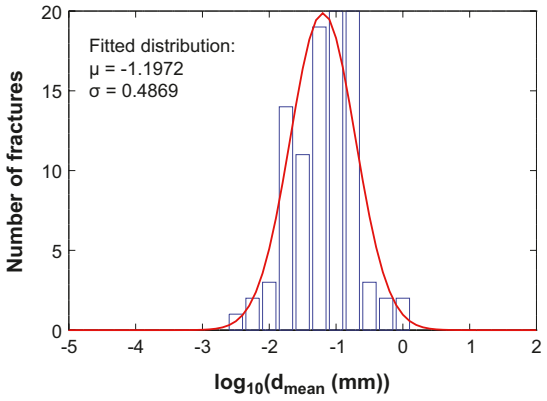

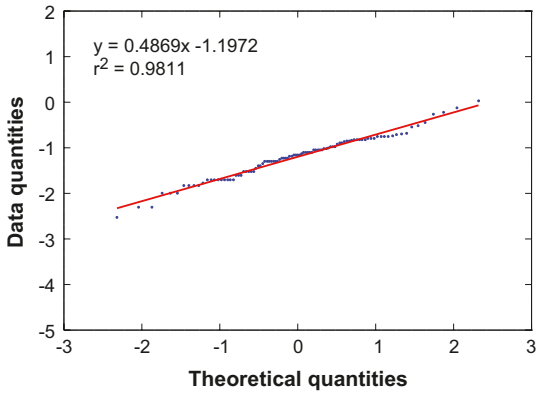

Hematite (RSMA01)

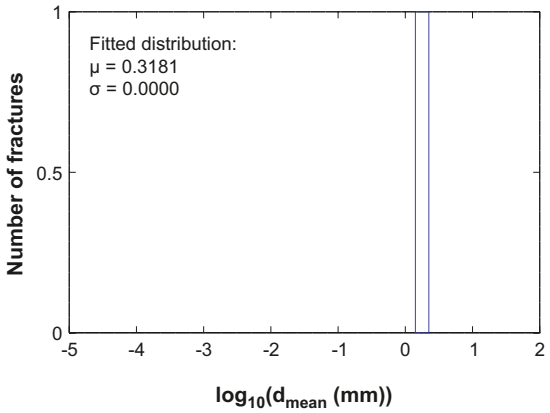

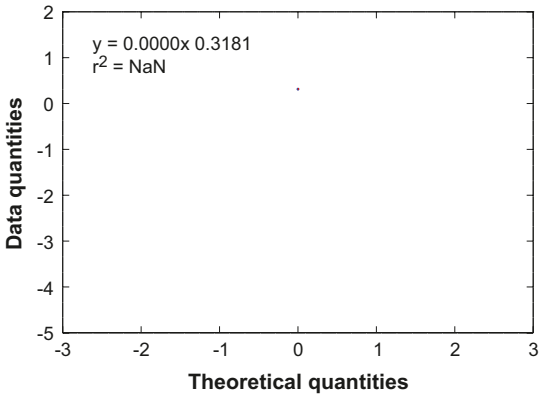

Pyrite (RSMA01)

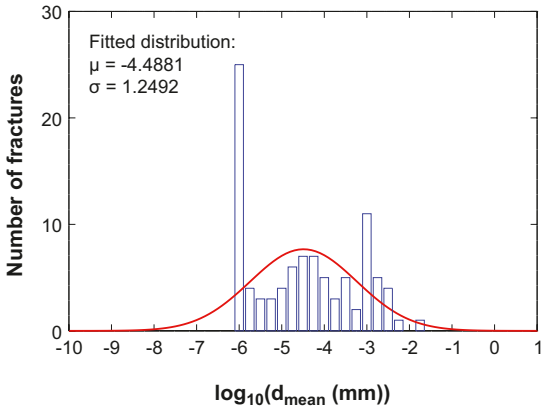

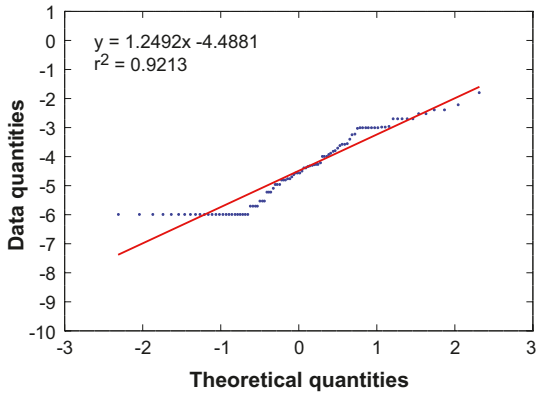

A3.2 RSMD01 (1,067 fractures)

Calcite (RSMD01)

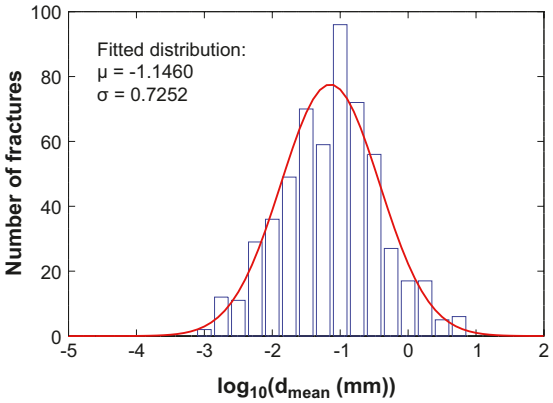

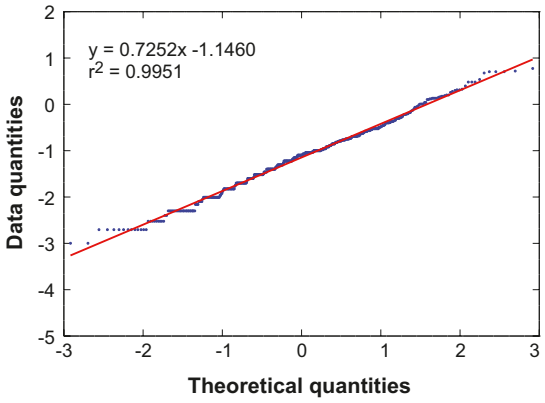

Chlorite (RSMD01)

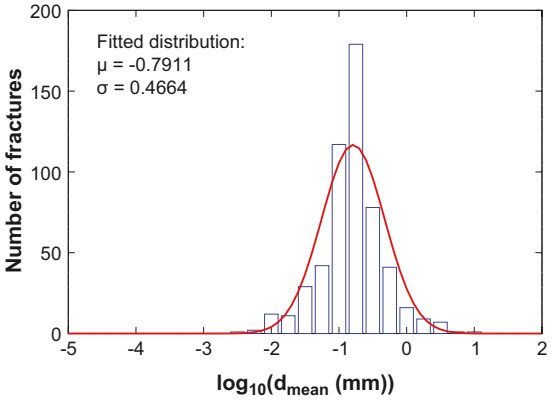

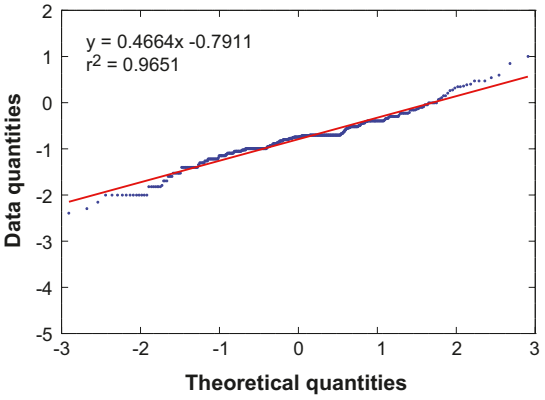

Clay minerals (RSMD01)

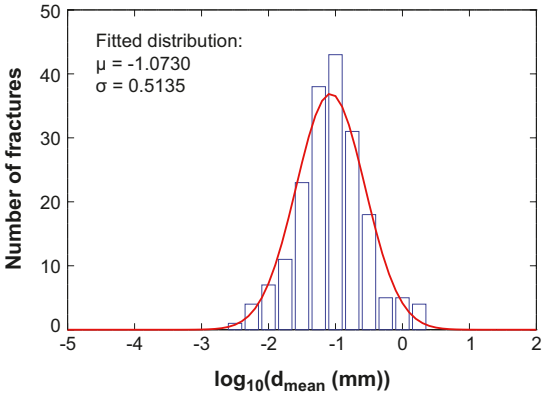

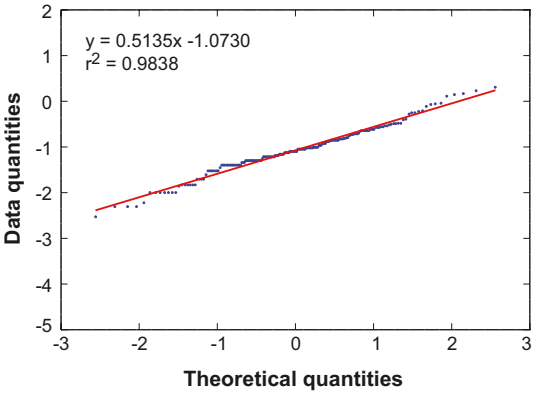

Hematite (RSMD01)

N/A

Pyrite (RSMD01)

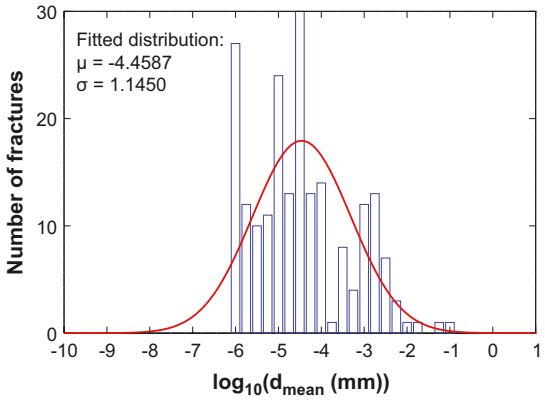

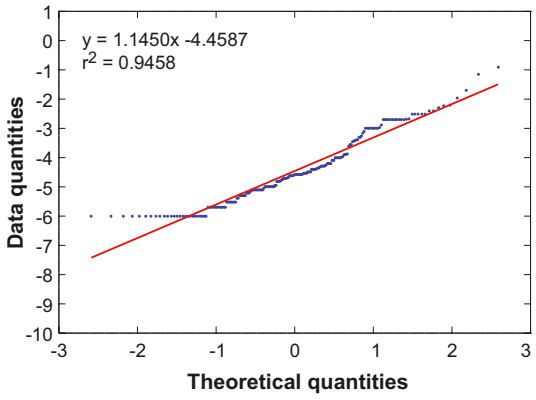

A3.3 RSMM01 (188 fractures)

Calcite (RSMM01)

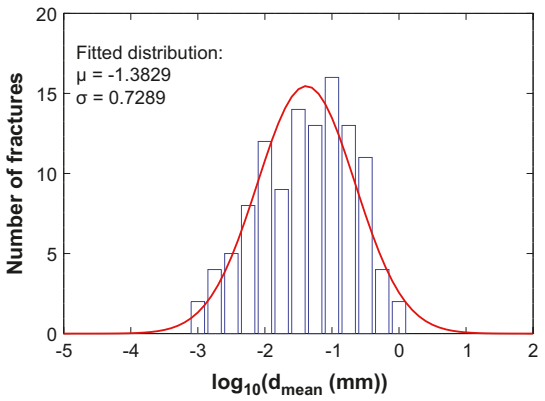

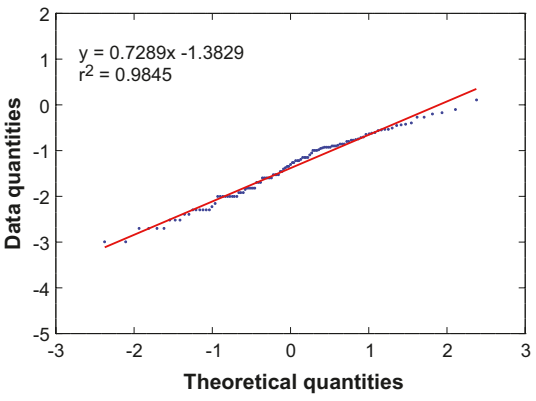

Chlorite (RSMM01)

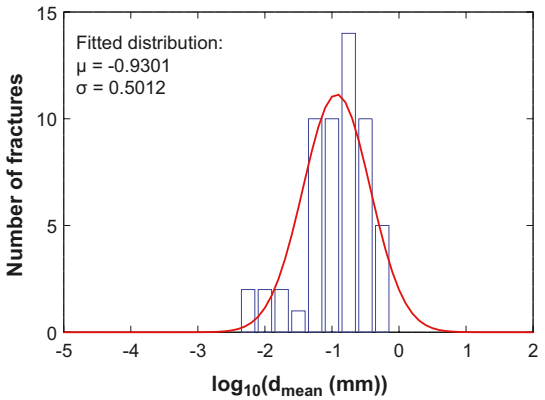

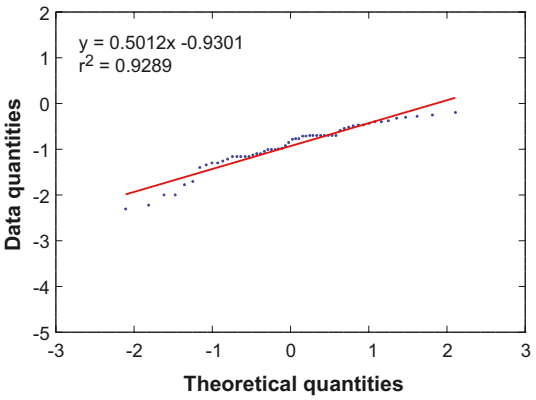

Clay minerals (RSMM01)

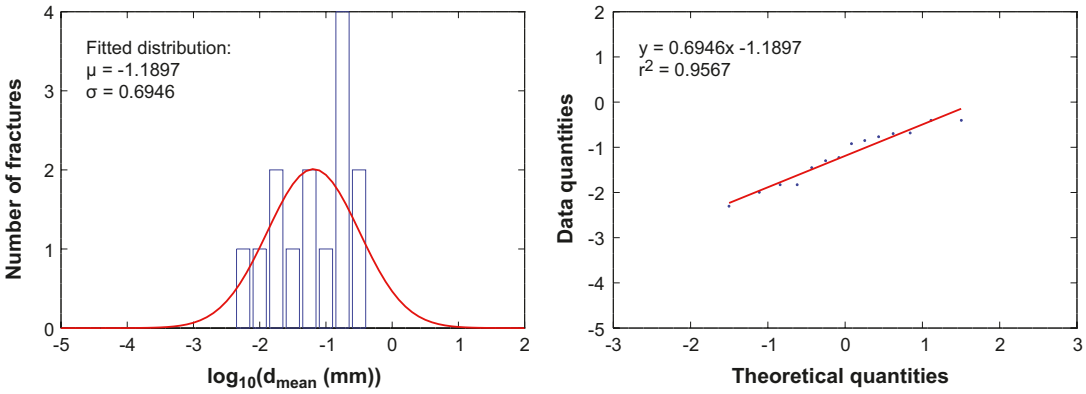

Hematite (RSMM01)

N/A

Pyrite (RSMM01)

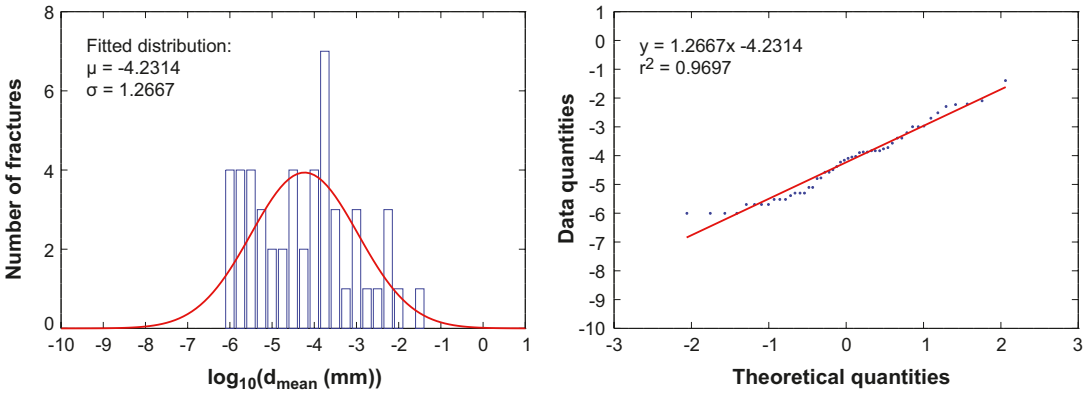

A4 Fracture domains

A4.1 All fracture domains (797 fractures)

Calcite (All FD)

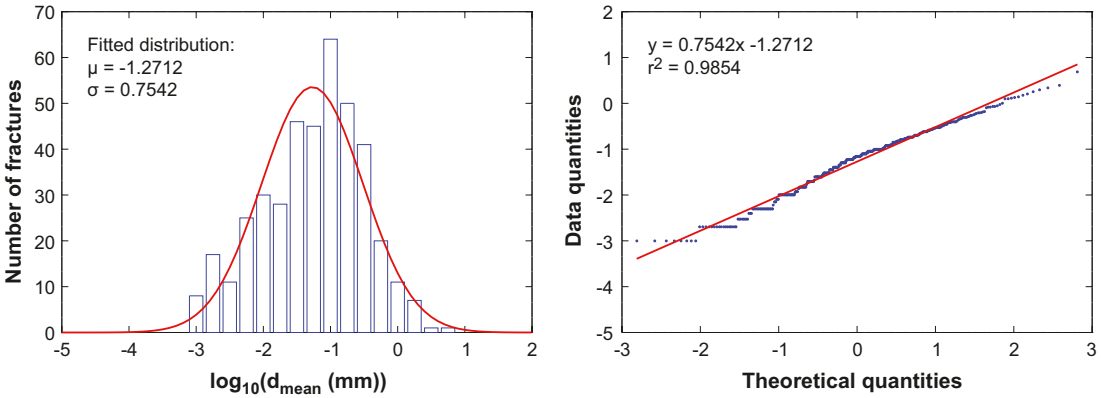

Chlorite (All FD)

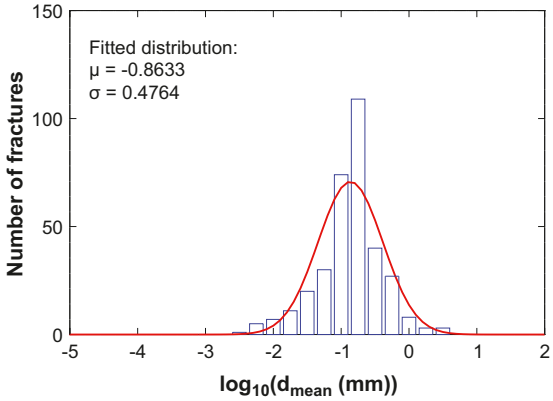

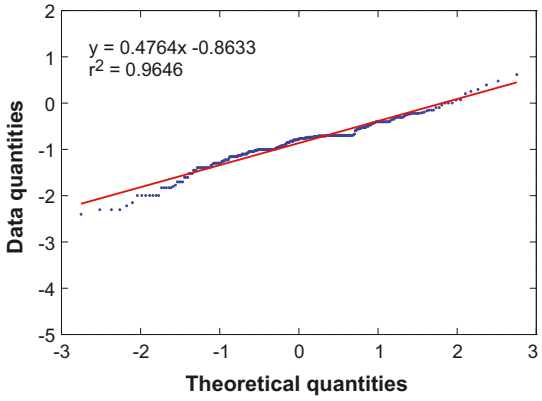

Clay minerals (All FD)

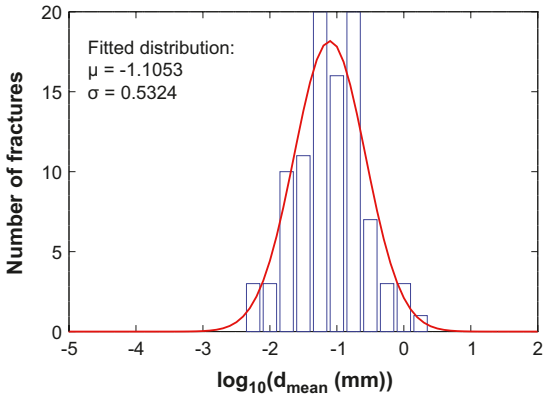

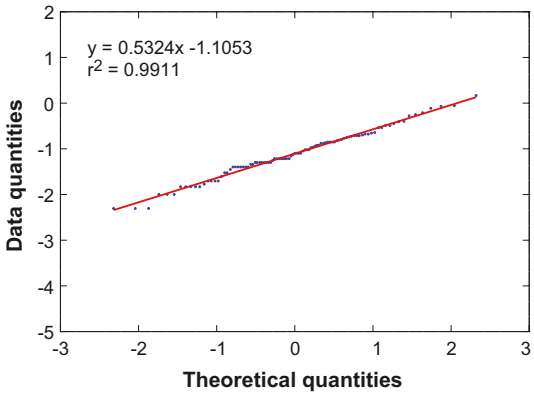

Hematite (All FD)

N/A

Pyrite (All FD)

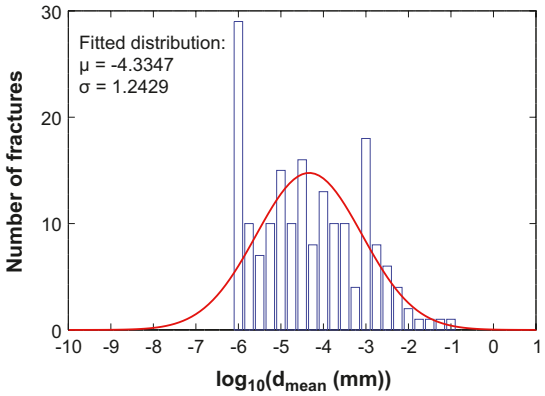

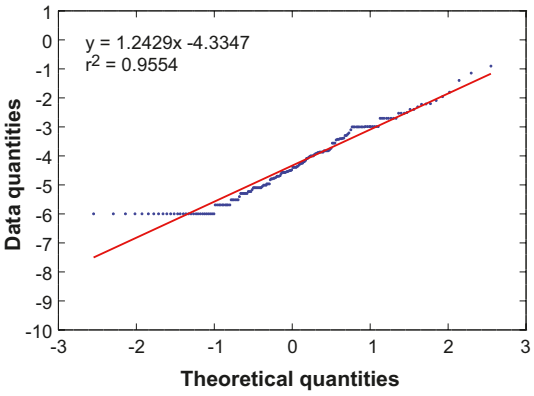

A4.2 FSM_C (295 fractures)

Calcite (FSM_C)

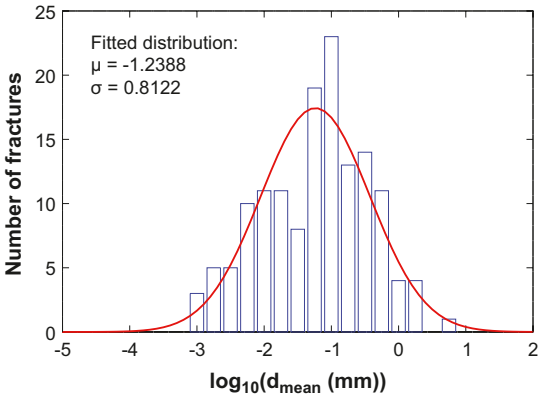

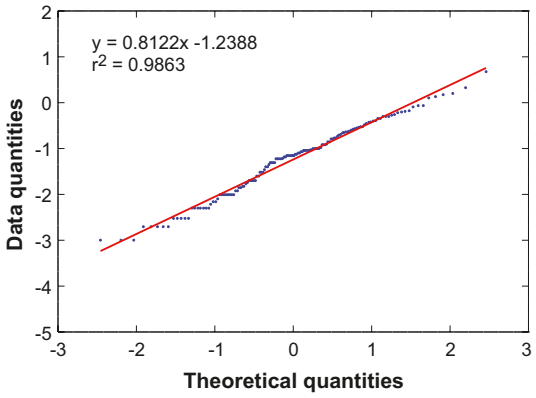

Chlorite (FSM_C)

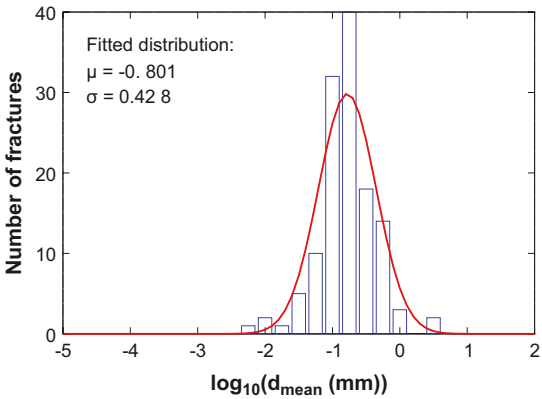

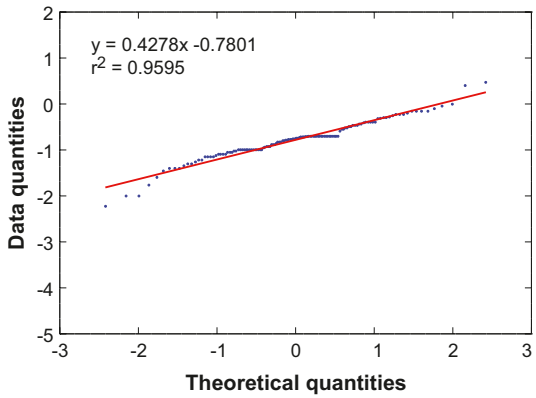

Clay minerals (FSM_C)

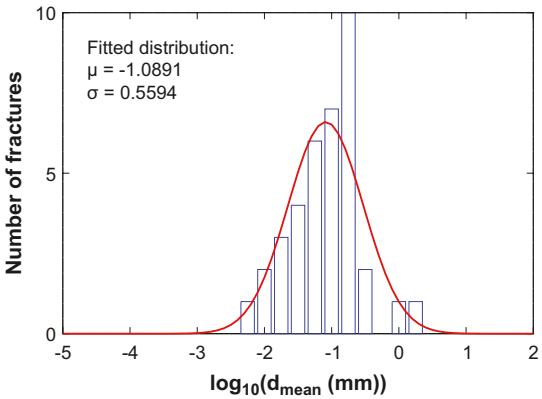

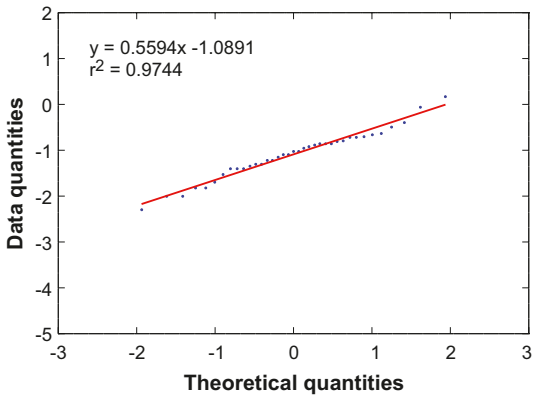

Hematite (FSM_C)

N/A

Pyrite (FSM_C)

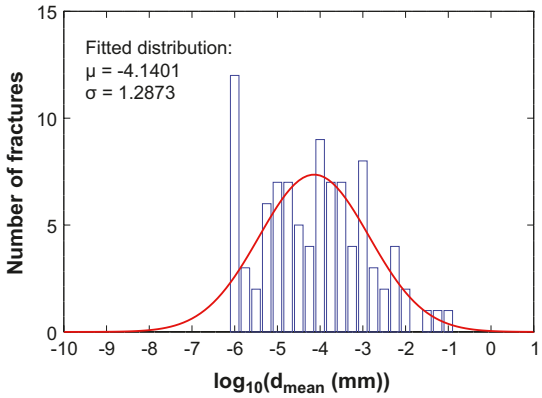

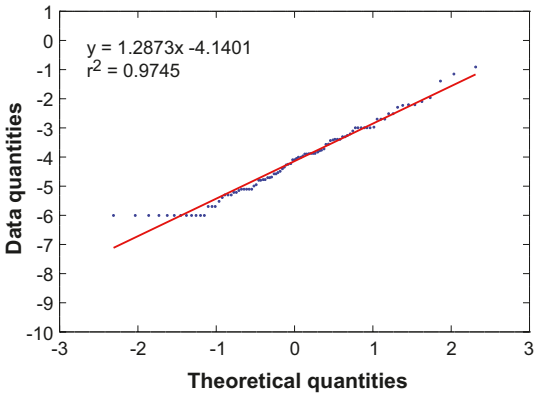

A4.3 FSM_EW007 (146 fractures)

Calcite (FSM_EW007)

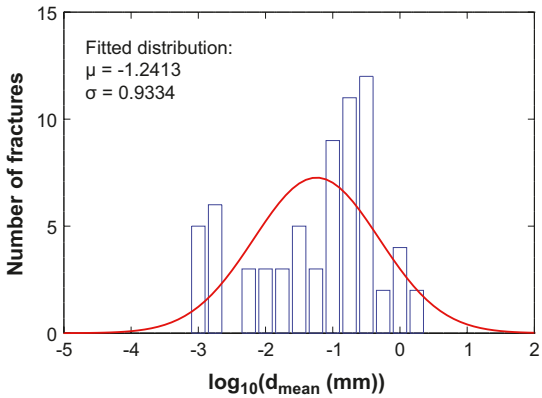

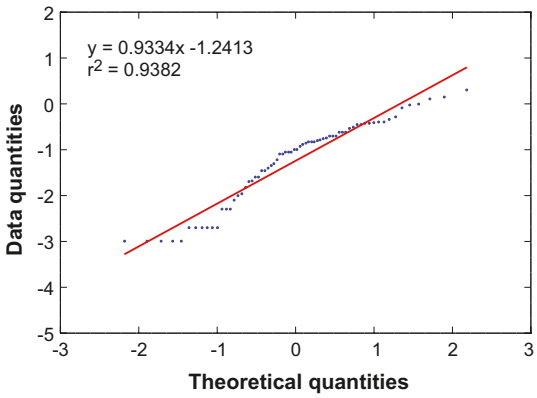

Chlorite (FSM_EW007)

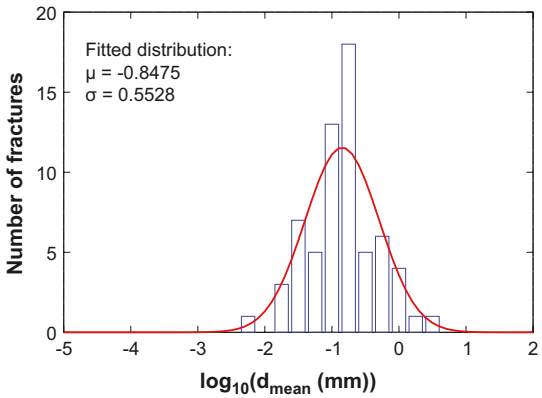

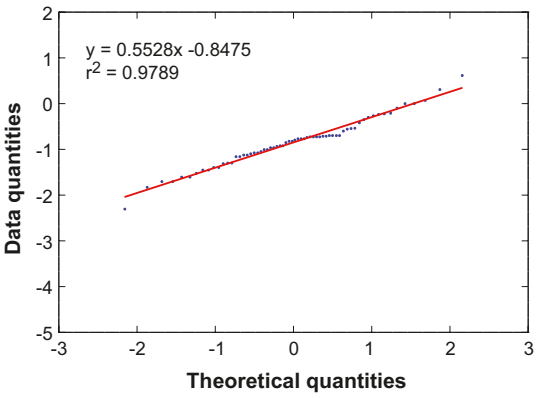

Clay minerals (FSM_EW007)

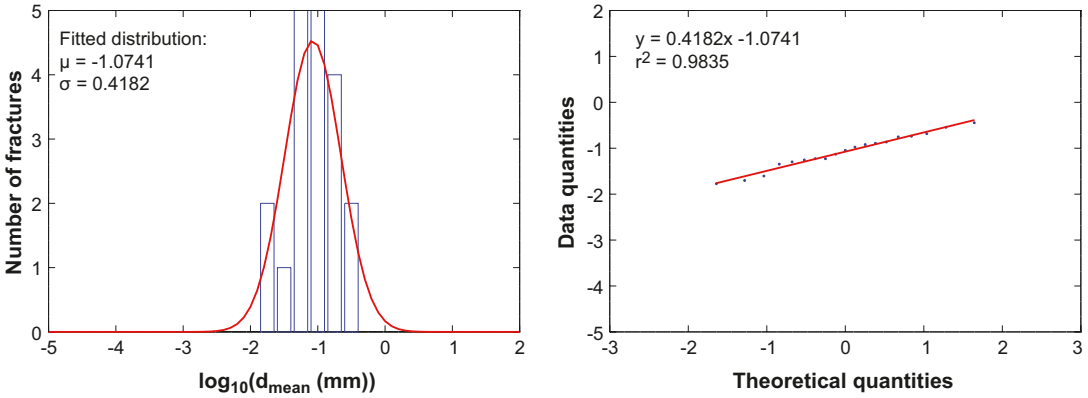

Hematite (FSM_EW007)

N/A

Pyrite (FSM_EW007)

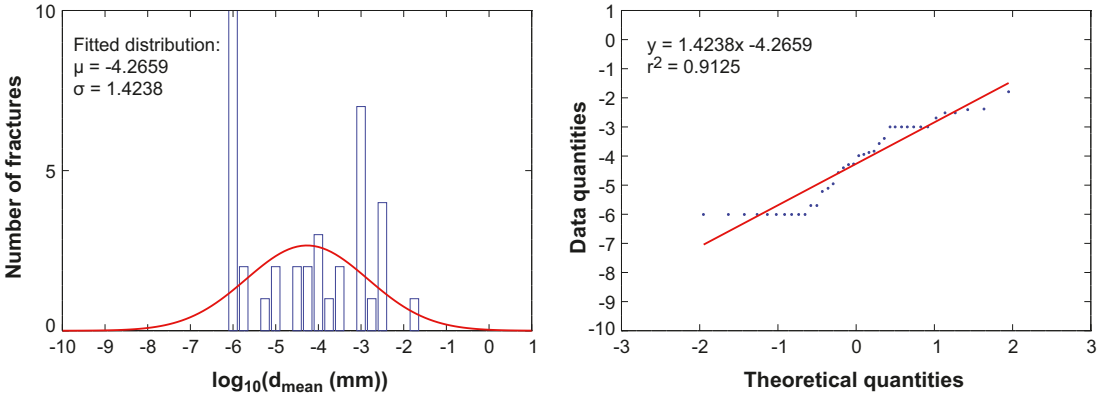

A4.4 FSM_NE005 (144 fractures)

Calcite (FSM_NE005)

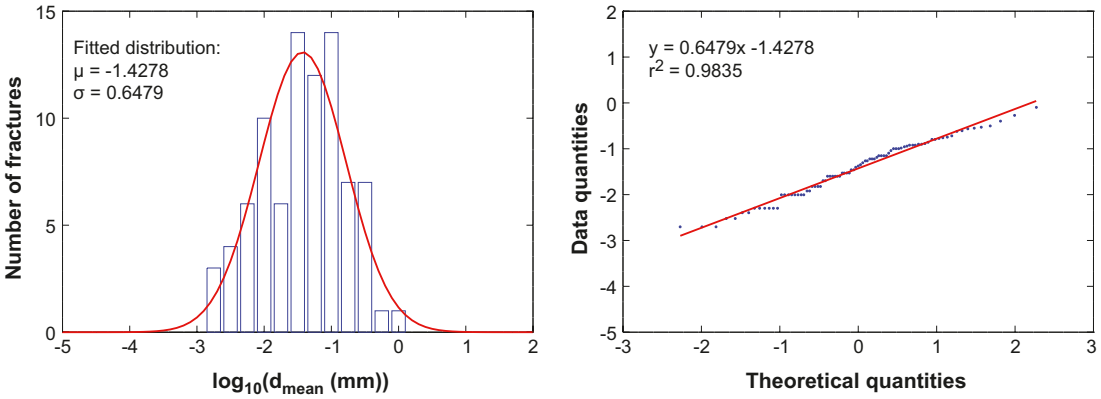

Chlorite (FSM_NE005)

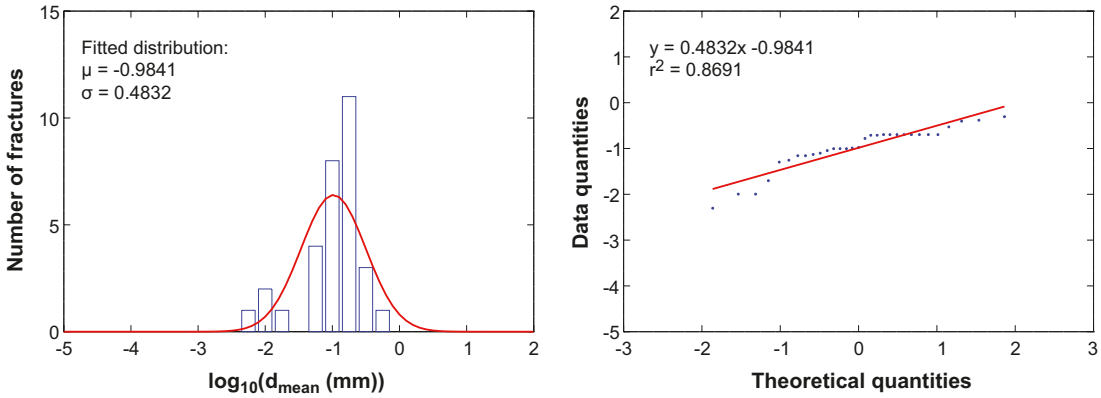

Clay minerals (FSM_NE005)

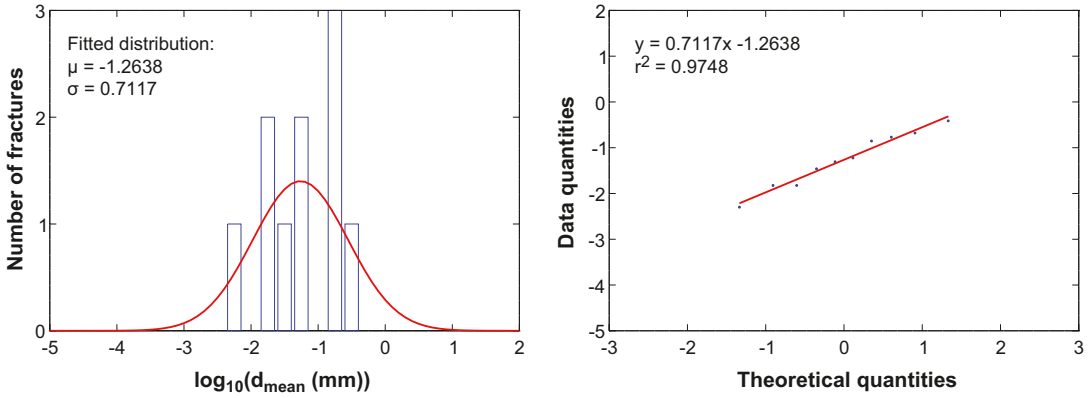

Hematite (FSM_NE005)

N/A

Pyrite (FSM_NE005)

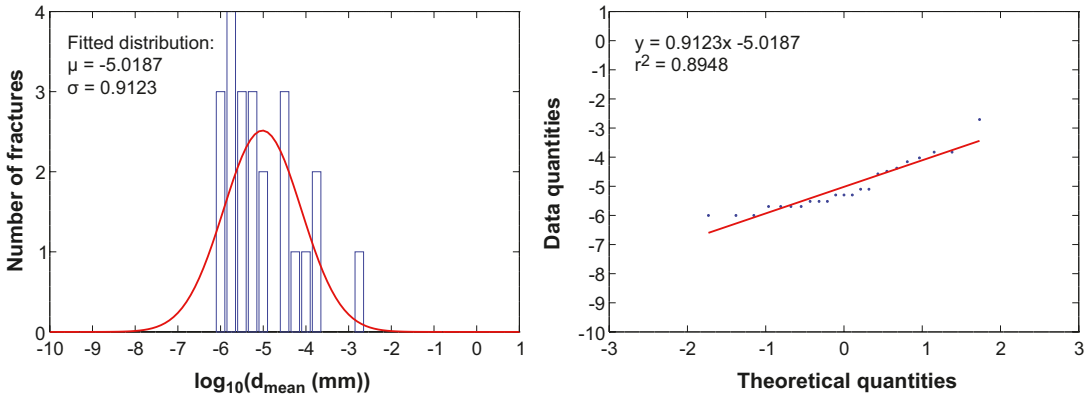

A4.5 FSM_S (115 fractures)

Calcite (FSM_S)

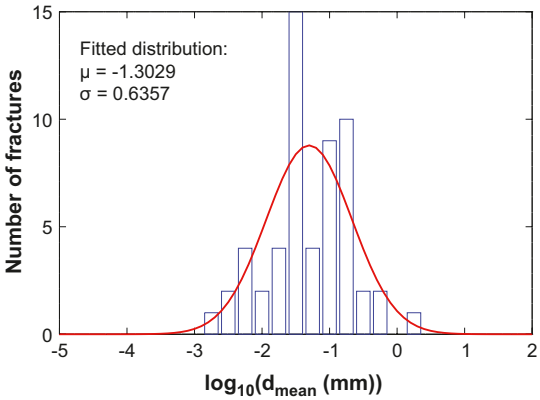

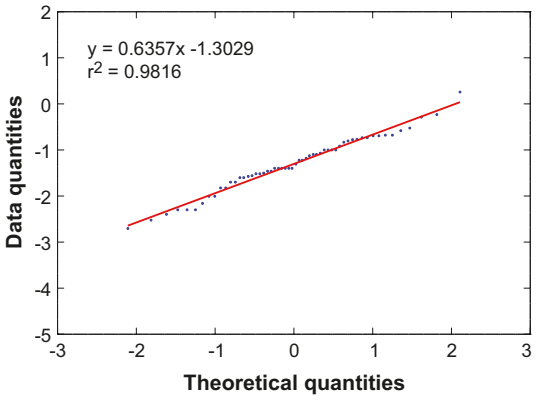

Chlorite (FSM_S)

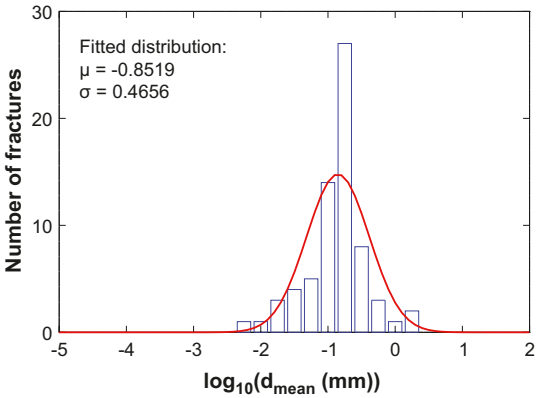

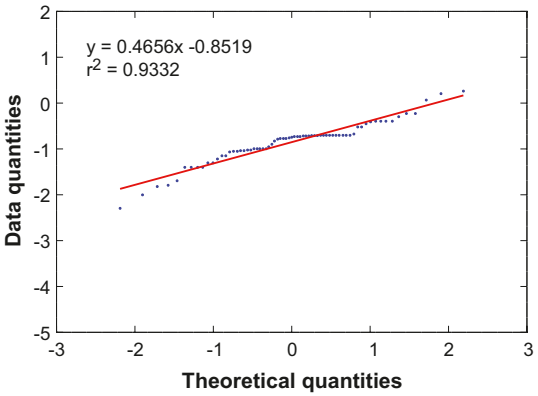

Clay minerals (FSM_S)

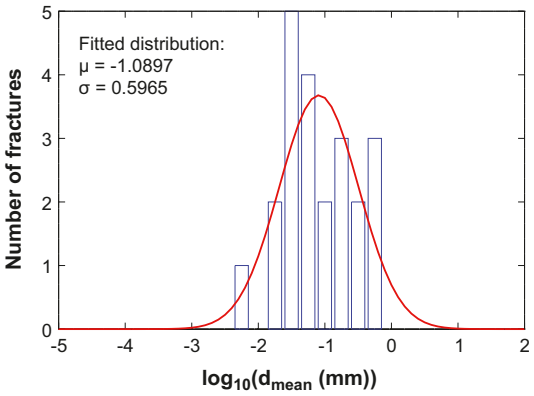

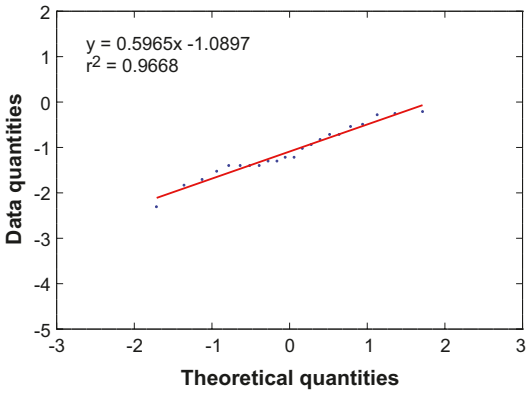

Hematite (FSM_S)

N/A

Pyrite (FSM_S)

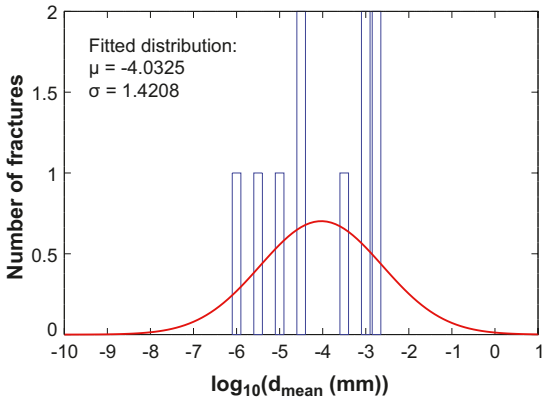

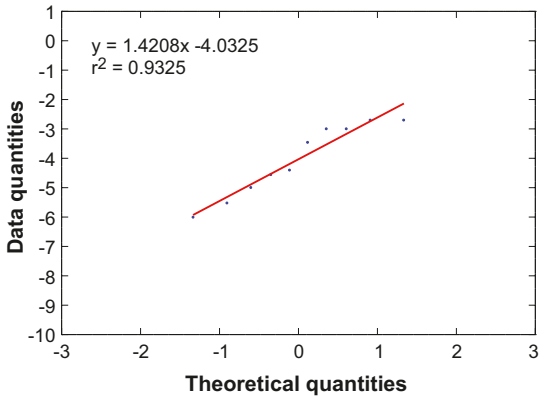

A4.6 FSM_W (97 fractures)

Calcite (FSM_W)

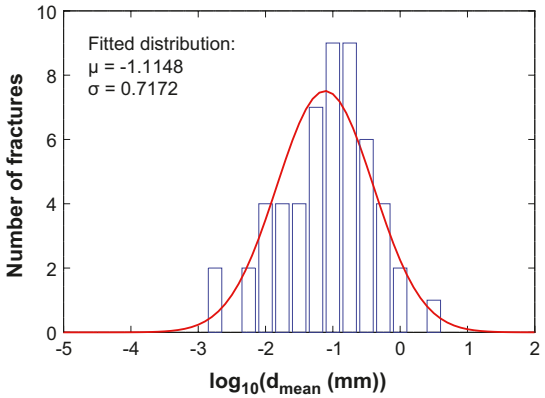

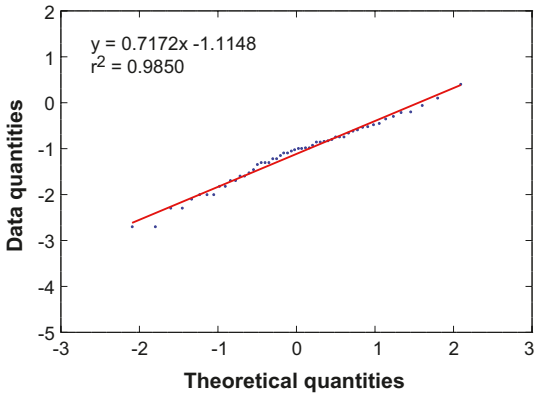

Chlorite (FSM_W)

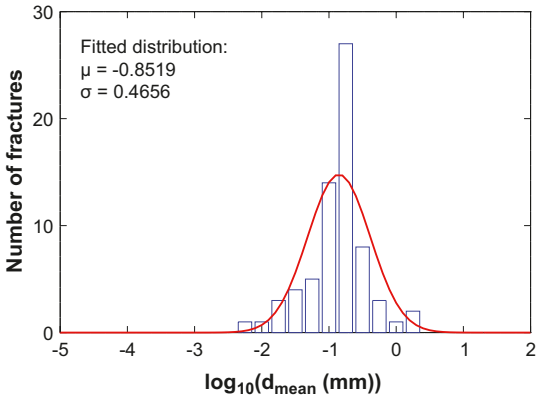

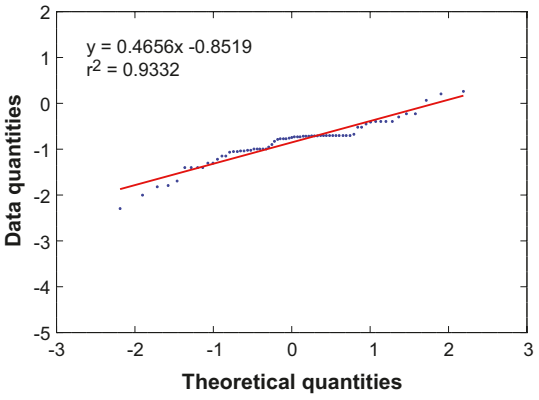

Clay minerals (FSM_W)

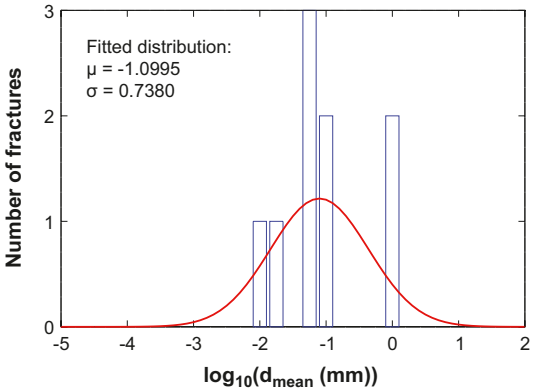

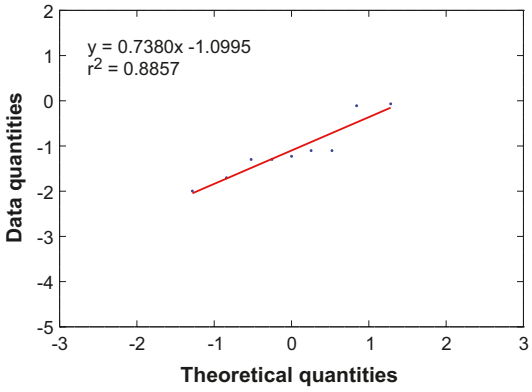

Hematite (FSM_W)

N/A

Pyrite (FSM_W)

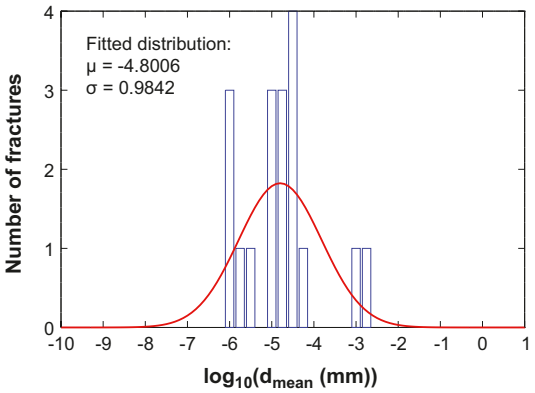

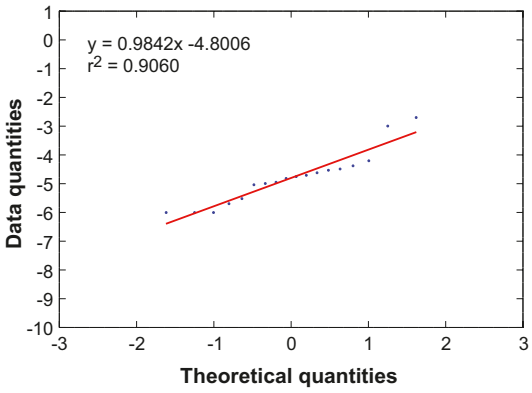

A5 Deformation zones

A5.1 All deformation zones (744 fractures)

Calcite (All DZ)

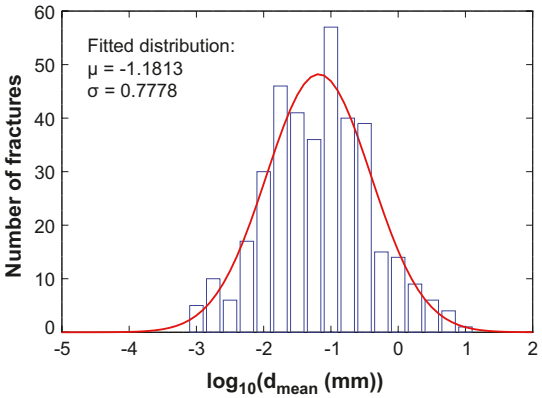

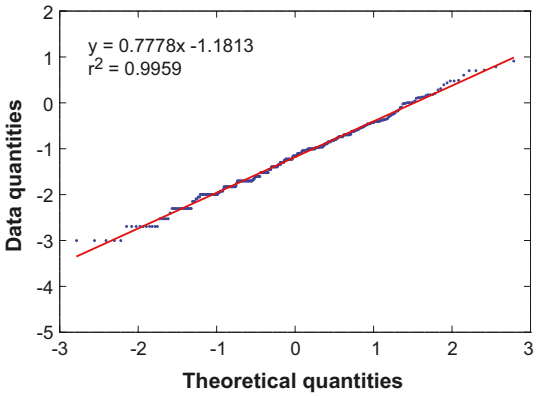

Chlorite (All DZ)

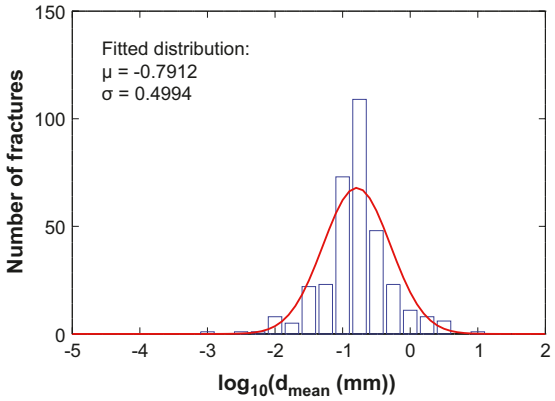

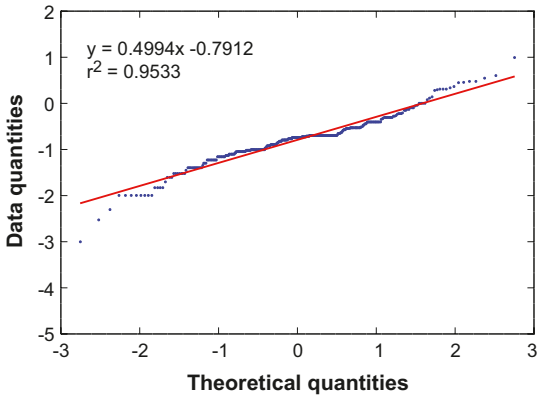

Clay minerals (All DZ)

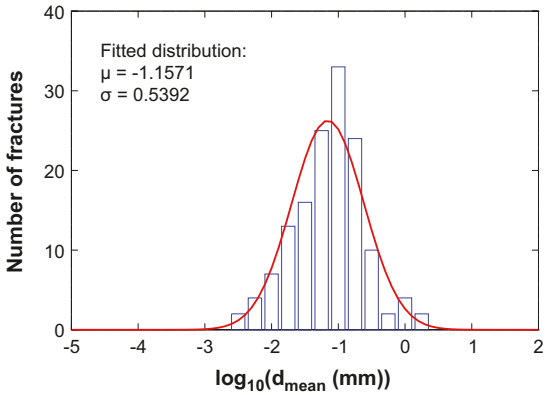

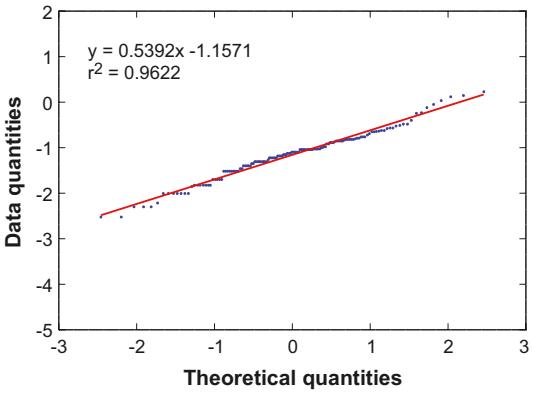

Hematite (All DZ)

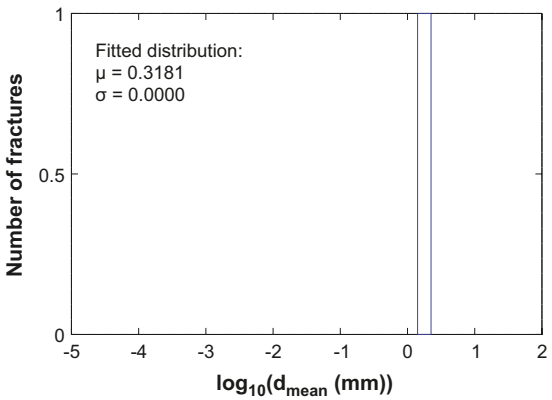

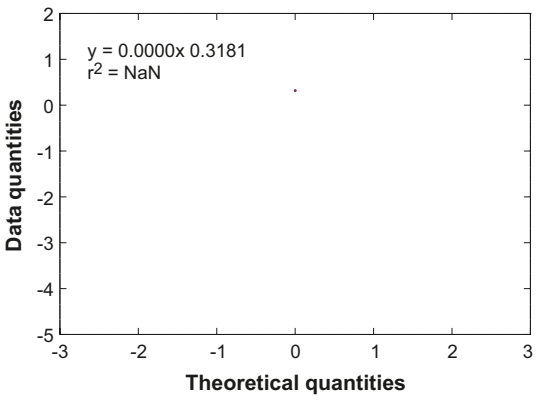

Pyrite (All DZ)

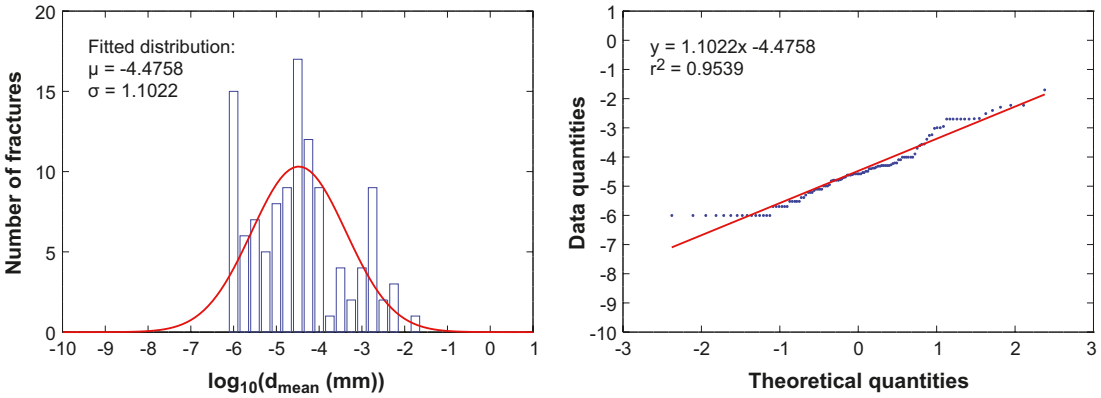

A5.2 GDZ (96 fractures)

Calcite (GDZ)

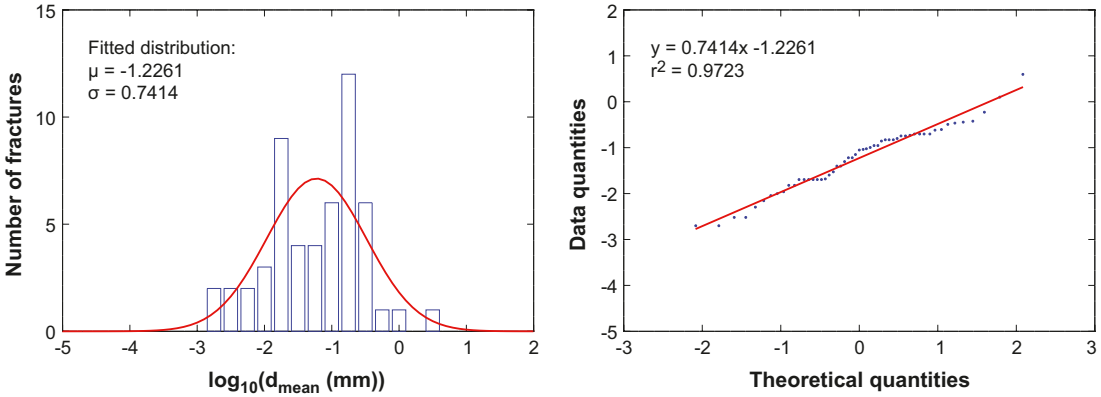

Chlorite (GDZ)

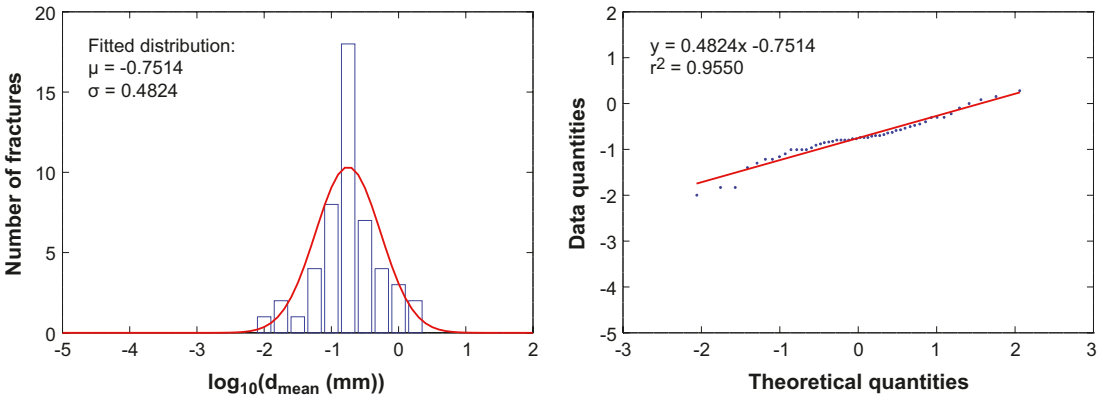

Clay minerals (GDZ)

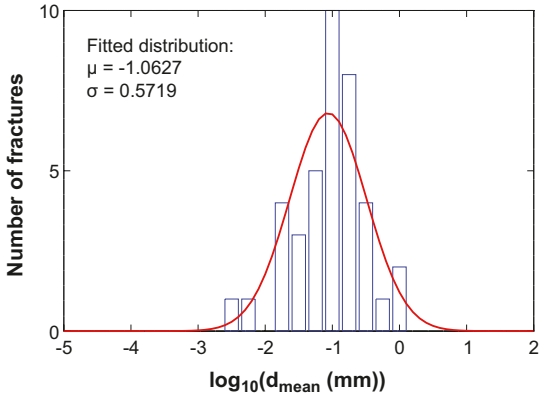

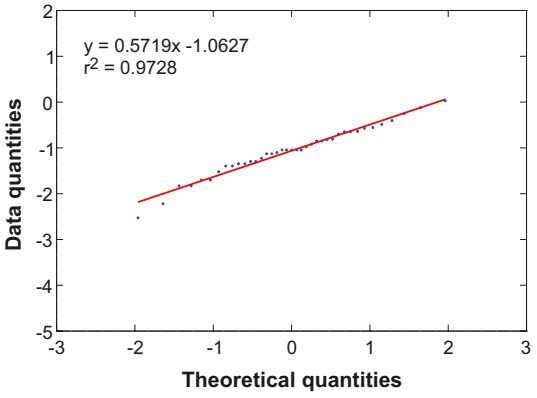

Hematite (GDZ)

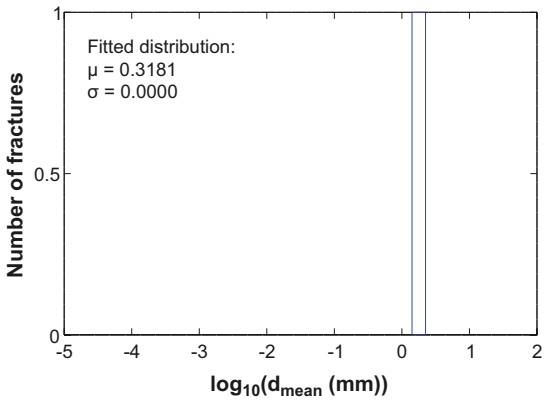

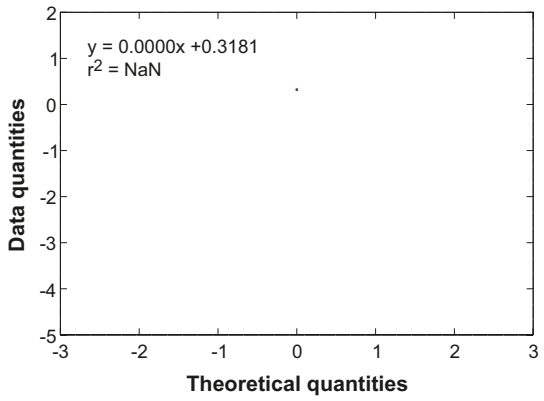

Pyrite (GDZ)

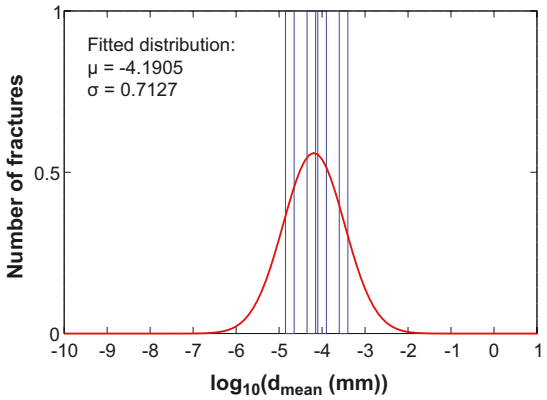

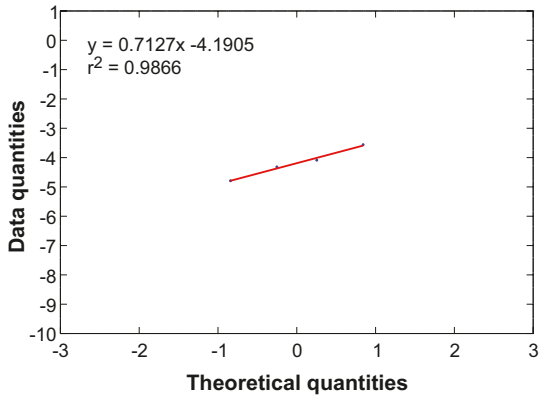

A5.3 E-W/NW-SE (57 fractures)

Calcite (E-W/NW-SE)

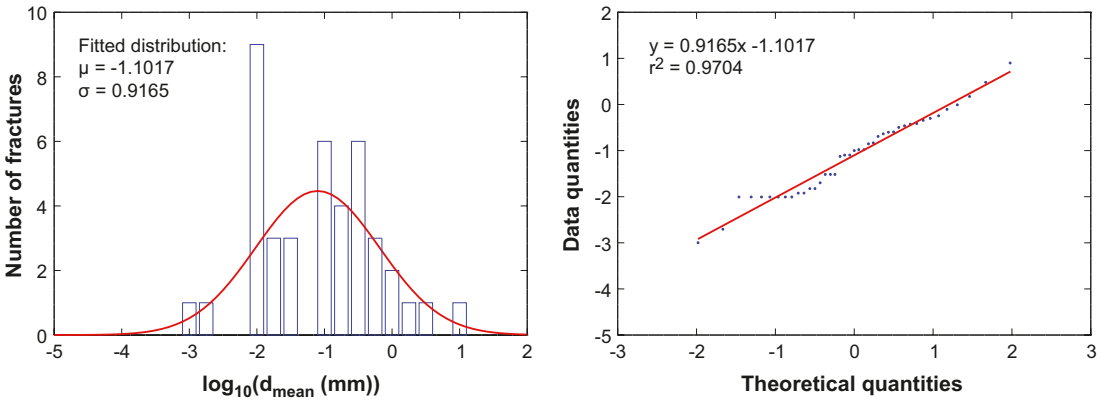

Chlorite (E-W/NW-SE)

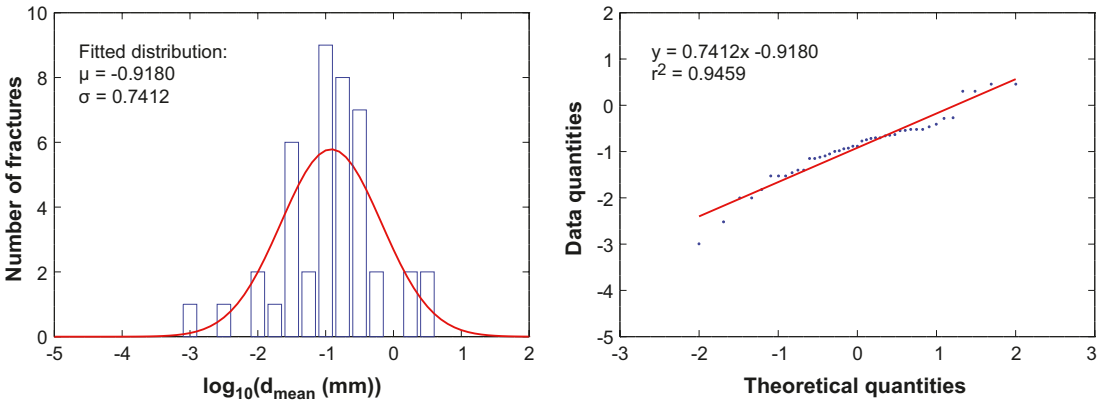

Clay minerals (E-W/NW-SE)

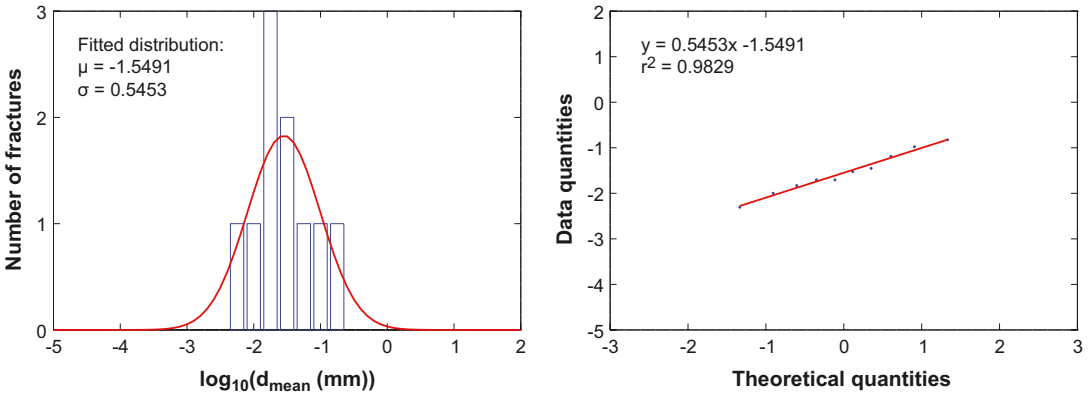

Hematite (E-W/NW-SE)

N/A

Pyrite (E-W/NW-SE)

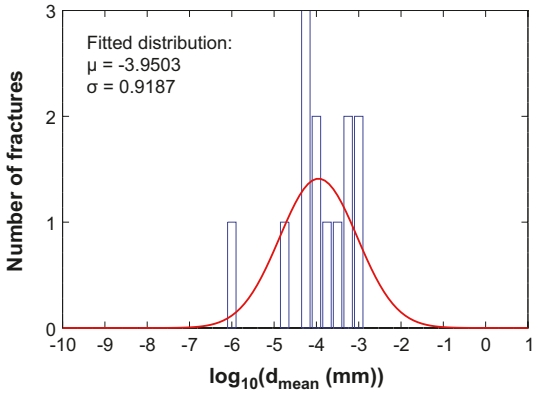

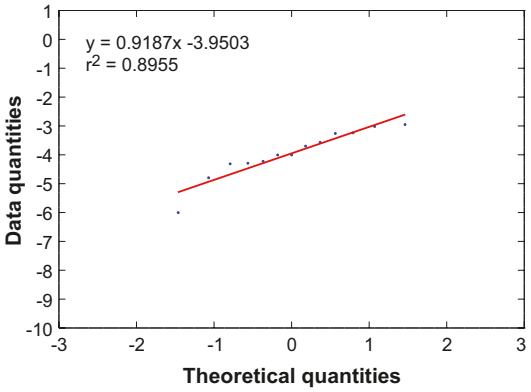

A5.4 N-S (139 fractures)

Calcite (N-S)

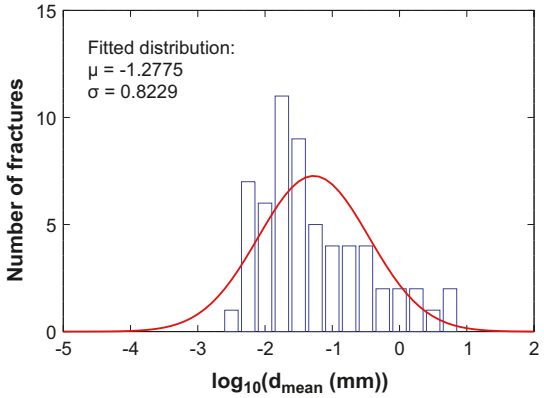

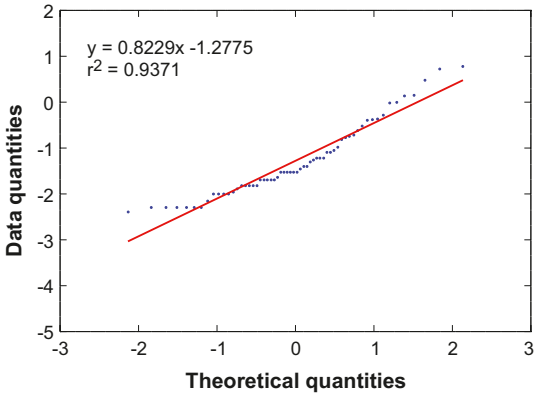

Chlorite (N-S)

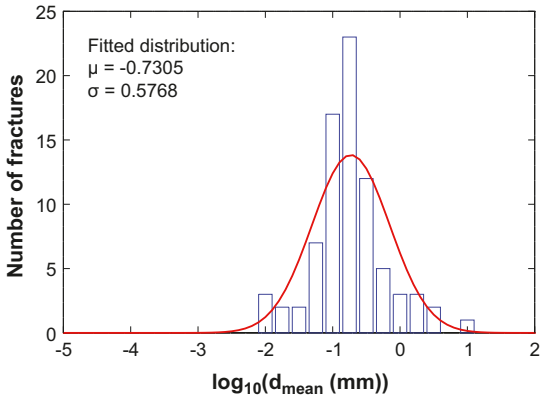

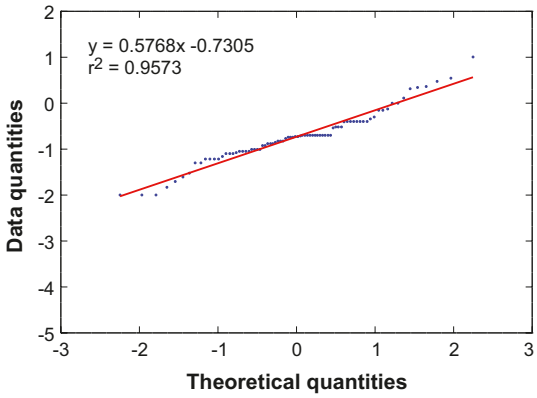

Clay minerals (N-S)

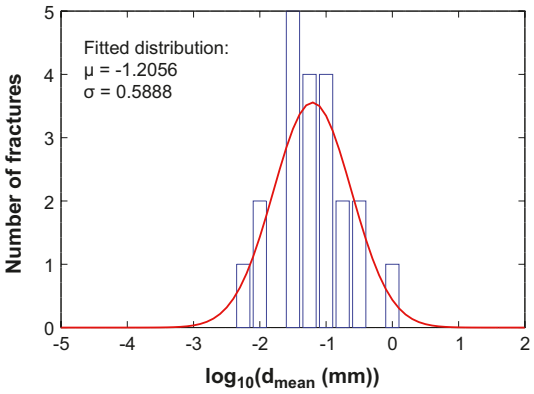

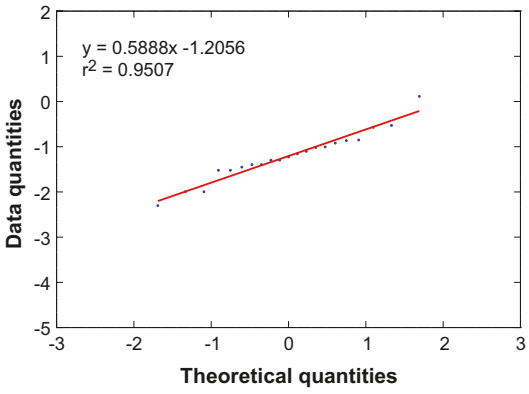

Hematite (N-S)

N/A

Pyrite (N-S)

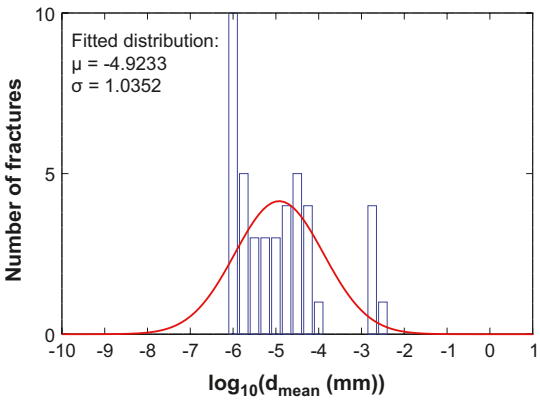

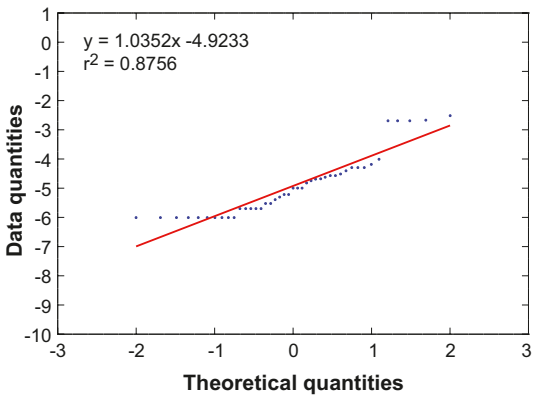

A5.5 NE-SW (452 fractures)

Calcite (NE-SW)

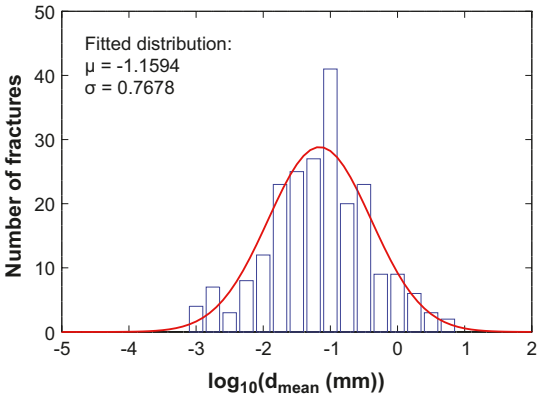

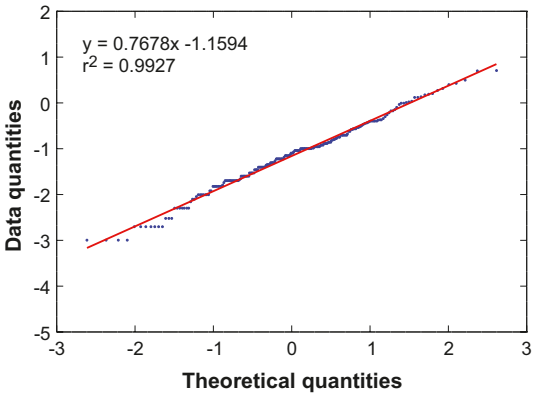

Chlorite (NE-SW)

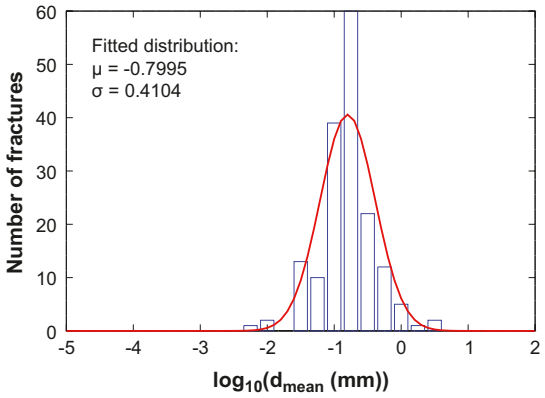

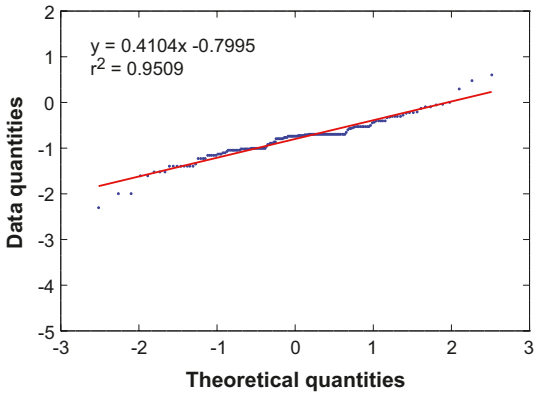

Clay minerals (NE-SW)

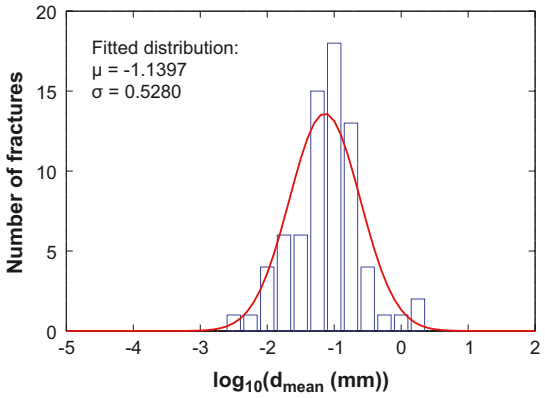

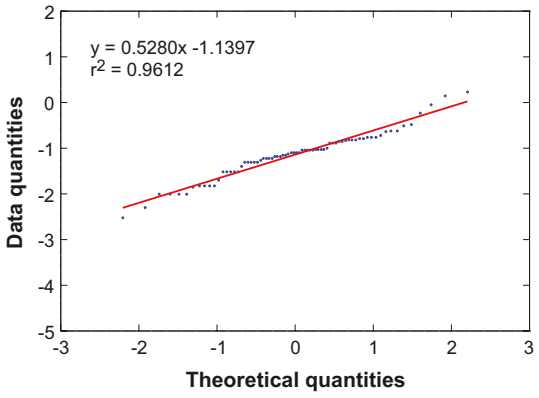

Hematite (NE-SW)

N/A

Pyrite (NE-SW)

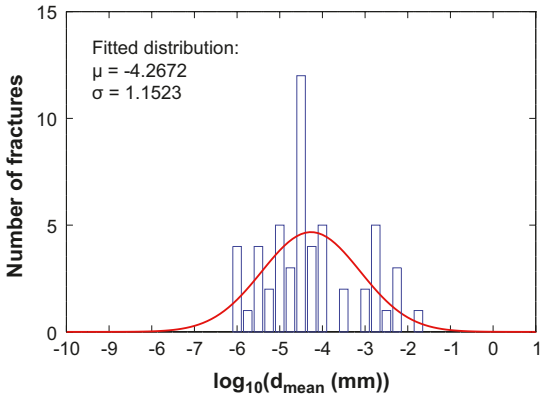

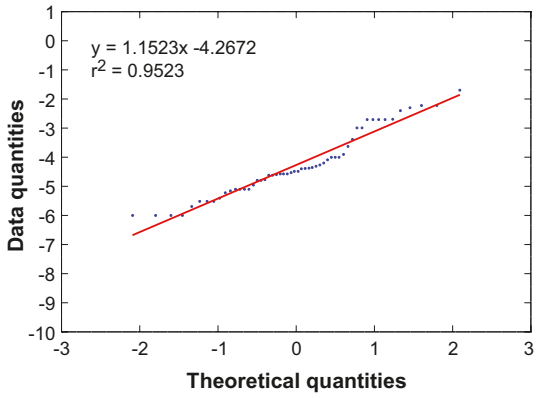

Appendix B

Mineral visible coverage, C_{vis}, in Laxemar

B1 All fractures in Laxemar (1,852 fractures)

B1.1 Calcite (All)

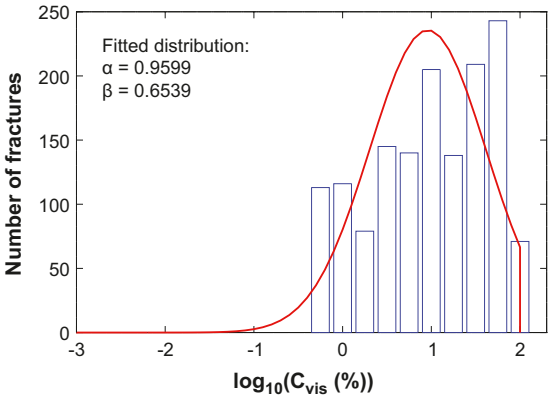

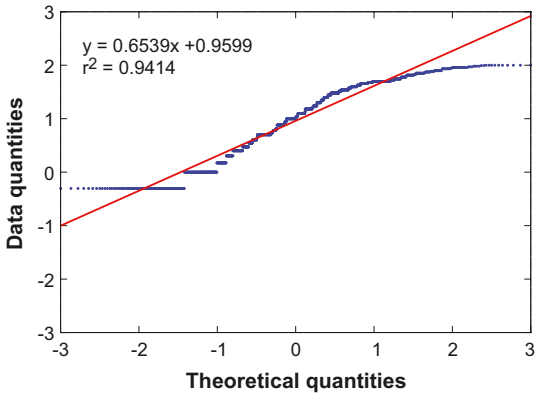

B1.2 Chlorite (All)

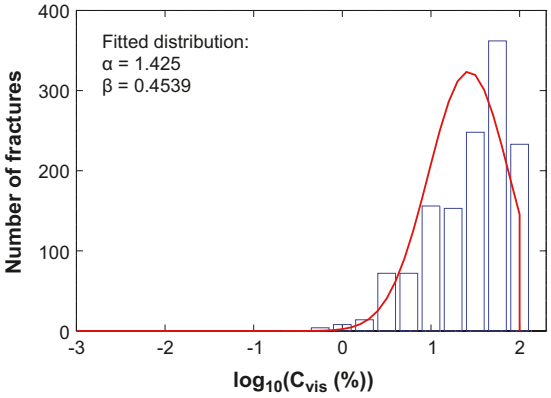

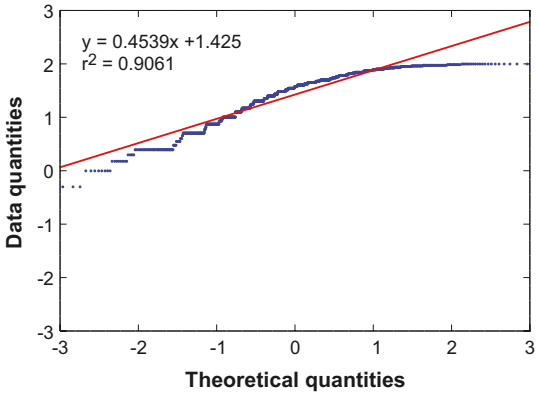

B1.3 Clay minerals (All)

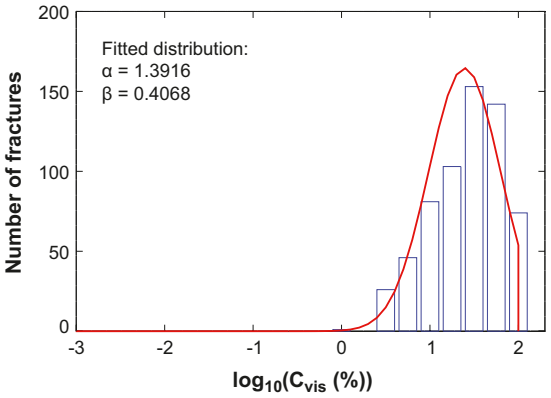

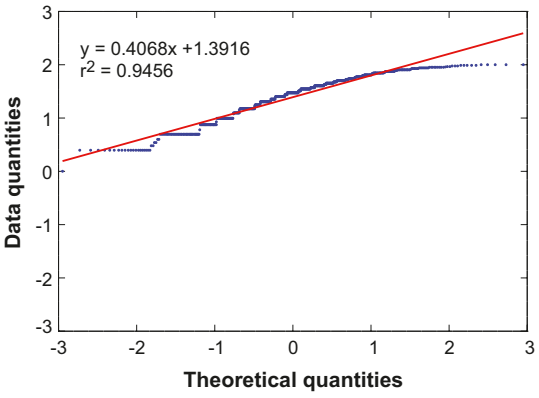

B1.4 Hematite (All)

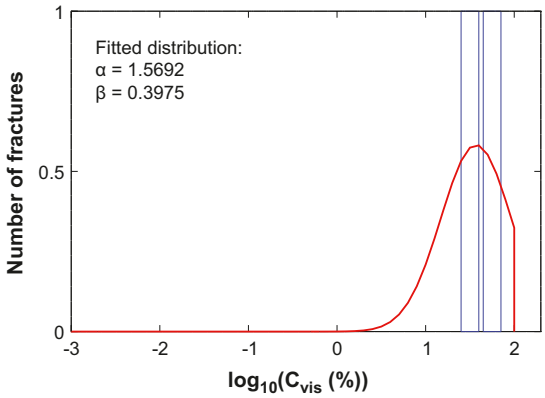

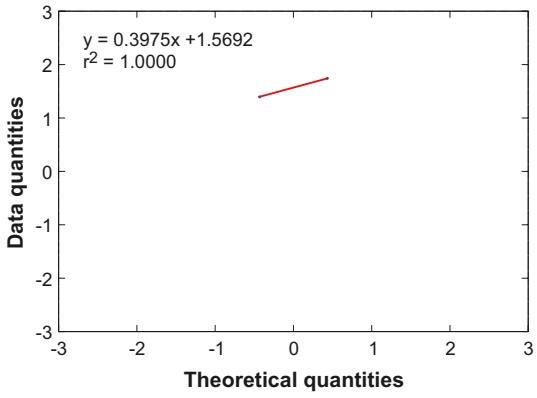

B1.5 Pyrite (All)

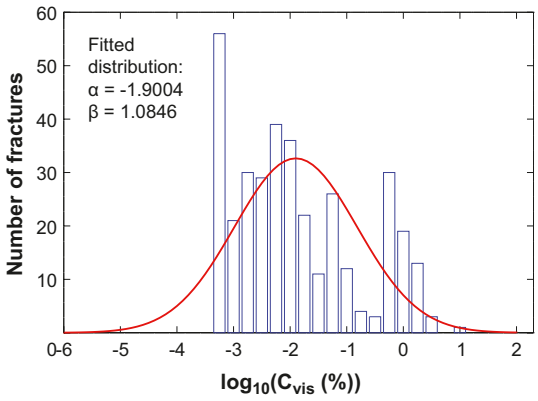

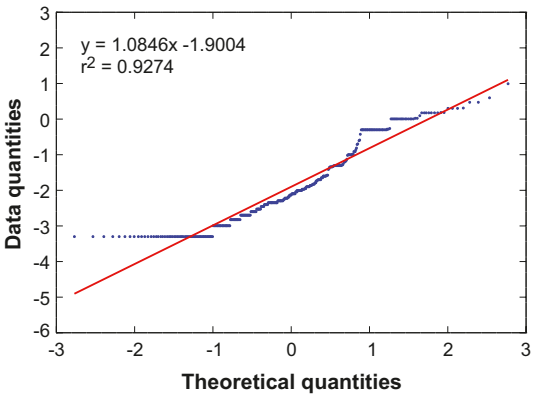

B2 Rock domain RSMD01 (1,067 fractures)

B2.1 Calcite (RSMD01)

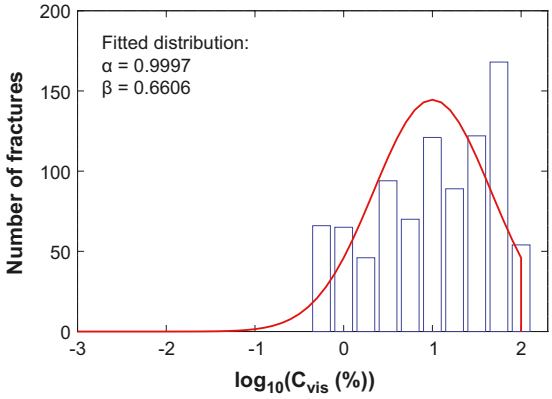

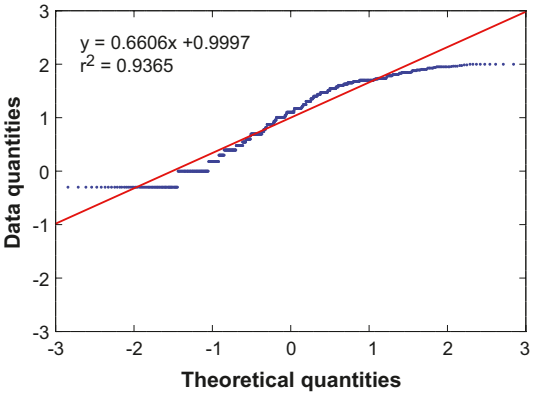

B2.2 Chlorite (RSMD01)

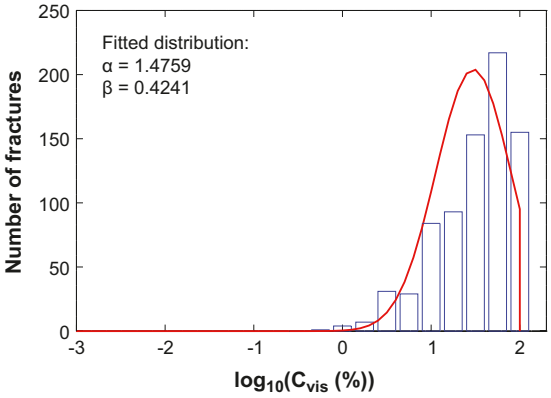

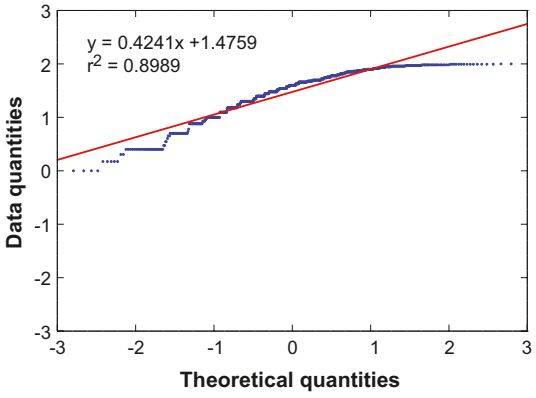

B2.3 Clay minerals (RSMD01)

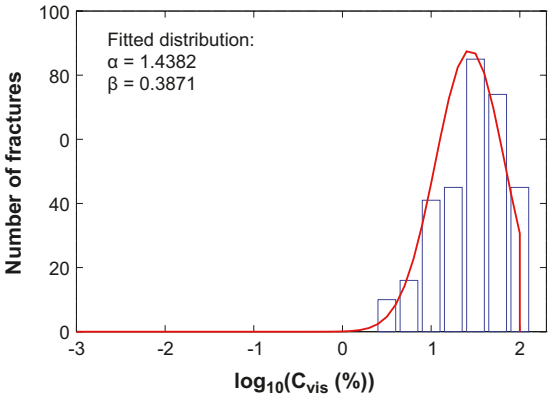

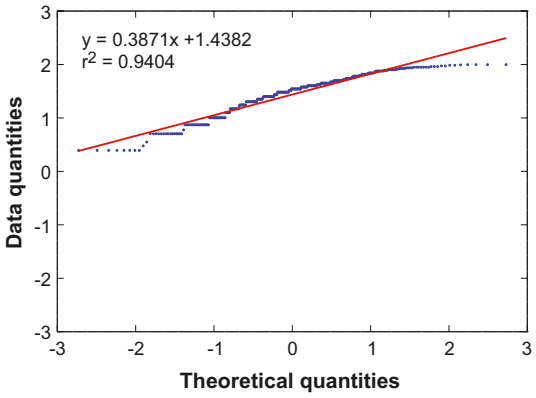

B2.4 Hematite (RSMD01)

N/A

B2.5 Pyrite (RSMD01)

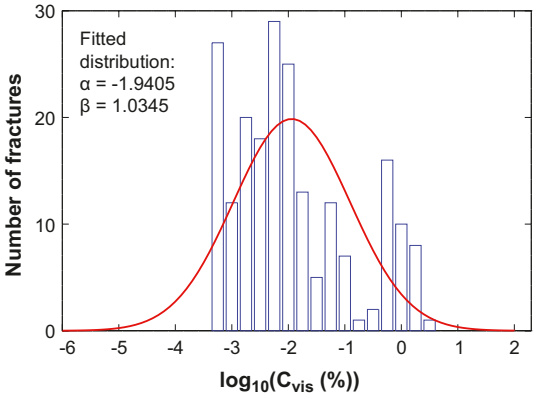

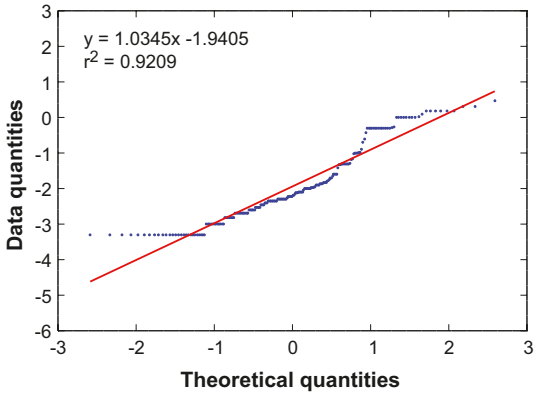

B3 All fracture domains (797 fractures)

B3.1 Calcite (All FD)

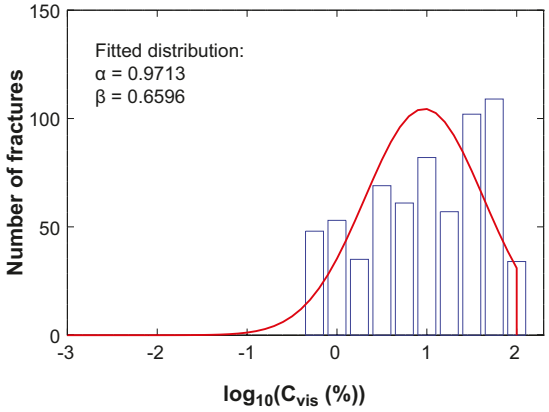

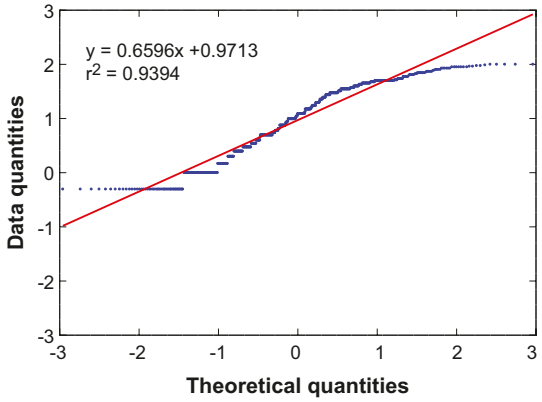

B3.2 Chlorite (All FD)

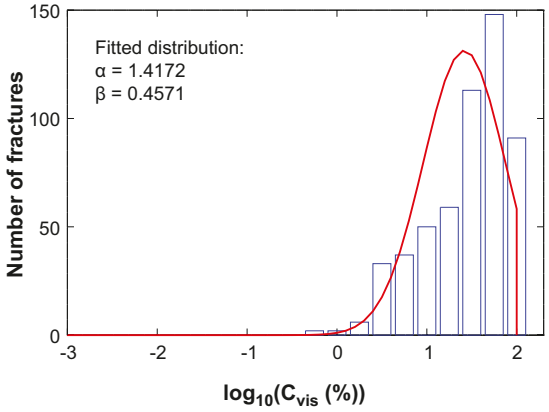

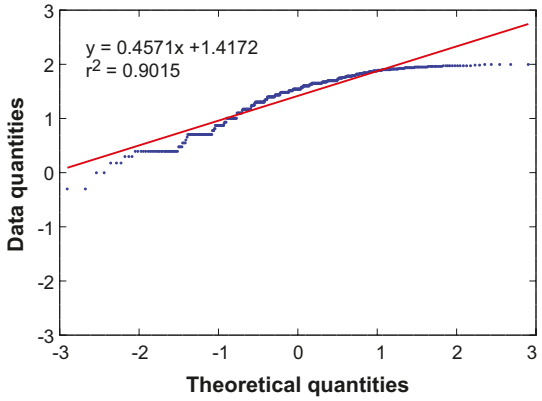

B3.3 Clay minerals (All FD)

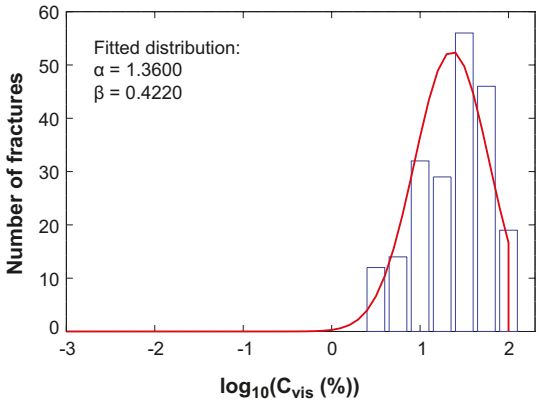

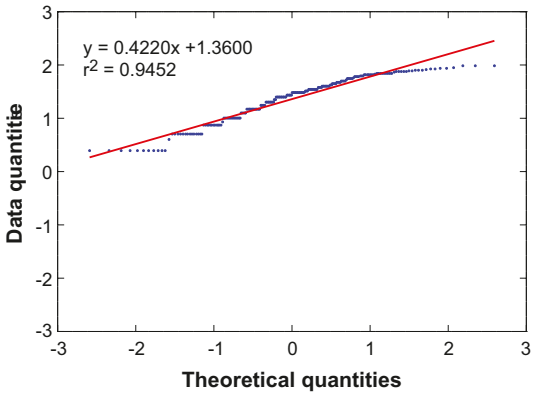

B3.4 Hematite (All FD)

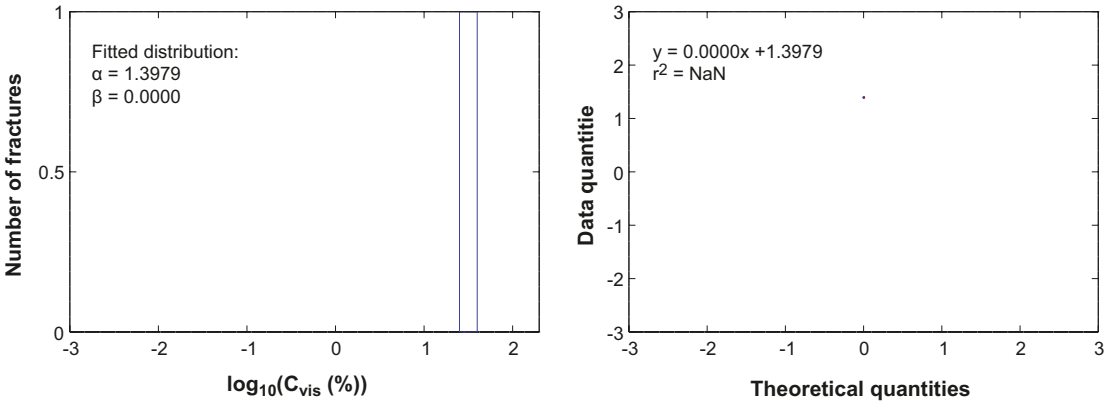

B3.5 Pyrite (All FD)

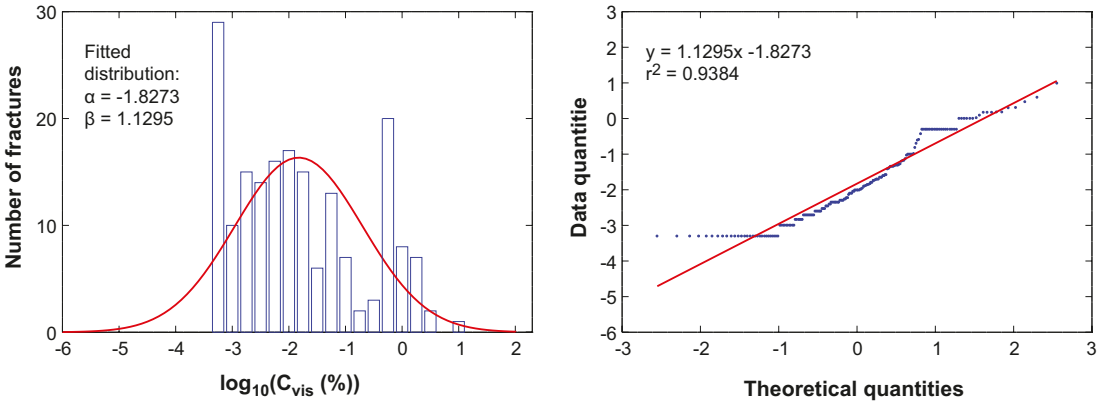

B4 All deformation zones (744 fractures)

B4.1 Calcite (All DZ)

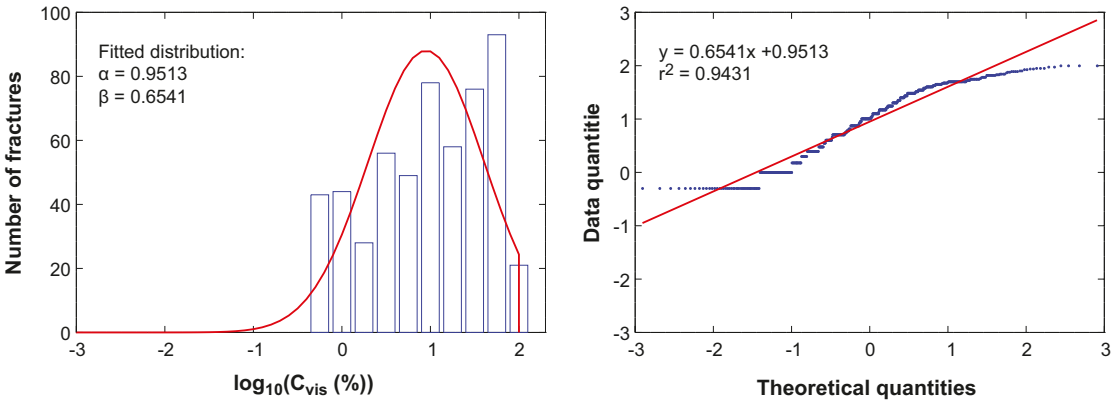

B4.2 Chlorite (All DZ)

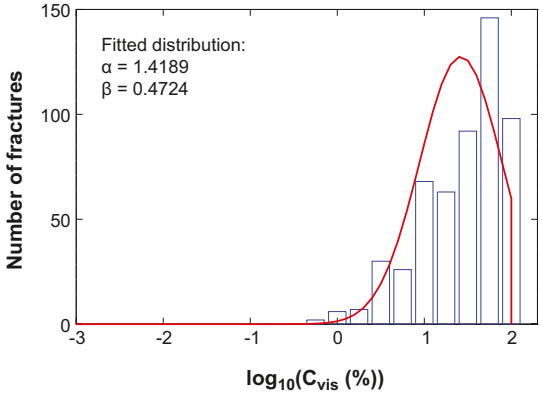

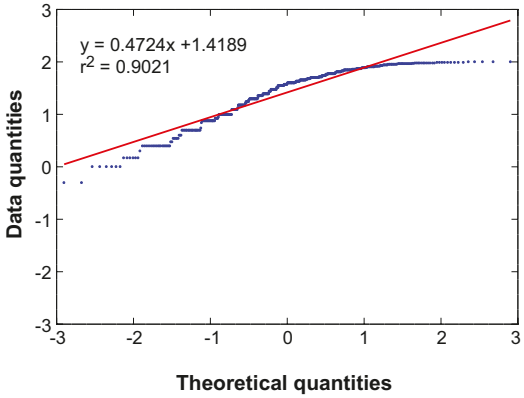

B4.3 Clay minerals (All DZ)

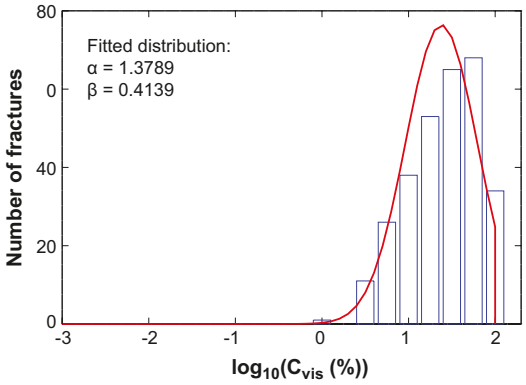

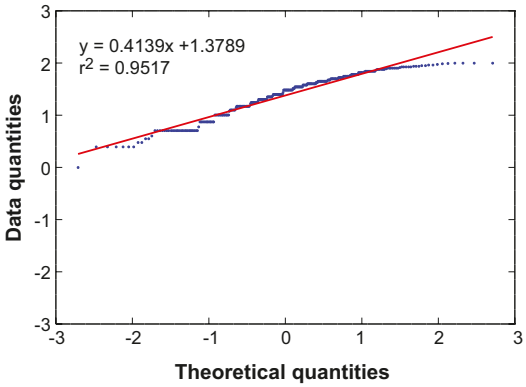

B4.4 Hematite (All DZ)

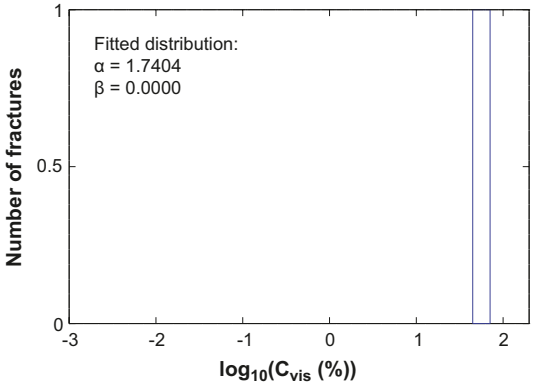

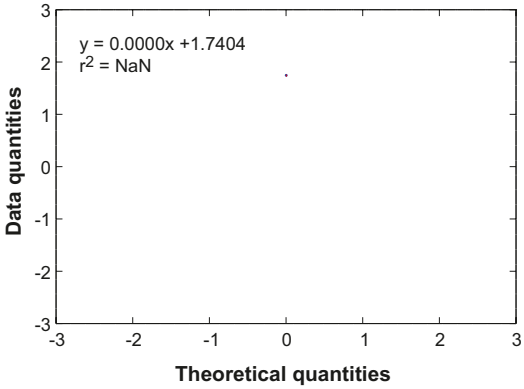

B4.5 Pyrite (All DZ)

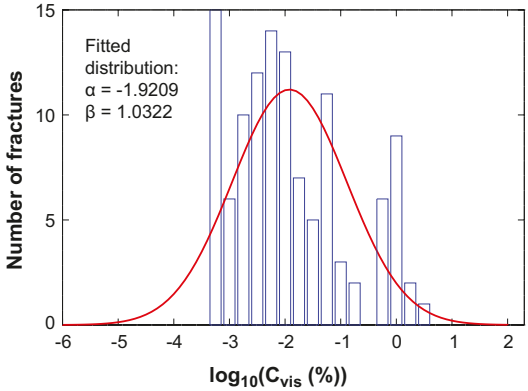

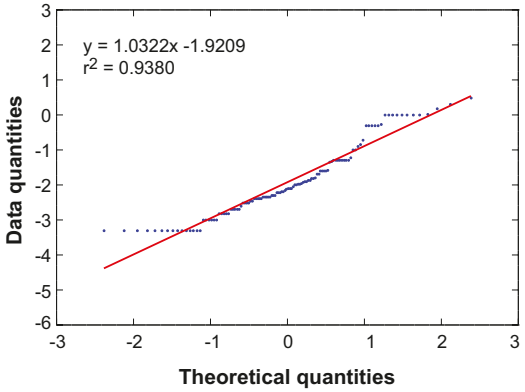

Appendix C

Information on data qualification

All data supplied as input to the SR-Site safety assessment modelling should be qualified, that is they should be both scientifically justifiable and quality assured. The data delivered in this report may be used as input to SR-Site and therefore, we have appended information in line with what is requested in an instruction of how data quantification should be performed, and what issues one should reflect upon in the process. This instruction is given in the SR-Site Data report /SKB 2010/. The structure of this section is according to the supplier part of this instruction.

C1 Modelling in SR-Site

This Section is reserved for the customer of the data (i.e. the SR-Site safety assessment modelling team).

C2 Experience from SR-Can

This Section is reserved for the customer of the data (i.e. the SR-Site safety assessment modelling team). What can be said is that in SR-Can, only some semi-quantitative information existed on amounts and coverages of fracture minerals /Drake et al. 2006/.

C3 Supplier input on handling of data in SR-Site and SR-Can

We are not aware of the strategy for implementing these data in SR-Site modelling. Furthermore, we have no suggestions on how, or if, this should be done.

C4 Sources of information and documentation of data qualification

All input data analysed in this report are produced within the Oskarshamn site investigation programme, and have been obtained in accordance with the SKB quality assurance system. The input data are presented in the site investigation report /Eklund and Mattsson 2008/.

The fracture mineral mapping has been performed according to the method description (MD 143.009) and activity plan (AP PS 400-07-061). The site investigation report, method description, and activity plan have been examined as part of the data qualification, and are found adequate.

Numerical data from the quantitative mineral mapping have been taken from the database Sicada (Data Delivery ID: Sicada_09_062, Delivery Date: 2009-05-06). The delivery is a combination of the databases GE054 mineral volume mapping and P_fract_core_eshi.

Information on the geological structures (rock domain, fracture domain, and deformation zone) is included in the Sicada delivery.

The programs used for sorting data into different data subsets, making illustrations, and performing statistical analyses are:

- GNU Octave version 3.0.0. John W. Eaton. Department of Chemical Engineering. University of Wisconsin, USA.
- Analyse-it version 2.12. Analyse-it Software LTD.

All data obtained in the site investigations are judged to be qualified. According to the data qualification instruction, a number of issues should be reflected and commented upon. This is done in Table C-1.

Table C-1 Issues to be reflected upon in data qualification.

	Question in data qualification instruction	Answer
Issues concerning input data	Is the acquirement of observed data, for example in the site investigation, performed in agreement with a widespread quality management system (e.g. the ISO 9000 series or equivalent)?	Yes
	Is it possible to trace relevant quality management documents (for example method descriptions, field notes, etc.) for the measurements?	Yes. Activity plan and method description have been examined. Questions have been dealt with through personal communication with the authors of the site investigation report.
	Is it possible to extract relevant information on the data quality, variability, and representativity from documents reporting the acquirement of data?	Yes. Available information in the site investigation report, activity plan, and method description has been examined. Information from calibrations given in the site investigation report has been examined.
	Are concerns associated with the observed data and nonconformities of the measurements transparently described?	Yes, This is done in the site investigation report. The nonconformities reported concern in many cases parts of the drill core where mapping could not be performed, as samples from the drill core had been taken to the laboratory, as part of other campaigns. However, the combined length of drill core sections that could not be mapped is small in comparison to that which could be mapped. Nonconformities arising from missing core pieces and sections are listed in /Eklund and Mattson 2008/.
	Is the performed data acquirement programme sufficient to catch data uncertainty and natural variability and do the acquired data represent that which was intended (site, rock domain, copper canister, population, etc.)?	Yes. These issues are discussed in this present report.
Issues concerning data refinement	Are concerns and nonconformities described in the supporting documents (for example site investigation reports) propagated to, and handled in, the data refinement?	Yes. Such concerns and nonconformities have been examined and are part of the input to this analysis. Questions have been dealt with through personal communication with the authors of the site investigation report.
	In refining observed data by use of more or less complex modelling, is this done in accordance with documented methods?	Refinement of data has been performed by elementary arithmetic operations. The statistical methods used in the analysis are well-defined standard methods.
	In case of more complex modelling, which may have implication for data qualification, is the details of the modelling described in a task description or in the document reporting the modelling results?	No complex modelling is used in the data refinement.
	Has comparative/alternative modelling been performed to evaluate artefacts induced in the modelling, and to evaluate whether the refined data are reasonable?	No alternative modelling has been performed, as no complex modelling is used in data refinement.

C5 Conditions for which data are supplied

No external conditions, such as temperature, should affect the observed data. However, there is a risk that some of the fracture minerals have been mechanically removed from the facture surface in the drilling and sample preparation. Furthermore, fracture minerals may have been affected by wear in previous drill core mapping, where they may also have been exposed to diluted HCl solution. Also de-stressing, general weathering and oxidation are conceivable sources of alteration.

C6 Conceptual uncertainty

When selecting drill core sections that should be mapped, the locations of flow anomalies have been used. As a flow anomaly has not been associated with a specific fracture, it has been assumed that all fractures in a section surrounding the flow anomaly should represent the flow path. This assumption is conceptually uncertain.

Even if a fracture may allow water flow, channelling is postulated to occur and there is no way of knowing if the fracture surface mapped has been exposed to flowing water. This is valid even if one, by some means, has the ability to conclude that the fracture plane conducts water, and also has been conducting water prior to the drilling of the borehole. This evokes conceptual uncertainty.

The quantitative mapping of the amount of fracture minerals is carried out on a surface with a diameter of approximately 5 cm. This surface is then set to represent the entire fracture plane which surface area is unknown. This introduces a major uncertainty.

In the fracture mapping, it is assumed that the coverage and thickness of a fracture mineral that is over layered by another fracture mineral can be estimated, without removing the covering layer. It is uncertain to what extent this is true.

The distributions presented in this report, and their associated shapes, are not based on process understanding of the occurrence of fracture minerals, but should be seen as empirical.

Only a fraction of all fractures in the potential repository host rock has been investigated. Some uncertainty still remains concerning to what extent the obtained results can be extrapolated to other parts of the repository host rock.

C7 Data uncertainty due to precision, bias, and representativity

In this Section the precision, bias, and representativity of the data are discussed. In the data qualification instruction it is requested to put numerical values on the data uncertainty, to the extent possible.

The data uncertainty introduced by the analysis made in this report is judged to be small in comparison to data uncertainty introduced when selecting the fractures and estimating the parameters during the mapping.

In the quantitative mineral mapping campaign, the data uncertainty of the estimated visible coverage and layer mineral thickness was investigated by performing calibrations. Concerning the visible coverage, the calibration was made on 39 samples prior to the campaign. Firstly the visible coverage was estimated by standard mapping methods, and thereafter the fracture surface was photographed and subsequent image analysis was performed. Figure C-1 displays the result from the calibration, indicating precision and bias errors of a few percents only.

No calibration was made for the total coverage. It is subjectively estimated that the error may be a factor of few larger for the total coverage than for the visible coverage.

For the layer mineral thickness, reasonably successful calibrations were made on eight samples. First the layer mineral thickness was estimated by standard mapping methods. Thereafter, the sample was sawed into two pieces, along the axis of the cylindrical drill core. The cuts were photographed and image analysis was performed. Figure C-2 shows the results from the calibration.

From the calibration, one can suggest precision errors of around 0.1 mm or less. However, the fracture mineral thickness of both the drill core edge and the saw cut may be biased as fracture minerals may have been mechanically removed by the drilling and sawing. Concerning d_{mean} and C_{vis} the precision should not significantly affect the mean value of the distribution but only the data spread. By examining the results in Chapters 3 and 4, generally the natural variability is the key contributor to the spread, why the achieved precision is judged as sufficient.

As discussed in Section 2.4.4 of this present report, the rounding in the mapping makes the results biased towards certain favoured data values. According to the method description (MD 143.009),

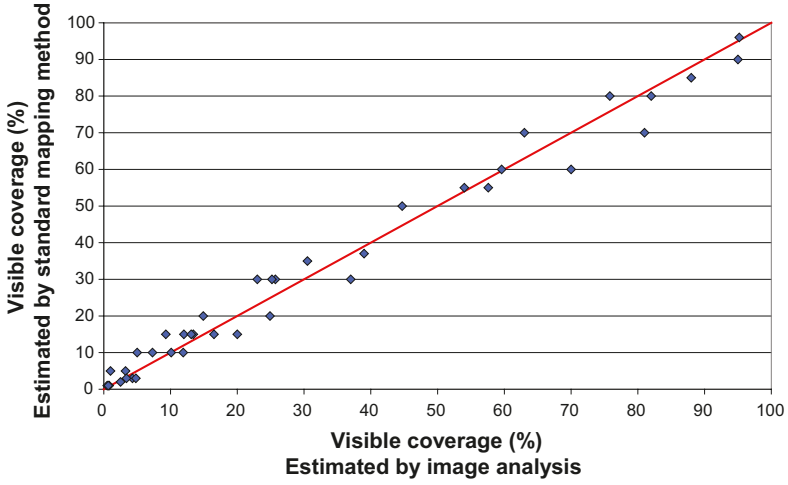

Figure C-1. *Results from calibration of visible coverage. Data from Appendix 3 in /Eklund and Mattsson 2008/.*

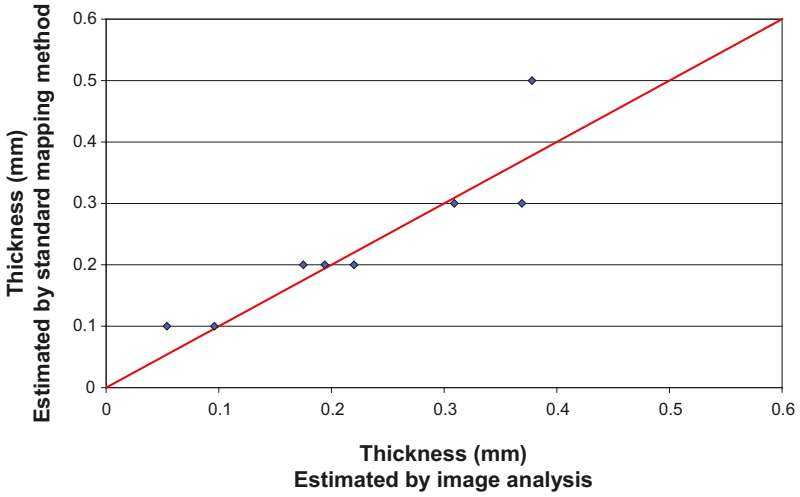

Figure C-2. *Results from calibration of layer mineral thickness. Data from Appendix 4 in /Eklund and Mattsson 2008/.*

the layer thickness is estimated in 0.1 mm steps, while coverages should be estimated as 1, 2, 3, 5, 7, 10, 15, 20, 25, 30, 40, 50, 60, 70, 80, 90, or 100%. Concerning $\log_{10}(d_{mean})$, as seen in the normal score plot in for example Figure 2-6, this does affect the slope and intercept of linear fitting, from where μ and σ of the normal distribution are acquired. The same holds true for $\log_{10}(C_{vis})$ and the α and β parameters of Equation 2-2. However, the effect is not major. It is subjectively estimated that the mean value should not be shifted by more than a factor (in many cases much less). Also there may be a bias towards lower fracture mineral amounts and coverages, due to mechanical wear and alteration in the drilling and in subsequent handling andstorage of the drill core. This bias is difficult to estimate but is probably not more than a factor or so.

The representativity discussion is divided in two issues. Firstly, the mapped fractures may or may not have conducted water prior to the excavation. This complicates the matter of assigning data for subsequent use in modelling where flow paths are of concern. It is difficult to estimate the error this evokes but it appears that the presence of fracture minerals is unrelated to the present groundwater flow rate (see Section 3.7). Therefore, the evoked error may be limited. Secondly, the limited set of open fractures mapped may not represent the entire rock volume of interest for a potential repository. However, the results of this report indicate that open fractures located in one part of the rock are populated by fracture minerals in a similar fashion as open fractures of another part of the rock.

All in all it is judged that the delivered d_{mean} and C_{vis} results are off by less than an order of magnitude but perhaps by as much as one or a factor of few. It is acknowledged that these estimates are subjective. More precise estimates of the uncertainty would be difficult to defend.

C8 Spatial and temporal variability

In Chapters 3 and 4, the spatial variability of d_{mean} and C_{vis} is investigated for different rock volumes. The averaged fracture mineral thickness and coverages do have a temporal variability over geological time periods, but it is assumed that during the time frame of consequence for repository safety, this variability is insignificant.

C9 Correlations

In this work, parameters from the site investigation report have been combined by elementary arithmetic operation (see Section 2.2). Otherwise, no correlation has been used.

C10 Results of supplier's data qualification

Results and recommended data for the Laxemar site concerning the averaged fracture mineral thickness and visible coverage are supplied in Chapter 5 of this report (Table 5-1 and Table 5-2), as suggested for use in subsequent modelling.